Ver:1.6

# ASTROSAT – INDIA'S FIRST MULTIWAVELENGTH ASTRONOMY SATELLITE

A simultaneous view of the Universe in UV and X-rays

ASTROSAT

INDIAN SPACE RESEARCH ORGANISATION

# ASTROSAT Handbook

| | |
|---|---|
| Ver 0.1 - Collation of all individual payload inputs into separate chapters - | Jan 11 2013 |
| Ver 0.2 - Updated with comments from individual payload teams | July 31 2013 |
| Ver 0.3 - Updated with comments from UVIT payload team | Aug 24 2013 |
| Ver 0.4 -Updated with comments from LAXPC payload team | Oct 01 2013 |
| Ver 1.0 - Revisions from SXT and inclusion of outline of Ch10 & 11 | Oct 18 2013 |
| Ver 1.1 - Revision from LAXPC payload team | Oct 23 2013 |
| Ver 1.2 – Corrected table 1 and replaced ASTROSAT figure | Nov 03 2013 |
| Ver 1.3 – Revision of LAXPC chapter | Jul 25 2014 |
| Ver 1.3a – minor corrections in text and tables | Nov 10 2014 |

**Ver 1.6** – Dec 18 2014

The current version is numbered as Ver 1.6 so as to avoid confusion since Ver 1.5 was circulated sometime back.

Changes are in the payload characteristics table in Introduction, minor corrections and addendum on brightness limits in UVIT, hardware section in CZT and last paragraph of CPM.

LAXPC remains the same as version 1.3.

SSM is yet to be updated.

## CONTENTS

Chapter 1

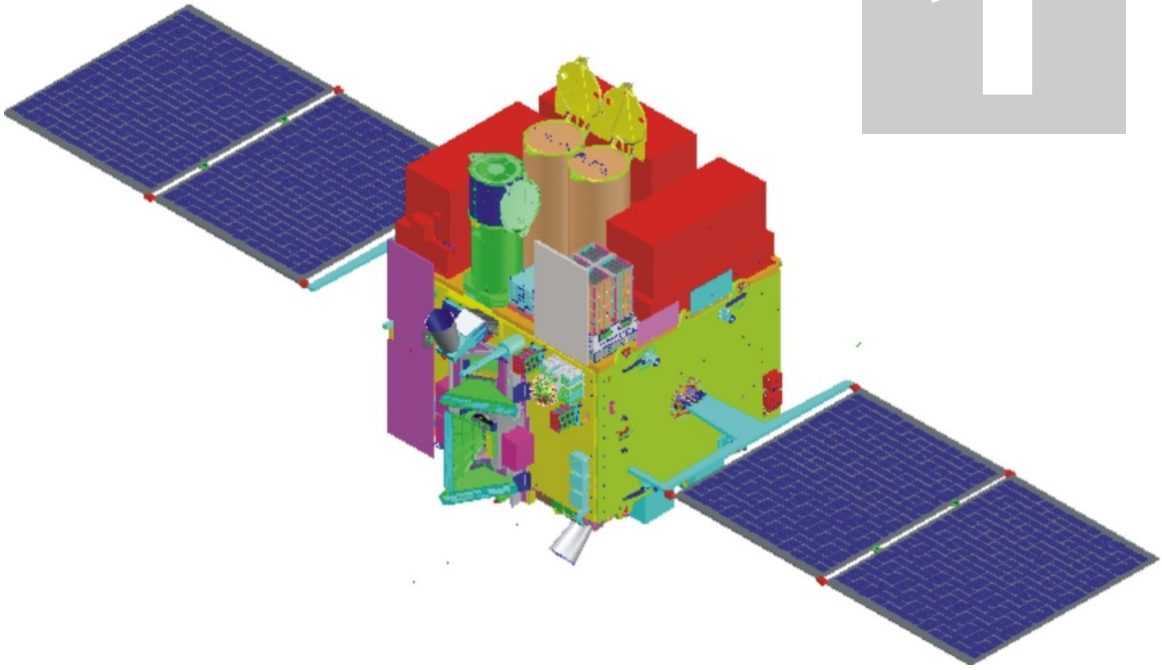

# ASTROSAT mission

*ASTROSAT – India's first dedicated astronomy satellite*

To understand the nature of cosmic sources, their radiation processes and environment, it is necessary to measure their emission over the entire electromagnetic spectrum. Since intensity of most cosmic sources varies with time, the variability being wavelength-dependent, it is necessary to make simultaneous observations in different wavebands. Most of the current space astronomy observatories are dedicated to a particular waveband e.g. X-ray, UV etc and therefore, usually multiwavelength studies have to be made from coordinated observations with different satellites. There are logistical problems in making simultaneous and coordinated studies of a specific object from different satellites and ground-based telescopes. As a result, despite a large number of such multiwavelength observation campaigns, very few sources have so far been studied over wide spectral band leading to poor understanding of the underlying physical processes. The most efficient and effective approach is to have a dedicated satellite such as ASTROSAT with several co-aligned instruments covering the desired spectral bands so that simultaneous observations in all the desired wavebands is possible.

## Primary Science Objectives of ASTROSAT

Understand high energy processes in binary systems
Search for black hole sources in the Galaxy.
Measure magnetic fields of neutron stars.
Study high energy processes in extragalactic systems.
Detect new transient X-ray sources.
Limited high-angular resolution deep field survey in UV

**These primary science objectives are being met with 5 science payloads.**

Large Area X-ray Proportional Counters (LAXPC)
Cadmium-Zinc-Telluride Imager (CZTI)
Soft X-ray imaging Telescope (SXT)
Scanning Sky Monitor (SSM)
Ultra Violet Imaging Telescope (UVIT)

The important parameters of the instruments are listed in the table. A complementary charged particle monitor is also onboard to provide data on particle flux.

## ASTROSAT - Payload Characteristics

| | UVIT | SXT | LAXPC | CZTI | SSM |
|---|---|---|---|---|---|
| Detector | Intensified CMOS, used in photon counting mode or integration mode | X-ray (MOS) CCD (at the focal plane) | Proportional counter | CdZnTe detector array | Position-sensitive proportional counter |
| Imaging / non-imaging | imaging | imaging | non-imaging | imaging | imaging |
| Optics | Twin Ritchey-Chretian 2 mirror system. | Conical foil (~Wolter-I) mirrors 2-m focal length | Collimator | 2- D coded mask | 1- D coded mask |
| Bandwidth | FUV (130-180 nm), NUV (200-300 nm), VIS (320-550 nm) | 0.3 - 8 keV | 3 - 80 keV | 10 - 100 keV | 2.5 - 10 keV |
| Geometric Area (cm2) | ~1100 | ~ 250 | 10800 | 973 | ~ 180 |
| Effective Area (cm2) | 10 - 50 (depends on filter) | 128@1.5 keV 22@6 keV | 8000@5-20 keV | 480 (10-100 keV, normal incidence) | ~11 @ 2 keV ~53 @ 5 keV for all 3 SSMs |
| Field of View (FWHM) | 28' dia | ~ 40' dia | 1° x 1° | 6° x 6° | 10° x 90° |
| Energy Resolution | <1000 A (depends on filter) | ~5-6%@1.5 keV ~2.5%@6keV | 12%@22 keV | 6% at 100 keV | 25% @ 6 keV |
| Angular Resolution | 1.8 arcsec (FUV, NUV) 2.2 arcsec (Vis) | ~2 arcmin (HPD) | ~(1-5) arcmin (in scan mode only) | 8 arcmin | ~12 arcmin |
| Time resolution | 1.7 ms | 2.4 s, 278 ms | 10 microsec | 20 microsec | 1 ms |
| Typical observation time per target. | 30 min | 0.5 - 1 day | 1 - 2 days | 2 days | 10 min |
| Sensitivity ( Obs. Time) | Mag. 20 (5σ) 200 s (for 130-180 nm) | ~15 μCrab (5σ) (10000 s) | 1 milliCrab (3σ) (100 s) | 0.5 milliCrab (3σ) (1000s) | ~28 milliCrab (3σ) ( 600s) |
| No. of Units | 2 | 1 | 3 | 1 | 3 |
| Total Mass (kg) | 230 | 90 | 414 | 50 | 48 |
| Total Power (W) | 85 (pk 117) | 80 | 65 | 50 | 30 |
| Sun-avoidance angle | 45 deg | > 45 deg | 30 deg | 30 deg | 30 deg from edge of FOV |
| Prime responsibility | IIA | TIFR | TIFR | TIFR | ISAC |

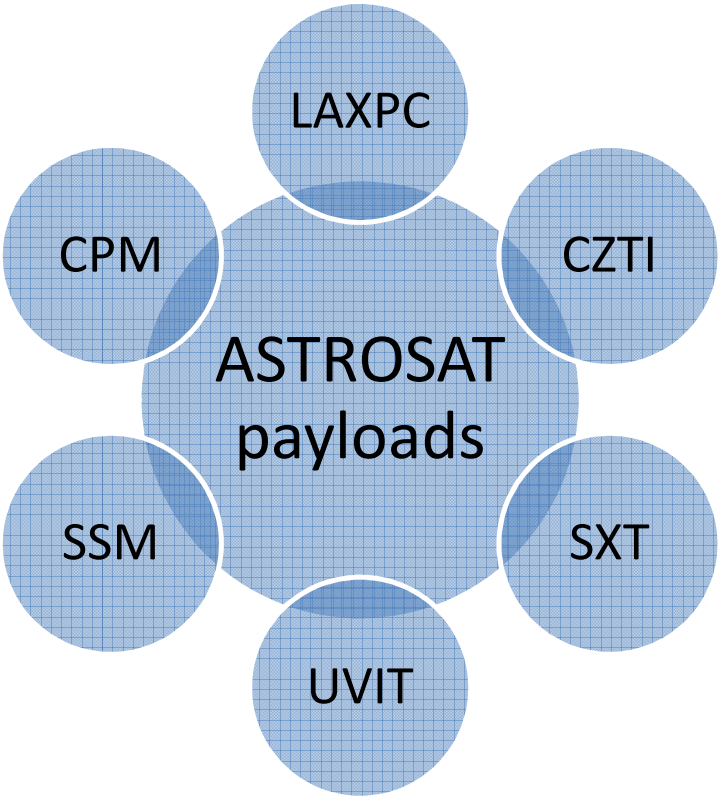
LAXPC
CPM
CZTI
ASTROSAT payloads
SSM
SXT
UVIT

Chapter 2

# Ultra-Violet Imaging Telescope

Imaging in the ultra-violet regime with a spatial resolution of 1.8" ( ~ X 3 better than Galex) in a field of ~ 28' provides many opportunities for Galactic and extra-galactic studies. Some of the objectives are listed below:

a) Time variations in UV of X-ray sources in coordination with the X-ray payloads
b) Star formation in nearby galaxies
c) Star formation in interacting galaxies
d) Star formation history of universe
e) Hot stars in Globular clusters
f) Planetary nebulae

## Instrument Overview

UVIT is primarily an imaging instrument. Images are made simultaneously in three channels: FUV (130-180 nm), NUV (200-300 nm), and VIS (320-550 nm), in a field ~ 28' circle. The spatial resolution (FWHM) is < 1.8" for the FUV and NUV channels, and it is ~ 2.2" for the VIS channel. In each channel, a set of filters are available, in the filter-wheels, for selecting a band. In the two ultraviolet channels, gratings are provided for low resolution (~ 100) slitless spectroscopy. The focussing optics is configured as twin R-C telescopes, each with a primary mirror with with effective diameter of ~ 375 mm.

The overall structure is shown in Fig. 2.1 Those parts of the telescopes which define locations of the optical elements are mostly made of Invar36, and the other parts are made of Aluminium alloy. The two telescopes are mounted on a cone-like structure of Titanium, which is attached to central cylinder of the spacecraft.

A cylindrical baffle extends over each of the telescopes for attenuating the radiation from off-axis sources. With these baffles the light reaching the detector from sources at 45 deg. from the axis is attenuated by a factor $10^9$; with such attenuation the light reaching the detector from full Moon at 45 deg from the axis is less than the average sky background. In addition to these baffles, the doors act as sun shades as long as Sun is at > 45 deg from the axis and the plane containing the optical axis and normal to the doors.

In order to avoid contamination of the optics due to ultraviolet assisted reactions, bright-earth is kept away from the axis by >12 deg., and the sun is kept behind the sun-shield at all times even if UVIT is not observing.

The geo-coronal lines are very strong in day time, and a significant amount of solar radiation could be scattered by the other instruments on the spacecraft into the baffles. Therefore, the nominal observation period is restricted to the night time (In special cases, observations in day time could be considered).
The intensified CMOS detectors can either be used in a high gain photon counting mode, or in a low gain integration mode (in which signal in a pixel of the CMOS detector could be contributed by multiple photons).
Pointing accuracy of the spacecarft is ~ 3', and for any pointing the aspect could drift by several tens of arcsec, at rates < 0.2"/s. In order to eliminate effect of this drift on the PSF, multiple short exposures (< 1 s each) are taken and are combined using shift and add. As the VIS field has adequate number of bright sources, images (taken in integration mode) from this channel are used to estimate the drift as a function of time.

There are three main contributors to the PSF: optics, detector, and drift of the aspect. Of these three the largest contribution is made by the detector and it is ~ 1" FWHM. The estimated overall FWHM, including the contributions of the optics and the drift, is 1.5".

The peak effective area, excluding the losses in the filters, is: ~ 15 $cm^2$ for the FUV, and ~ 50 $cm^2$ for NUV & VIS. An exposure calculator is available to estimate the expected signal levels for point sources observed through the various filters. In addition, a simulator is available which can generate the output image expected from an observation with UVIT, for an extended source with known distribution of the intensity.

# CONFIGURATION OF UVIT IN ASTROSAT

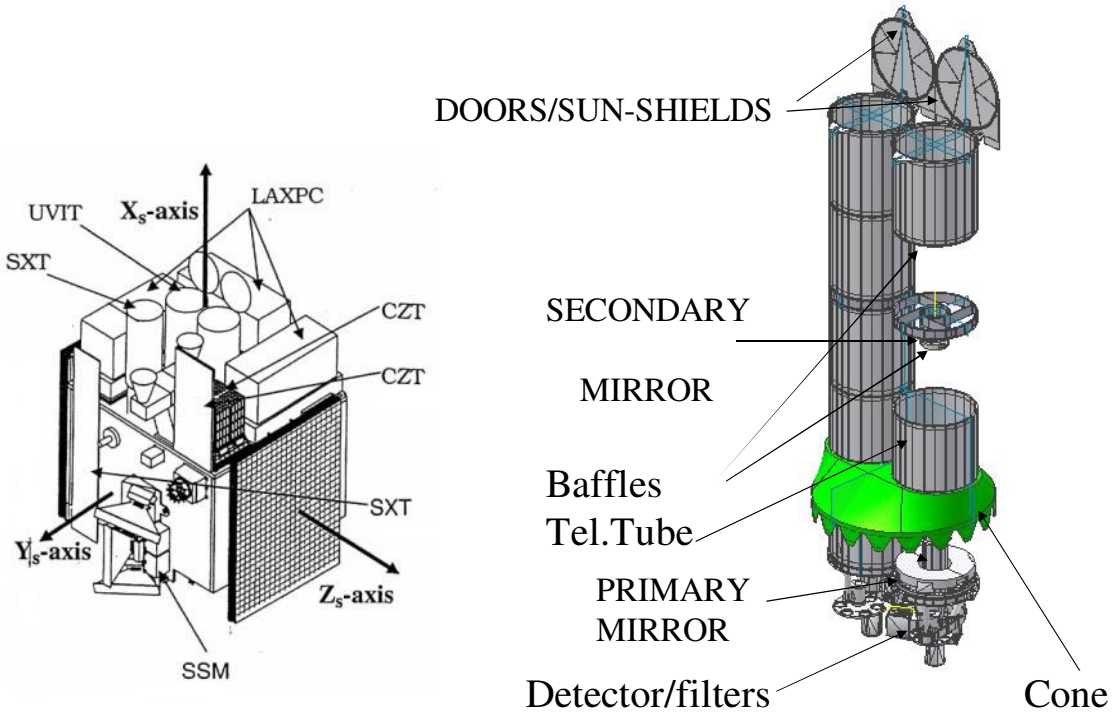

*Fig. 2.1 Configuration of the instruments in ASTROSAT is shown on the left. UVIT is shown on the right. The two telescopes are mounted on "Cone" which is fixed on the S/C.*

## Optics

Optical layouts of the two telescopes are are shown in Fig. 2.2 & Fig. 2.3. Both telescopes have hyperbolic f/4.5 primary mirrors of diameter ~ 380 mm (optical diameter ~ 375 mm), and hyperbolic secondary mirrors of optical diameter 140 mm. The overall focal length of the telescopes is ~ 4750 mm. The reflective coatings are Al with $MgF_2$ layer. The expected reflectivity is: ~ 70% per surface in FUV, and > 80% per surface in NUV & VIS. Roughness of the coated surfaces is < 1.5 nm rms, to keep the scattering < 1% per surface.

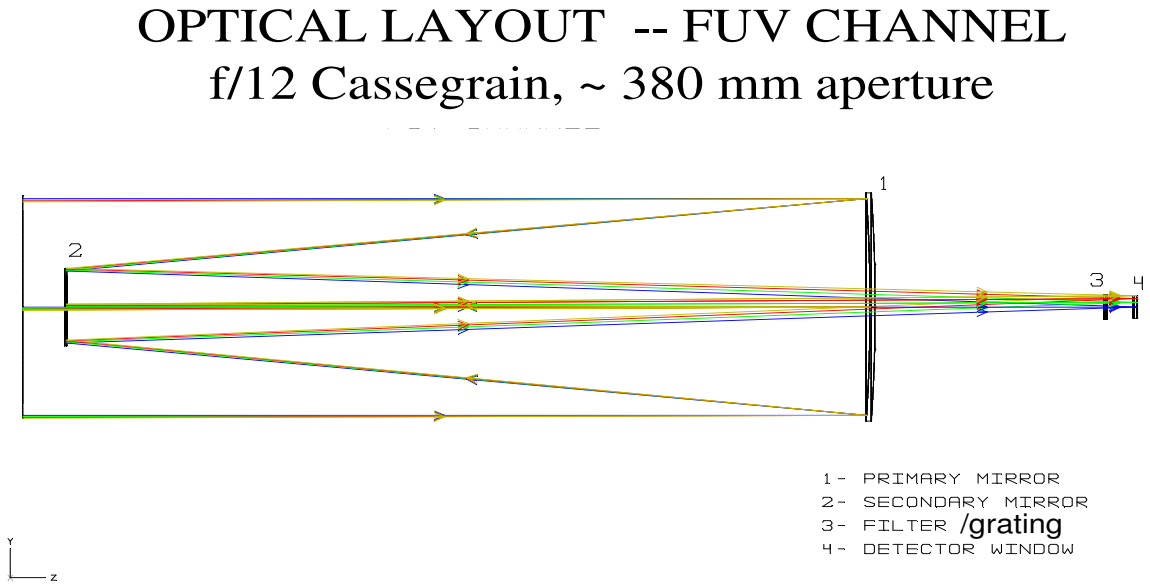


*Fig. 2.2 Optical layout of the FUV telescope is shown. The primary mirror has a working diameter of 375 mm. The detector has a diameter of ~ 40 mm. The filters, each of diameter 50 mm, and the grating are mounted in a wheel at a distance of ~40 mm from the detector.*

The plate scale is ~ 43"/mm. With a surface figure better than 1/50 waves rms (at 632 nm) for each of the mirrors, the PSF includes > 60% energy in diameter 1" at all wavelengths. In the NUV/VIS telescope, a beam splitter is used to reflect NUV and transmit VIS. Transmission leads to aberration in the VIS beam, and a cylindrical lens in used to reduce the aberration below 2" FWHM

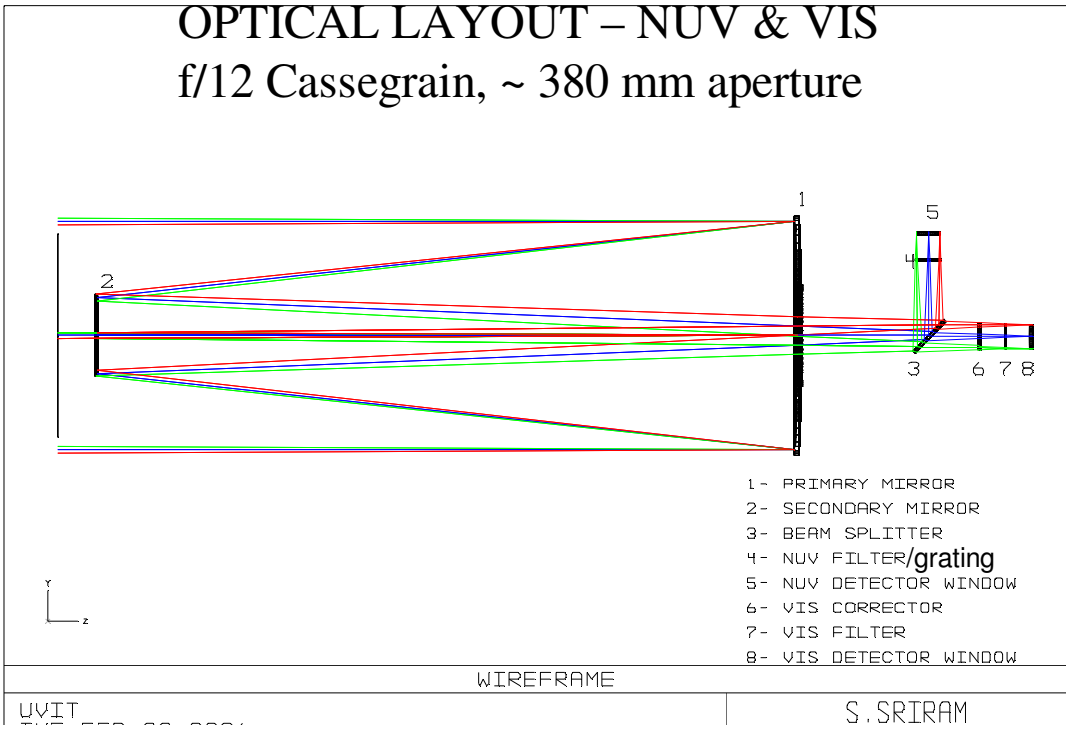


Fig. *2.3 Optical layout of the NUV /VIS telescope is shown. The primary mirror has a working diameter of 375 mm. A dichroic beam splitter is used for spectral division of the beam in NUV (reflection) and VIS (transmission). The detector has a diameter of ~ 40 mm. The filters, each of diameter 50 mm, and the grating (only for the NUV channel) are mounted in a wheel at a distance of ~ 40 mm from the detector.*

## Filters

Filters for the three channels are listed in Tables 2.1 to 2.3**.** The transmission curves for the filters and the beam splitter are shown in Fig. 2.4 to 2.15. Thickness of each filter/grating is chosen such that the best focus is obtained at the same location for all the filters/grating of a channel. In OBS_ID, filters are identified as "F0, F1, ..." . Filters "F0, F1, ..." correspond to Slot No. "0, 1, ..." in the tables 2.1 to 2.3.

**Table 2.1 FUV filter specification**

| Slot. No. | Filter Type | Filter Thickness mm | Pass Band nm |
|---|---|---|---|
| 0 | Block | | |
| 1 | CaF2 | 2.50 | > 125 |
| 2 | Barium Fluoride | 2.40 | > 135 |
| 3 | Sapphire | 2.00 | > 142 |
| 4 | Grating - 1 | 4.52 | > 125 |
| 5. | Silica | 2.70 | > 160 |
| 6. | Grating – 2 | 4.52 | > 125 |
| 7. | CaF2 | 2.50 | > 125 |

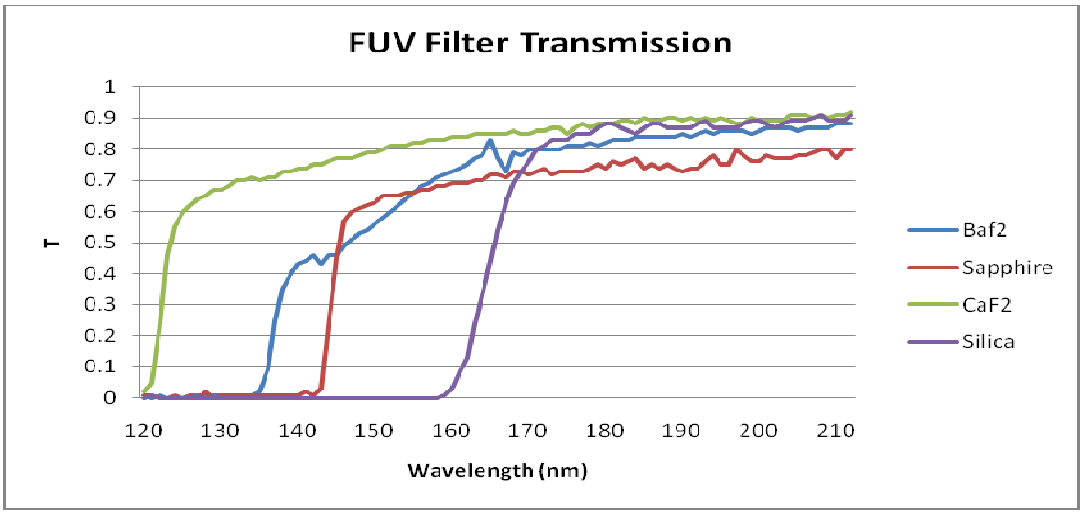


*Fig.2.4: Spectral transmission of FUV filters measured in MGKML.*

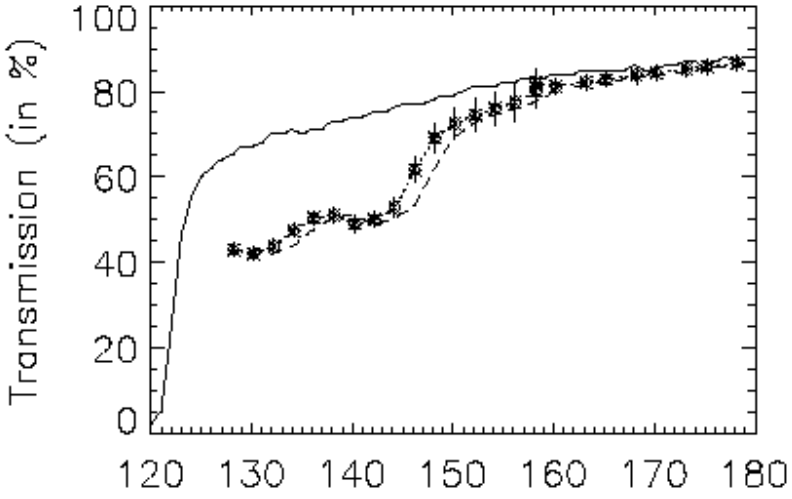


*Fig. 2.5: Measured CaF2 transmission in MGKM Lab. of IIA. Exposure to water vapour, in the air, leads to reduction in the transmission from 125 nm to 150 nm. A recovery of the transmission is affected by long exposures to high vacuum*

Table.2.2 NUV filter specification

| Slot. No. | Filter Type | Filter Thickness mm | Pass Band nm |
|---|---|---|---|
| 0 | Block | | |
| 1 | Silica | 3.00 | > 200 |
| 2 | NUV15 | 2.97 | 200 – 230 |
| 3 | NUV13 | 3.15 | 230 – 260 |
| 4 | Grating | 4.52 | > 200 |
| 5. | NUVB4 | 3.33 | 250 – 280 |
| 6. | NUVN2 | 3.38 | 275 – 285 |
| 7. | Silica | 3.30 | > 200 |

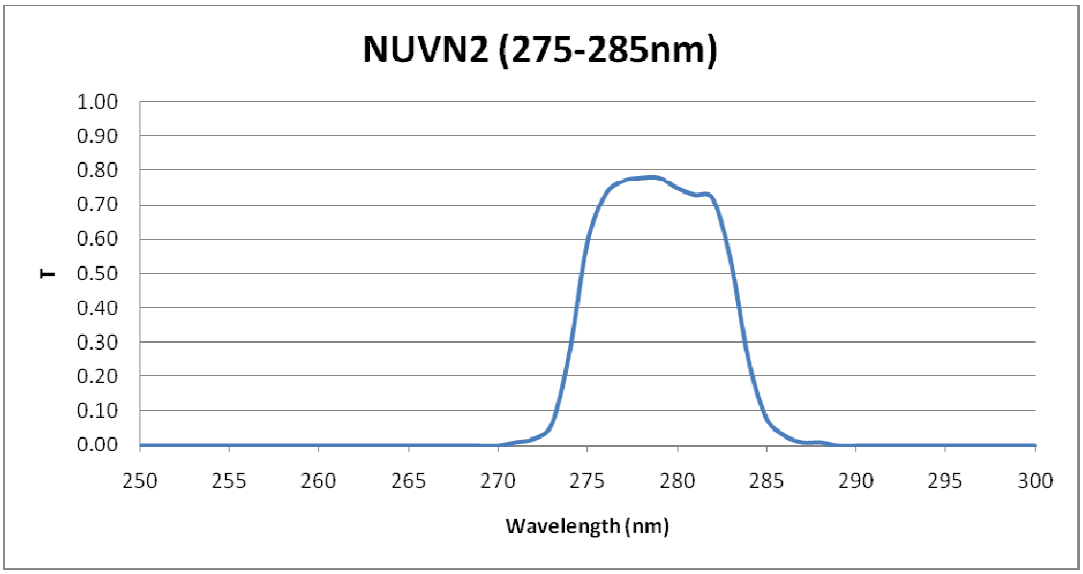


*Fig. 2.6 Spectral transmission of NUVN2 filter measured in MGKML.*

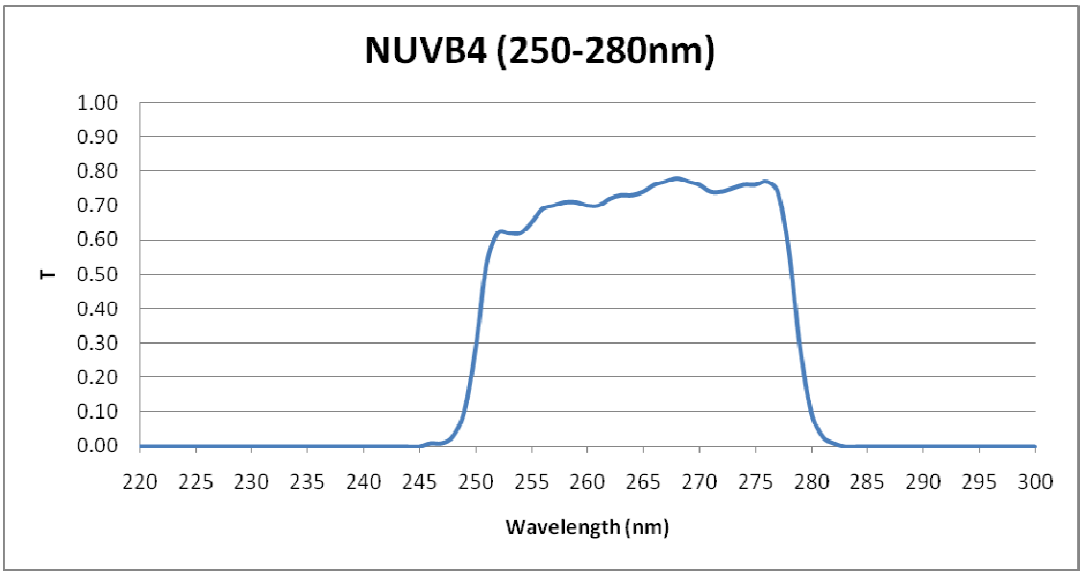


*Fig. 2.7 Spectral transmission of NUVN2 filter measured in MGKML.*

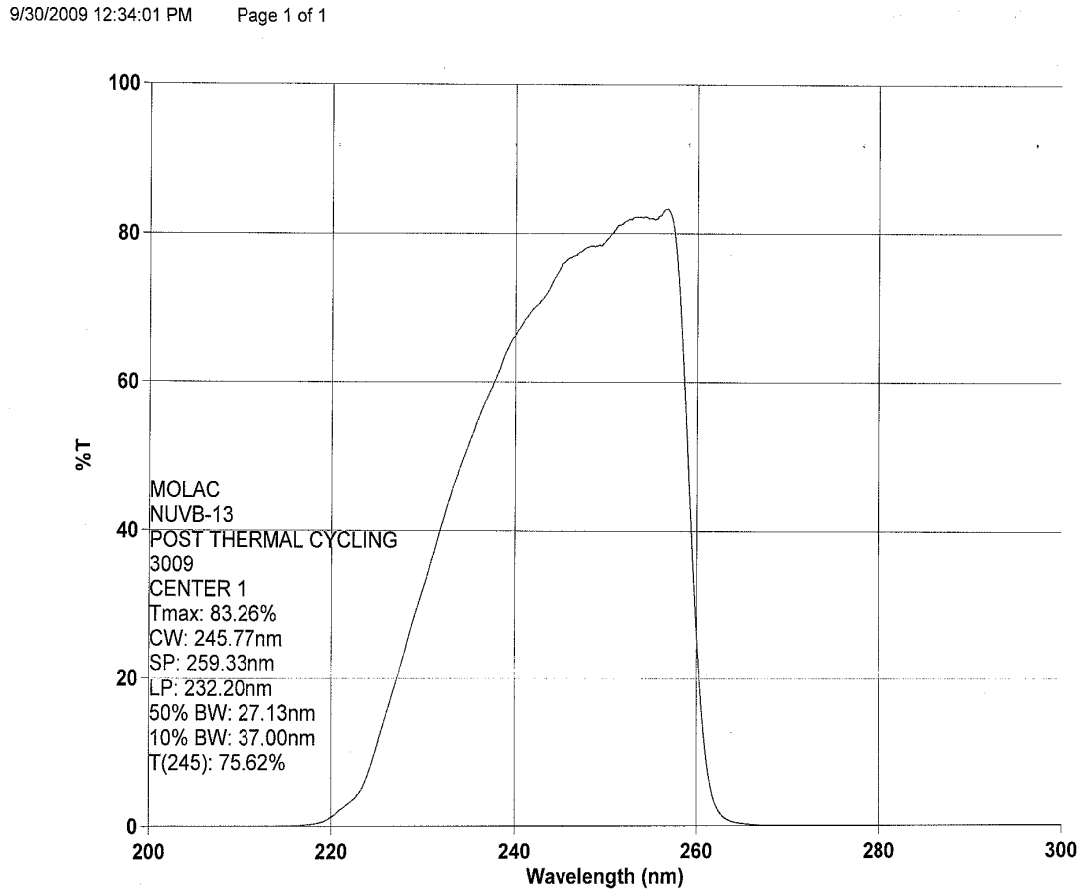


Fig *2.8: Spectral transmission of NUVB-13 filter obtained from supplier*

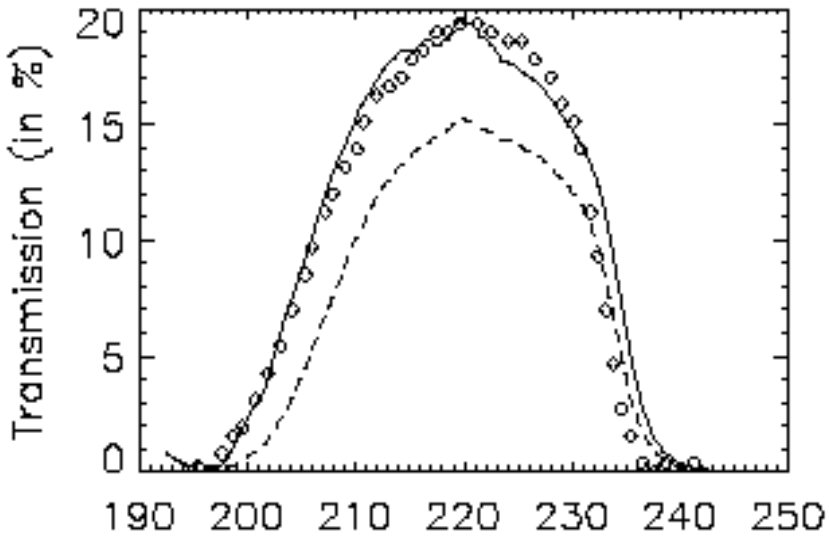


*Fig. 2.9 Transmission curve for NUVB15 filter measured at LEOS Laboratory. Solid line: Vendors curve at the centre of the filter. Data Points (diamond): Measurements at the edges. Dashed line: Measurements at the centre. In these measurements wavelengths are shifted by +2.5nm to match curve from the vendor .*

**Table 2.3 VIS filter specification**

| Slot.No. | Filter Type | Filter Thickness mm | Pass Band Nm |
|---|---|---|---|
| 0 | BLOCK | --- | |
| 1. | VIS 3 | 3.00 | 400 – 530 |
| 2. | VIS 2 | 3.00 | 370 – 410 |
| 3. | VIS 1 | 3.00 | 325 – 365 |
| 4. | Neutral Density Filter | 3.00 | > 380 |
| 5. | BK7 - Window | 3.00 | > 320 |

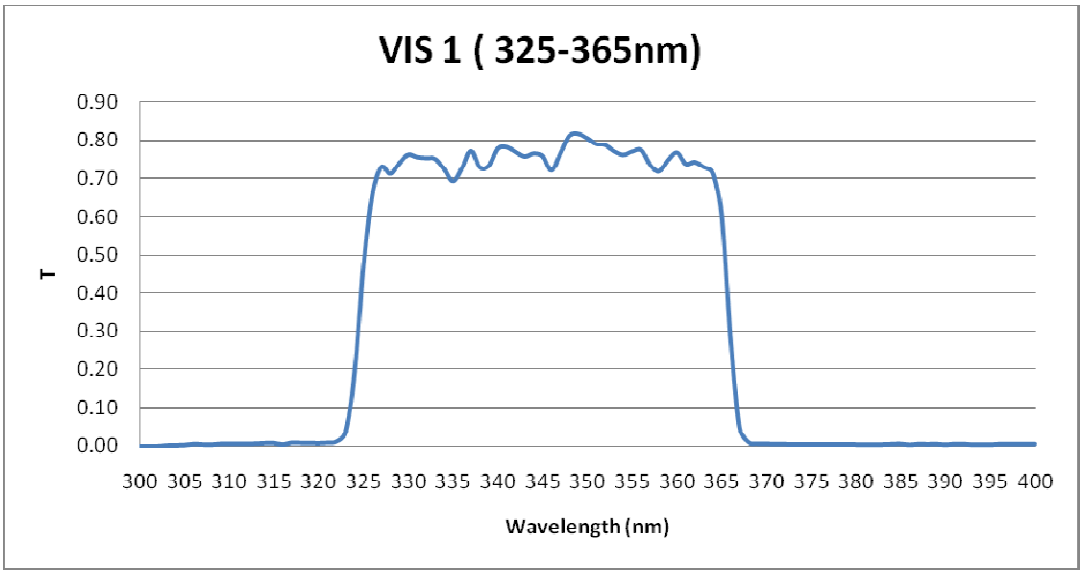

Fig2.10: Spectral transmission of VIS-1 filter measured in MGKML.

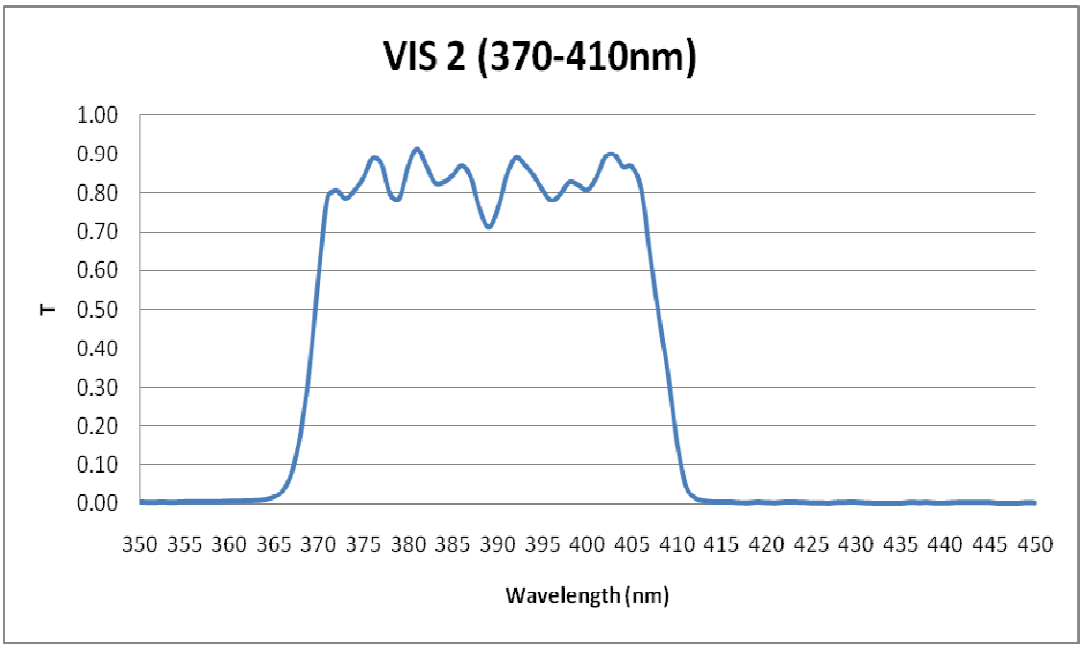


Fig. 2.11: Spectral transmission of VIS-2 filter measured in MGKML.

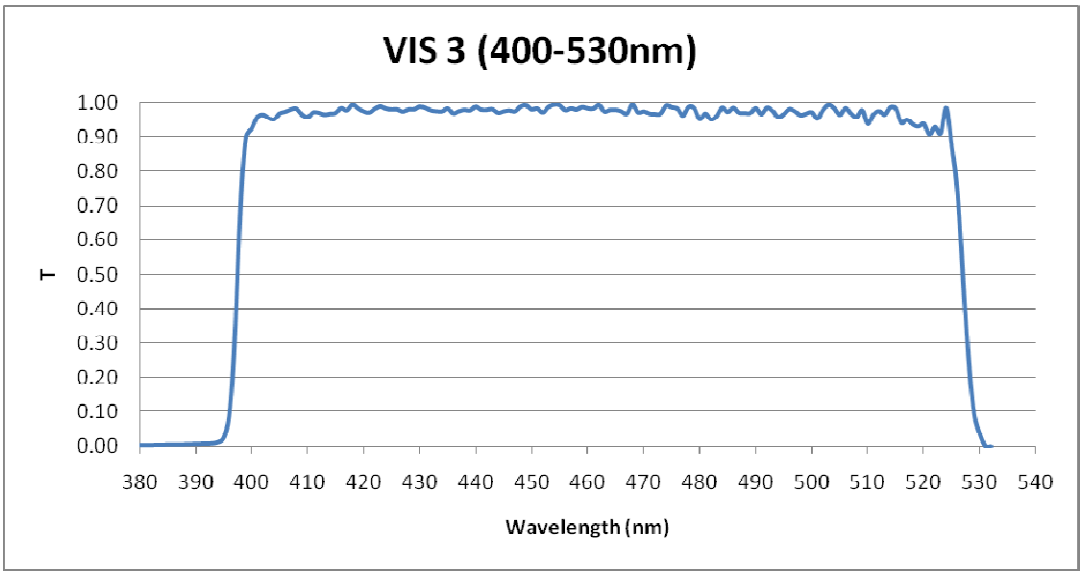


Fig2.12: Spectral transmission of VIS-3 filter measured in MGKML.

## Data Sheet

SCHOTT

**NG4**

| Density | |
|---|---|
| ρ [g/cm³] | 2.43 |

| Reflection factor | |
|---|---|
| $P_d$ | 0.92 |

| Bubble content | |
|---|---|
| Bubble class | 2 |

| Reference thickness | |
|---|---|
| d [mm] | 1 |

| Chemical resistance | |
|---|---|
| FR class | 1 |
| SR class | 2.2 |
| AR class | 1.0 |

| Spectral values guaranteed | | | |
|---|---|---|---|
| τi (405 nm) | = | 0.27 | ± 0.03 |
| τi (546 nm) | = | 0.31 | ± 0.03 |
| τi (694 nm) | = | 0.39 | ± 0.04 |

| Transformation temperature | |
|---|---|
| Tg [°C] | 483 |

| Thermal expansion | |
|---|---|
| $\alpha_{300\text{-}70°C}$ [$10^{-6}$/K] | 6.7 |
| $\alpha_{20/300°C}$ [$10^{-6}$/K] | 7.2 |
| $\alpha_{20/200°C}$ [$10^{-6}$/K] | |

| Refractive index n | | |
|---|---|---|
| λ [nm] | Element | n |
| 587.6 | He | 1.51 |

| Temperature coefficient | |
|---|---|
| $T_k$ [nm/°C] | |

| Notes |
|---|
| Ionically colored glass |
| Neutral density filter |
| All data without tolerances are to be understood to be reference values. Guaranteed values are only those values listed in the section "Spectral values guaranteed". |

**Colorimetric evaluation**

| Illuminant | A ( Planck T = 2856 K ) | | |
|---|---|---|---|
| d [mm] | 1 | 2 | 3 |
| x | | | |
| y | | | |
| Y | | | |
| $\lambda_d$ [nm] | | | |
| $P_e$ | | | |

| Illuminant | Planck T = 3200 K | | |
|---|---|---|---|
| d [mm] | 1 | 2 | 3 |
| x | | | |
| y | | | |
| Y | | | |
| $\lambda_d$ [nm] | | | |
| $P_e$ | | | |

| Illuminant | D65 ( $T_c$ = 6504 K ) | | |
|---|---|---|---|
| d [mm] | 1 | 2 | 3 |
| x | | | |
| y | | | |
| Y | | | |
| $\lambda_d$ [nm] | | | |
| $P_e$ | | | |

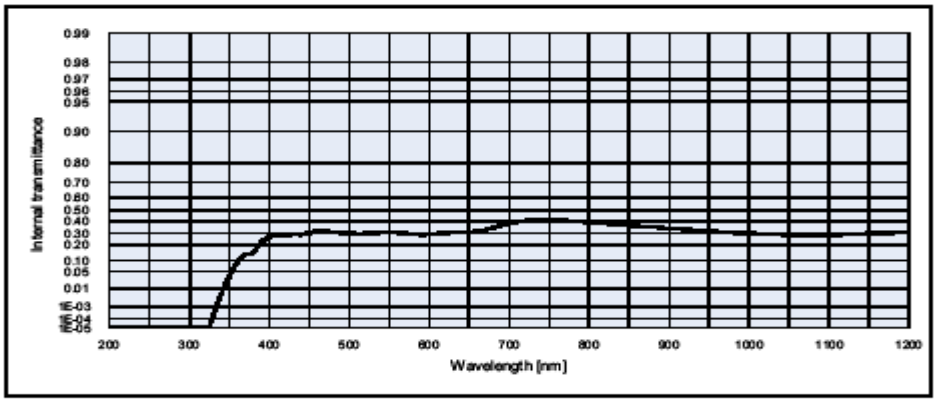


STATUS 2008

Page 1/2

*Fig. 2.13 Internal transmission of VIS ND filter (Schott NG4) given by the vendor for 1 mm thickness. The actual thickness used is 3 mm and the net transmission is ~0.025at 450nm.*

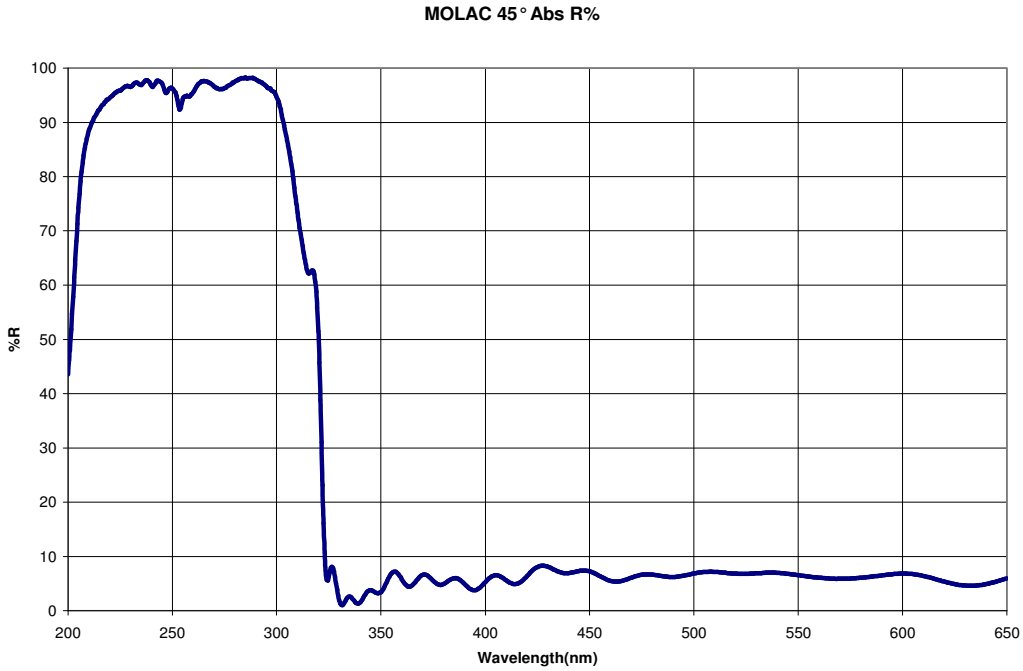


*Fig. 2.14: Reflection efficiency of Beam splitter obtained from supplier.*

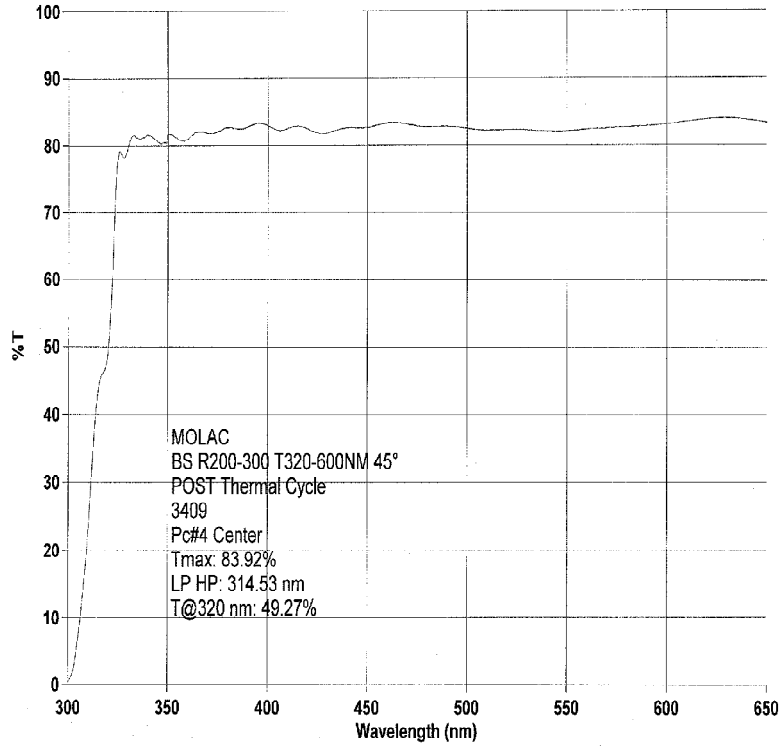


*Fig. 2.15: Transmission efficiency of Beam splitter obtained from supplier*

## Gratings

The gratings, with 400 lines/mm, are ruled on CaF2 substrate of 4.52 mm thickness; the area of ruling is 36 mm X 36 mm (pl. see table 2.4). The dispersion obtained on the detector plane is 1.2 nm/ arcsec & 0.6 nm/arcsec in the first and second orders respectively at 136 nm, The transmission of the gratings is shown in Fig. 2.16 to 2.18. Aberrations are introduced by the grating and the PSF is ~ 2" FWHM.

**Table 2.4 FUV/NUV Grating specification**

| .No | Parameter | FUV Grating | | NUV Grating |
|---|---|---|---|---|
| | Substrate | CaF2 | CaF2 | CaF2 |
| 2 | Grooves (lines/mm) | 400 | 400 | 400 |
| 3 | Diameter (mm) | 52.00 | 51.95 | 51.99 |
| 4 | Thickness (mm) | 4.52 | 4.52 | 4.52 |
| 5 | Ruled area | 36x36mm | 36x36mm | 36x36mm |
| 6 | 1st order peak wavelength (nm) | 190 | 240 | 210* |
| 7 | 2nd order peak wavelength (nm) | 140 | 156 | 154 |
| 8 | Crossover (nm) | 150 | 175 | 166* |

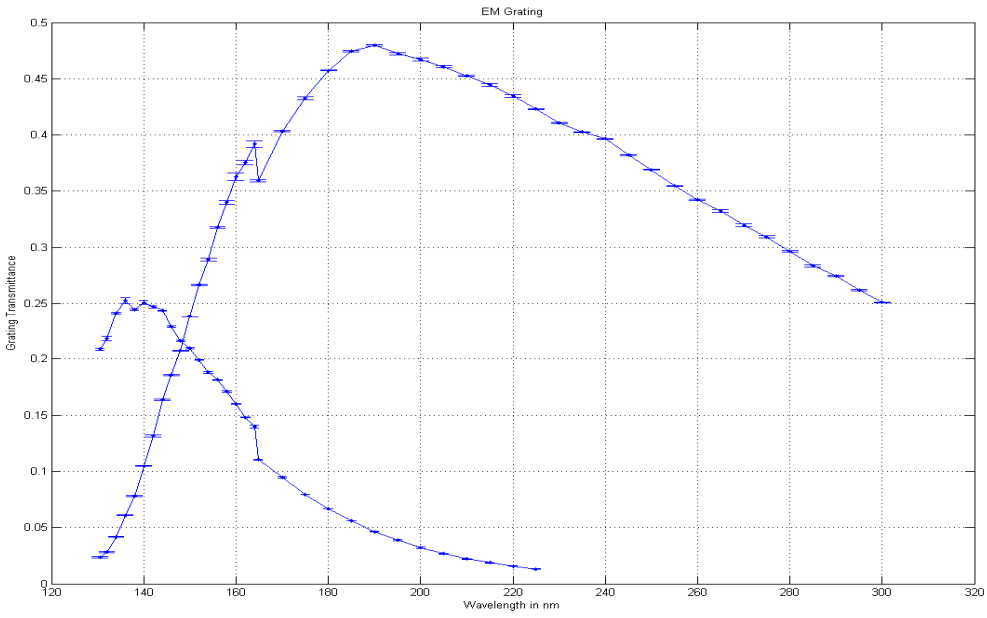

*Fig. 2.16 : Transmission efficiency of FUV grating-1 measured in MGKML.*

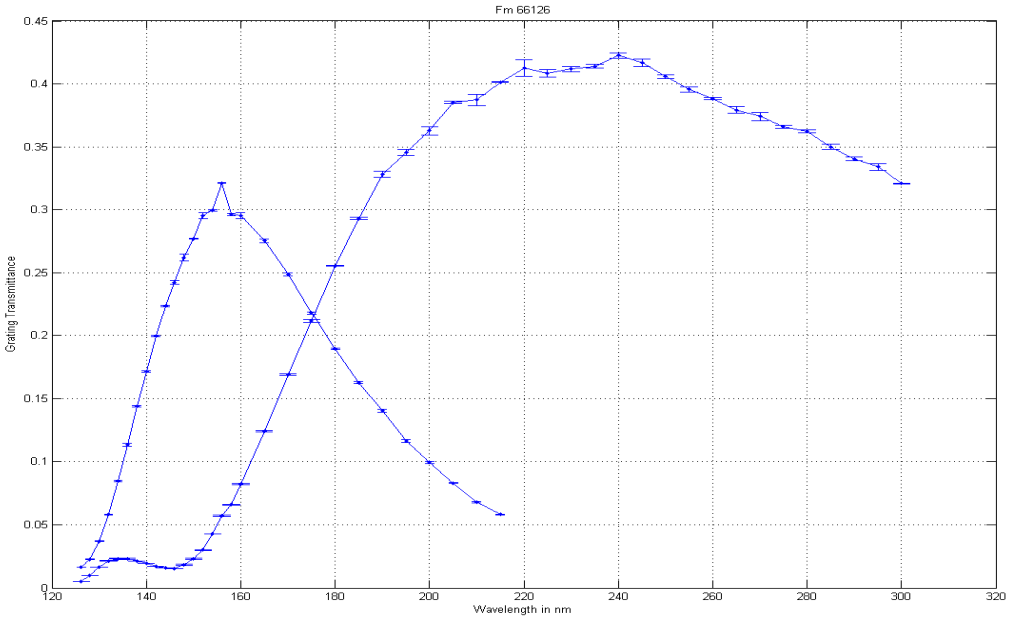


*Fig. 2.17 : Transmission efficiency of FUV grating-2 measured in MGKML.*

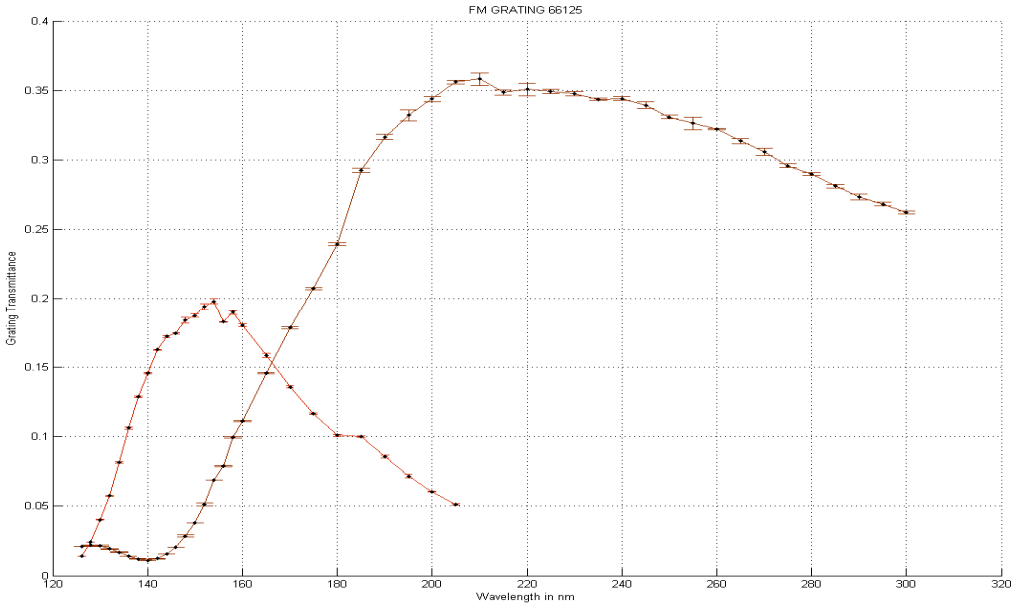


*Fig. 2.18 : Transmission efficiency of NUV grating measured in MGKML.*

## Detectors

All the three detectors are intensified CMOS type with an aperture of ~ 40 mm diameter. Construction of the three detectors and their electronics are identical except for the photo-cathodes and the window. A 5 mm thick $MgF_2$ window is used for the FUV detector, while 5 mm thick silica windows are used for the NUV and the VIS detectors. A sketch of the detector module is shown in Fig. 2.19

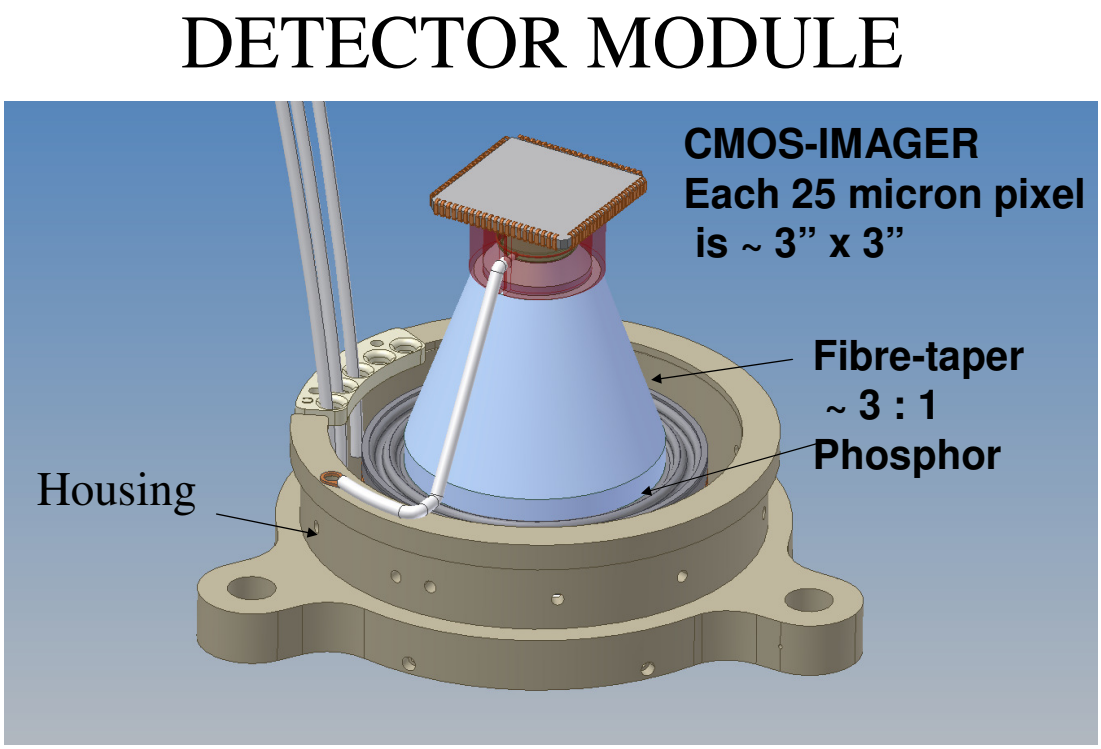


*Fig. 2.19 : Configuration of the detector module is shown. At the bottom, and hidden by the housing, are the 5 mm thick window with photo-cathode deposited on it, and a set of two micro-channels-plates for multiplication ( by up to about a million) of the photo-electron. The electrons are accelerated by ~ 5 kV and strike the phosphor to emit a pulse of photons. The light from phosphor is transmitted to Star-250 (C-MOS Imager) by a fibre-taper. The fibre-taper also matches the 40 mm diameter of the window to size of the C-MOS Imager (512 X 512 pixels of 25 X 25 microns).*

Gap between the photo-cathode and micro-channel-plates is kept small (~ 0.1 mm ) to minimize drift of the photoelectrons. With such small gaps, contribution of the detectors to the PSF is no more than ~ 1" FWHM.

The detectors can either be operated in photon counting mode (with a very high multiplication by the micro-channel-plates) where a list of coordinates of centroids of the detected photons is transmitted, or in integration mode with the multiplication kept at a low value where the raw frame of CMOS is transmitted. Typically the ultraviolet detectors are used in photon counting mode and the visible detector is used in integration mode. Either the entire array of 512 X 512 pixels can be read, at a max. rate of ~29 frames/s, to capture the full field, or a part of the field can be read in "window" mode at rates up to ~600 frames/s, depending on area of the window.

## Thermal Effects

Variations in temperature can effect observations in several ways. Relative thermal expansion shifts focus of the telescope, and surface of the mirrors can get distorted. To minimize these effects, temperature of the telescopes is kept $20^0$ +- $3^0$ C and the structure is made of Invar. The mirrors are mounted on flexible supports made of Invar to minimize thermal stresses. There is no provision for adjustment of the focus in orbit, but the effect of temperature variations on the focus is expected to be small.

Transmission of the filters/gratings and quantum efficiency/gain of the detectors too can change with temperature. The temperature of these elements is kept in range $15^0$ C to $30^0$ C. The thermal effects are not calibrated on ground. As the photon counting mode is not very sensitive to the gain of the detector, this mode is affected less than the integration mode.

Correction for the drift is based on assuming that there is no relative drift between the three channels. Temperature variations can lead to relative drift between the channels, and this can only be modeled with in-orbit data.

## Backgrounds

UVIT background has several sources. These are discussed below.

**a) Dark counts in the detector:**

At 20 degree C the dark photon counts are (as per the test data from Photek, UK , who supplied the CPUs of the detector systems):

| VIS | NUV | FUV |
|---|---|---|
| 1266/s | 50/s | 8/s |

**b) Bright limb of earth**

At angles less than 45 from the axis, bright earth can give background which is in excess of the Zodiacal light.

**c) Zodiacal light**

Zodiacal light is ~ mag 22 per sq arcsec in the V band. This corresponds to ~ 5 $x10^{-18}$ erg/(s A $cm^2$ $arcsec^2$) or ~ 0.08 detected photons per second per sq arcsec for an effective area of 50 sq cm for a band 5500 A to 6500 A.

This background falls very slowly between 6000 A and 3000 A and it falls very fast at the shorter wavelengths. The photon flux per A is less by ~ 6 (300) at 3000 A (2000 A) as compared to that at 6000 A.

**d) Geocorona**

Geocoronal lines are excited by solar radiations and vary in intensity by large factors. Typical counts of detected photons in the detectors, without filter, are listed below:

| Geocoronal Line | Counts per second | | | |
|---|---|---|---|---|
| | FUV Detector (Effective Area 15 Sq cm) | | NUV Detector (Effective Area 50 Sq cm) | |
| | Night | Day | Night | Day |
| 1216 A Ly ά | 129000 | 1290000 | | |
| 1304 A OI | 860 | 129000 | | |
| 1356 A OI | 64 | 12900 | | |
| 2471 A OII | | | < 170 | < 34000 |

It is clear that due to these lines observations cannot be made during the daytime in FUV channel. Further, the $CaF_2$ filter (the widest band filter in FUV) could have leak of a few percent for Ly ά, and the nighttime counts could be in range ~ 1000/s to 5000/s.

## Photon Counting and Integration Modes

The detectors can operate in two distinct modes:

i) Photon Counting Mode

ii) Integration Mode

In the photon counting mode, a very high multiplication is obtained in the MCPs such that each photo-electron generated in the short exposure (<100 ms) is detected as a light pulse in the CMOS imager, and its centroid is found. Thus, for each frame of exposure a list of centroid-positions is obtained from the detector. The expected spatial resolution in this mode is < 1.8" FWHM.

In the integration mode, multiplication of the MCPs is kept low, and signals in all the pixels of the CMOS detector are obtained. In this mode, many (weak) pulses of light, from many photo-electrons, could fall at the same location; the signal at any location is a measure of how many photo-electrons were detected.

Photon counting mode gives a much better spatial resolution (<1.8" FWHM for FUV and NUV channels) as compared to the integration mode (~ 5" FWHM) . However, if in a single exposure two or more photon events occur within a separation ~< 3 pixels of the CMOS imager (~ < 10"), these are detected as a single event or rejected as unacceptable event (see later discussion on choice of modes).

For imaging full field, minimum exposure time is ~ 34 ms. Therefore, given the background levels, imaging in the VIS channel in photon counting mode would lead to overlapping photon events. Further, the total flux of visible photons is such that in photon counting mode life of the MCPs would be exhausted in about one year. Hence, imaging in the VIS channel is normally done in integration mode.

## Operational Constraints

**Avoidance of ram-angle, Sun, and bright-Earth for safety:**
In order to avoid any damage to coating of the primary mirror, due to atomic oxygen, a minimum angle of $12^0$ is kept between the ram direction and the roll-axis, i.e. axis of UVIT. In order to avoid damage/UV-assisted contamination due to radiation from Sun/bright-Earth, a minimum angle of $45^0$ / $12^0$ is kept between the axis and Sun / bright-Earth at all times even if UVIT is not observing.

**Avoidance of bright objects:**
Every field to be observed is checked for avoidance of very bright objects in a neighborhood of $2^0$ radius; from $2^0$., 1 part in $10^4$ of the FUV flux could be scattered in the field.

**Saturation with bright objects:**
Any bright object which can give a detected photon count rate >1 count pr frame per ~ 10" X 10" would see serious saturation effects. Thus, to observe relatively bright objects in photon-counting mode a high frame rate can be used with partial field of view. (Minimum exposure time for the full field is ~ 34 ms, and it is ~ 2 ms for a field of 6' X 6'.

## Choices in Photon Counting Mode and Integration Mode

The nominal mode of observations for the ultraviolet channels is photon counting. Due to its large background, nominal mode of observations in the visible channel is integration mode with a low gain of MCP. To observe bright sources in the ultraviolet, either a high frame rate with a reduced (windowed) field can be used or the integration mode can be used. (As mentioned earlier, the spatial resolution in the integration mode is ~ 5" as compared to < 1.8" in the photon counting mode.)

In the photon counting mode a set of choices are available, in the hardware of the detector system, for selecting: a) thresholds for signals, in the pixels of Star250, to define a genuine photon event, and thus reject noise; a large threshold would reduce effective quantum efficiency, while a small threshold would bring in more noise-events, b) choice of centroiding algorithm for the events from a 3 square/5 square/3 cross windows. In addition, during the ground processing, a threshold can be set for rejecting bright pixels at the corners of the events to eliminate close pairs of photon events – this is required to minimize errors in determination of position of the centroid.

In the integration mode, the hardware allows selection of the gain of MCP by control of the high voltage. Thus, for a very bright source a very low gain can be selected to avoid saturation of the pixels of Star250.

## Observing in Partial Fields

For the full field (~ 28' circle), the maximum double frame rate is ~ 29/s. For those sources which have an intensity > ~ 5 photons/s/(10" X 10"), many frames would have close double photon events at this frame rate. In order to avoid double photon events for such sources a higher frame rate can be obtained by selecting a partial field for observations: the field is selected in units of pixels of Star250. The maximum frame rate is roughly in inverse proportion to area of the field. Thus, given the full field as 512 X 512 pixels, a rate of >600 frames/s is obtained for a field 100 X 100 pixels.

Choice is provided for the following sizes of partial fields, centered on the axis:

1. 100 X 100
2. 150 X 150
3. 200 X 200
4. 250 X 250
5. 300 X 300
6. 350 X 350
7. 512 X 512

In Photon Counting, frame rate is fixed at

1. ~ 640/s for 100X 100
2. ~ 300/s for 150 X 150
3. ~ 180/s for 200 X 200
4. ~ 115 /s for 250 X 250
5. ~ 82/s for 300 X 300
6. ~ 61/s for 350 X 350
7. ~29/s for 512 X 512.

If Integration is selected, exposure time per frame can be selected as per the following:

1. For 100 X 100: in range 0.02 s to 0.30 s, steps of **0.02s**
2. For 150 X 150: in range 0.05 s to 0.45 s, steps of **0.02s**
3. For 200 X 200: in range 0.08 s to 0.65 s, steps of **0.02s**
4. For 250 X 250: in range 0.12 s to 0.80 s, steps of **0.05s**
5. For 300 X 300: in range 0.17 s to 0.95 s, steps of **0.05s**
6. For 350 X 350: in range 0.25 s to 1.10 s, steps of **0.05s**
7. For 512X 512: in range 0.50 s to 1.70 s , steps of 0.1s

Please note that the design allows for selection of partial field of any size and at any position of the full field. However, for simplifications of the operations only some choices of square shaped partial fields, around the centre, are given. An off-centre partial field would call for a certain orientation of the field in addition to correct pointing of the axis, while safety of UVIT require that the field be oriented such that the sun is behind the doors.

## Timing Observations

While the main focus of UVIT is not for timing observations, it is possible to record absolute time of each photon event, along with its position, with an accuracy < 5 ms. For such observations, the analysis on ground would generate a time series of all the detected photons along with their positions on the sky.

## Observation Sequence

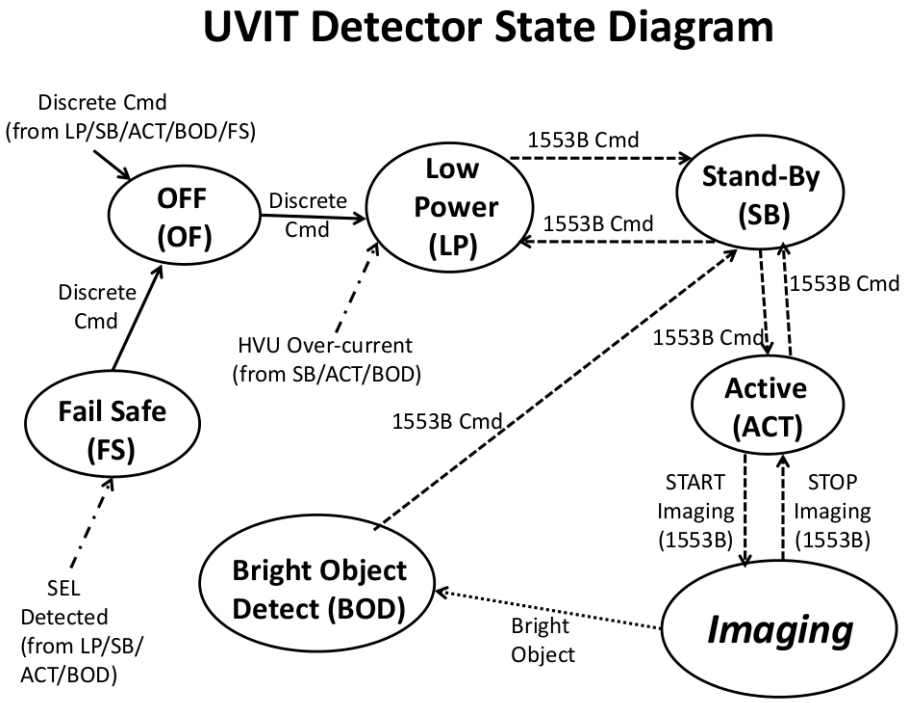


*Fig. 2.21 : State diagram for UVIT*

## Modes of operation of UVIT

### Description of Filter-Detector systems:

A brief description of the UVIT's Detector-Filter system will help comprehend the details of their OPERATION, which is somewhat complex. It will also help clarify the various acronyms used in the text.

The UVIT Filter system (for each of the 3 channels) consists of two distinct physical sub-units : Filter-Wheel-Motor Assembly (FWMA) & Filter-Wheel Drive Electronics (FWDE). The FWMA is located between the back of the primary mirror of the telescope and the Detector system. The FWDE is located on the spacecraft deck (inside the cuboid structure). Electrical signals run via ~ 4.5-m long cables between the FWDE & FWMA via a patch-board located near the focal volume of the 2 telescopes. All 3 FWDE units are housed inside the same mechanical enclosure / box.

The Detector assembly (for each of the 3 channels) consisting of the intensifier tube, fiber-optic-taper, CMOS image sensor and its fan-out board, electrical connectors & HV cables, is termed as 'Camera Proximity Unit' (CPU). The CPU is located at the focal plane of the respective channel (at the back of the telescopes; behind the primary). The High Voltage Unit (HVU) for the corresponding channel which generates the 3 voltages (V_PC, V_MCP & V_A), is located near CPU itself minimizing the lengths of the HV cables. The HV cables are an integral part of the CPU & connect to the HV connectors on the body of the HVU. The drive electronics for the

CMOS sensor as well as the signal processing (including centroiding) is located in a separate unit called 'Read-out Electronic Assembly' (REA) located on the spacecraft deck (similar to FWDE). All 3 REA units for the 3 channels are housed inside a single mechanical enclosure / box, called the Electronics Unit (EU). The electrical cables between REA & CPU are through long cables via the patch-board (see above). Similarly REA & HVU are electrically connected through similar long cables via the patch-board. It is important to note that while all commands for Filter system (FWDE) are through conventional dedicated conductors between spacecraft system (Bus Management Unit, BMU) and the FWDE, carrying relevant electrical signals (for Pulse or Data commands), the control of various selectable parameters of the Detector & related read-out Electronics system as implemented within each REA, is programmed via the serial (1553B) communication link with the spacecraft sub-system BMU.

While all the science data from the Detector system flow through the spacecraft's Data Handling Unit (DHU), the status of the Filter wheel are available exclusively through the Low Bit-rate Telemetry (LBT).

### Modes of the Detector :

Each of the 3 Detector sub-systems (corresponding to the 3 wavelength channels) are identical in regard to the 'Modes' in which they can be at any given time. The modes are like 'states' and they are named as :

a) Off
b) Low Power
c) Standby
d) Active
e) Bright Object Detected
f) Fail Safe

In 'Off' mode, all three units REA, HVU & the CPU are in powered off state. Only a discrete pulse command can take the detectors sub-system from 'Off' state to 'Low Power' state.

In 'Low Power' state, the REA is powered but the HVU and the CPU are still off, and 1553B communication line is now operational (ready to accept commands & respond to telemetry requests from the BMU).

Using a 'change-state' command via 1553B link, the detector can be taken from the 'Low Power' mode to 'Standby' mode and vice-versa. In this 'Standby' mode, in addition to the REA, the HVU and the CPU are also powered on (however, all the three control voltages of the HVU, viz., for Photo-Cathode, Micro-Channel-Plate & Anode are Low/zero).

In order to attain full functionality (of imaging), the detector system must be taken from 'Standby' mode to 'Active' mode via a 1553B command. Once in 'Active' mode, issuance of 'Star Imaging' with all the imaging parameters, initiates ramping up of the HVU & imaging as per programmed parameters. The science data stream now starts feeding the DHU sub-system. The imaging can be stopped by issuing a 'Stop Imaging' command (without leaving the 'Active' mode, meaning that we can re-start imaging with say, some different imaging parameters) or directly making a state-change to 'Standby'. All imaging is carried out in 'Active' mode only. Imaging parameters can be loaded only by the 'Star Imaging' command.

From the above, it should be clear that only certain sequences of changes of state of the detector system are meaningful (as evident from the state-diagram - Fig. 2.21 & Table 1). On receipt of any command implying

departure from the allowed sequences, the command is ignored - and a suitable error flag raised for follow up safety actions by the BMU.

Table 2.5: State table of the detector system for exception cases

| UVITDS State Table for Exception Cases | | | |
|---|---|---|---|
| State | Can be Driven to "OFF by a Discrete Command | Can be Driven to "Fail Safe" by an SEL detect | Can transition to "Low Power" by an HVU Overcurrent Detection |
| Off | Not Applicable | Not Applicable | Not Applicable |
| Low Power | Yes | Yes | Not Applicable |
| Standby | Yes | Yes | Yes |
| Active | Yes | Yes | Yes |
| Bright Object Detected | Yes | Yes | Yes |
| Fail Safe | Yes | Not Applicable | No |

## Emergencies

### Emergencies related to the Detectors

Recovery from any of the emergencies described here, involve action from ground station (i.e. there is no auto-recovery based on onboard logic).

1. While imaging, a Bright Object Detected (BOD) flag is generated in case certain conditions (above selectable thresholds) are encountered. These thresholds are: (i) intensity level (event height), (ii) size (event length in pixels along one axis) & (iii) persistence of this condition (over successive number of frames; to avoid 'false alarm'). The BOD flag/alarm is a 1bit hardware logic signal over a dedicated line (per UVIT channel), which is periodically monitored by the spacecraft system BMU. On receipt of BOD alarm, the BMU suspends all previously planned operations of UVIT & takes necessary action (issuance of commands) to take all 3 channels of UVIT into a 'safe' state. This includes: parking the filter wheels in 'light Block' condition, taking each of the 3 REAs to finally 'Low Power' mode via intermediate steps.

2. Another form of 'alarm'/emergency, possibly related to bright objects in the field is: Over Current (OC) of any of the High Voltage supplies. In this case, the channel detecting OC itself goes in to 'Low Power' mode & signals a flag to the BMU in the LBT telemetery (one bit in the1553B frame). BMU on receipt of the OC flag, will take action sequence leading to Power Off for all 3 channels (the sequence includes : suspension of all previously planned operations of UVIT; safe parking of filter wheels; all relevant intermediate steps to arrive at the Power Off' condition).

3. Yet another form of 'alarm'/emergency (possibly related to high charged particle background), occurs when the onboard electronics detects a Single Event Latchup (SEL) situation. The affected channel itself moves to a FAILSAFE state (with its secondary power system internally disabled), while the BMU detects this state from its periodic monitoring of the supply (+3.3 V) line. The BMU then takes all 3 channels to Power Off state following the usual sequence of intermediate steps.

4. An additional type of emergency occurs, when the 1553B command acknowledgment frame received from REA, has any one (or more) of the 'errorflagbits' in 'set' state. This implies at least one of the programmed selectable imaging parameters is 'wrong' (incompatible with current state) & hence that command frame has been ignored by REA. This means an error has occurred possibly in the mission planning software & hence the UVIT operations need to be shutdown till the cause is understood (just like any of the emergencies). On encountering this kind of emergency, the BMU takes all 3 channels to 'Low Power' state via usual sequence of intermediate steps.

5. Housekeeping values out of acceptable range : when any of the few selected temperatures & power supply voltages is found to be out of its acceptable operating range, this emergency is triggered. Although this out-of-range condition may have been detected in one channel, all the 3 detector systems of all the 3 channels are taken to 'Low Power' state via usual sequence of intermediate steps.

**Emergencies related to the Filter wheels:**

In case the filter wheel status shows abnormality (e.g. being in 'acquire'/slewing state for a time much longer than normal), BMU takes all 3 channels of UVIT to 'Low Power' state via usual sequence of intermediate steps (including parking the filters to 'light block' configuration).

## Typical Observing Sequence

From the safety point of view of the UVIT payload, during all slews of the spacecraft, the Filter wheel is parked at the SAFE ('lightblock') configuration. Even when a UVIT channel is not being used for any observations, that channel is normally left in 'Standby' mode [this is to minimize the number of hard OnOff cycles over the mission life].

A typical observation sequence (for exposure with one filter) consists of the following steps [starting with filter at 'SAFE' parked configuration and Detector in 'StandBy' state, as stated above; assuming imaging in Photon Counting mode] :

The spacecraft (BMU) verifies that:
(A) the UVIT is presently in a 'SAA Safe ZONE'
(B) selected UVIT health parameters (temperatures & supply voltage monitors) are within allowed range
(C) the spacecraft attitude (AOCS) is at the target position

(1) Change state of the REA from 'Standby' to 'Active' mode;

(2) Collect DARK1 (for Star250 C-MOS imager) Image frames in Integration Mode, and High Voltages 'Low' [this involves 'Start Imaging', data collection & 'Stop Imaging' sequence of operations];

(3) Move from 'Active' state to 'StandBy';

(4) Prepare the Filter Wheel for motion by issuing 'Safe Reset';

(5) Move the Filter Wheel by issuing 'Target angle' (Filter selection for this observation);

(6) 'Kill time' for sufficient duration so that the Filter would have reached the destination;

(7) Disable Filter Wheel Motor (coils de-energized) to save power;

(8) Move from 'StandBy' to 'Active' state;

(9) Begin Imaging by issuing 'Start Imaging' command, which includes all imaging parameters;

(10)'Kill time' appropriate for the duration of the current exposure;

(11)Issue the 'Stop Imaging' command;

(12)Move from 'Active' state to 'StandBy';

(13)Park the Filter Wheel in SAFE ('lightBlock') configuration;

(14)'Kill time' for sufficient duration so that the Filter would have reached the destination;

(15)Disable Filter Wheel Motor (coils de-energized) to save power;

(16)Move from 'StandBy' to 'Active' state;

(17)Collect DARK2 (for Star250 C-MOS imager) Image frames in Integration Mode, and High Voltages 'Low' [this involves 'Start Imaging', data collection & 'Stop Imaging' sequence of operations];

(18)Move from 'Active' state to 'StandBy';

[Now the channel is back to its starting position; Detector (REA) in 'StandBy' & Filter wheel at 'SAFE'.]

### Observations in Daytime

The backgrounds in daytime, due to geocorona and due to scatterings in ASTROSAT, are very large. However, in specific cases observations during the daytime are possible, with reduced sensitivity, as long as the sun is > 45 deg. away from the field and limb of the earth is > 12 deg. away.

### Optimisation for observations of multiple nearby sources in multiple filters

Change of a filter takes ~ 30 s. In addition, before every change of the filter the high voltages on the detector are taken to zero and then ramped up after the new filter is in position, which takes another ~30 s. Thus, observations of nearby multiple sources ( e.g. sources separated by < 10’ observed in a window of (6’ X 6’) can be finished in one filter by changing pointing from one source to the next before changing to the next filter. In case the sources are far from each other, the largest overhead would be time to change pointing and it is best to finish all the observations on one object before moving to the next.

## Quantum Efficiencies

Quantum efficiencies of the detectors have been measured in photon counting mode, with reference to a NIST calibrated photo-diode. These are shown in Fig. 2.22

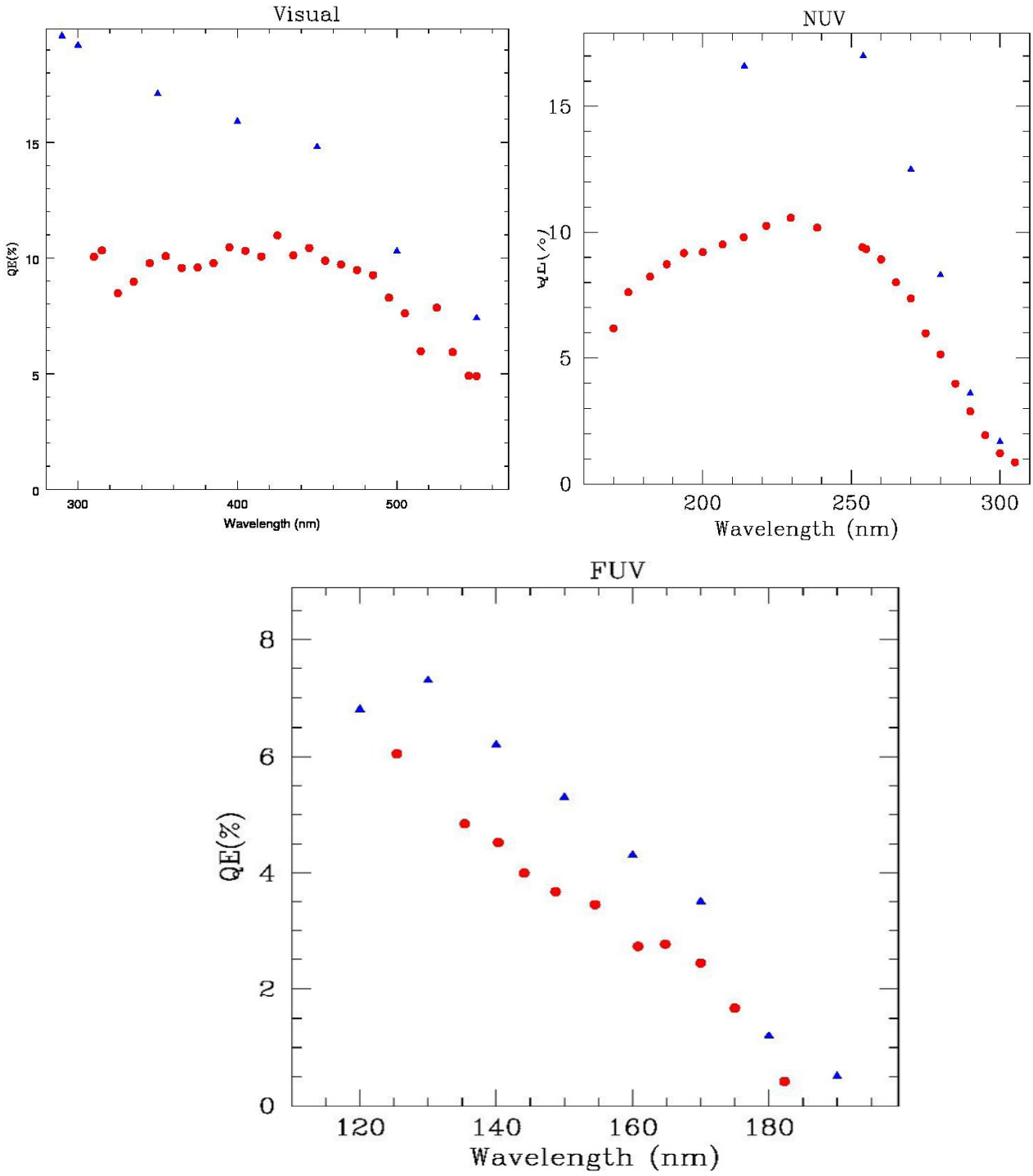


*Fig. 2.22 : QE values for Ph. Counting mode are shown as red circles. The blue diamonds are QE values for the photo-cathodes measured by the vendor.*

## Effective Area

Based on the tests done on the various optical components, the effective areas have been estimated as a function of wavelength for all the filters. These are shown in Fig. 2.23, 2,24, and 2.25.

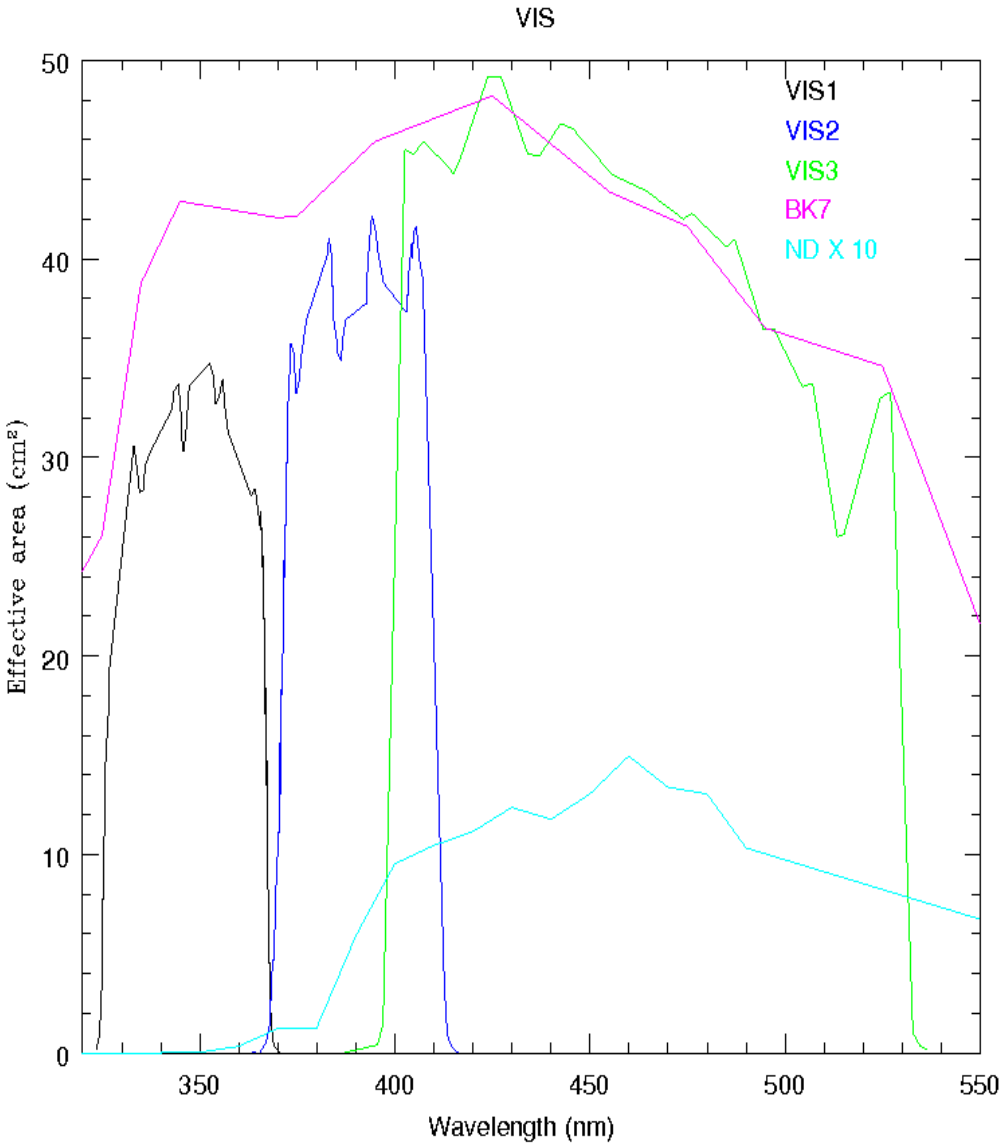


*Fig. 2.23: Estimates of the effective area are shown for the filters of VIS channel.*

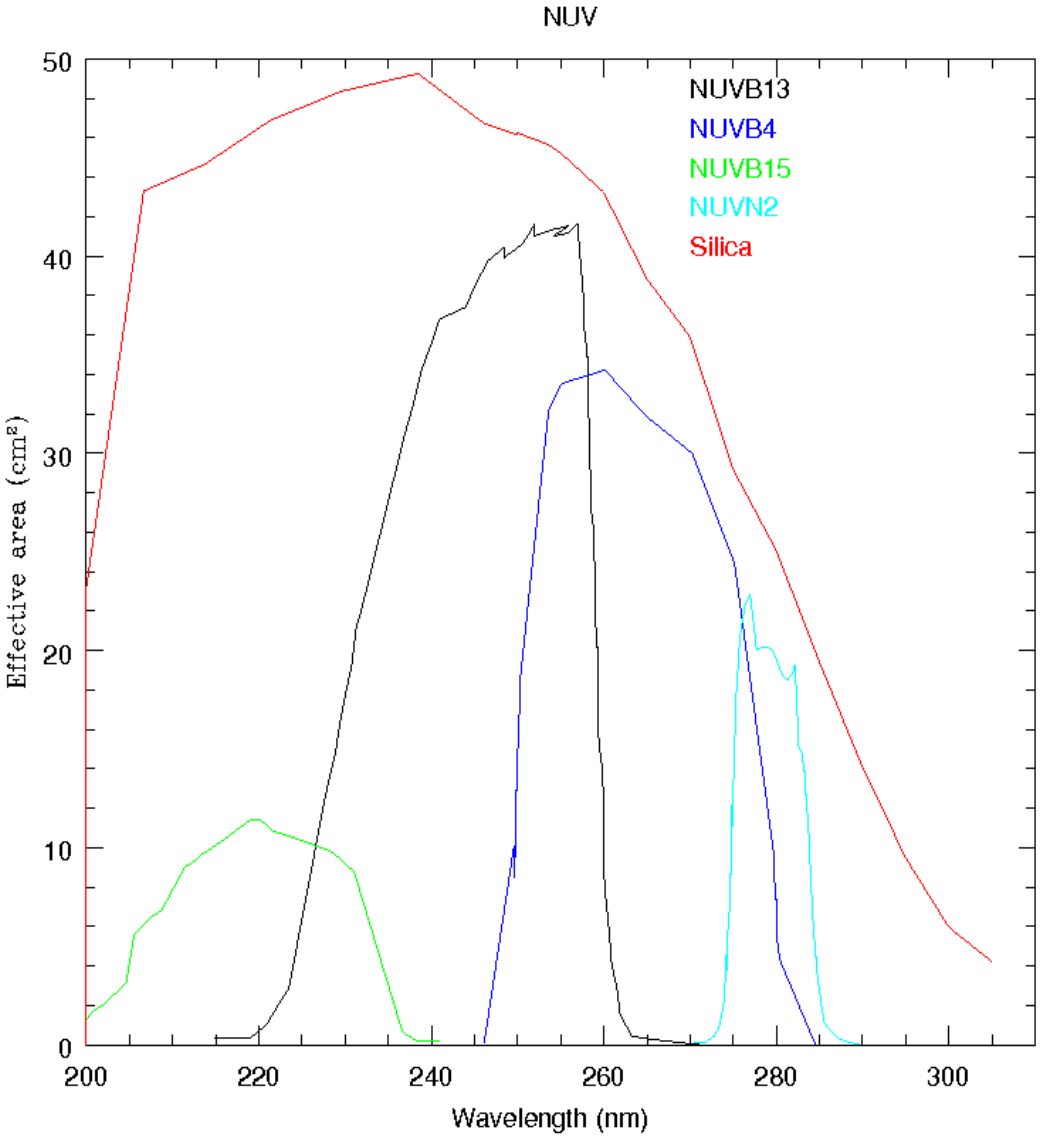


*Fig. 2.24: Estimates of the effective area are shown for the filters of NUV channel.*

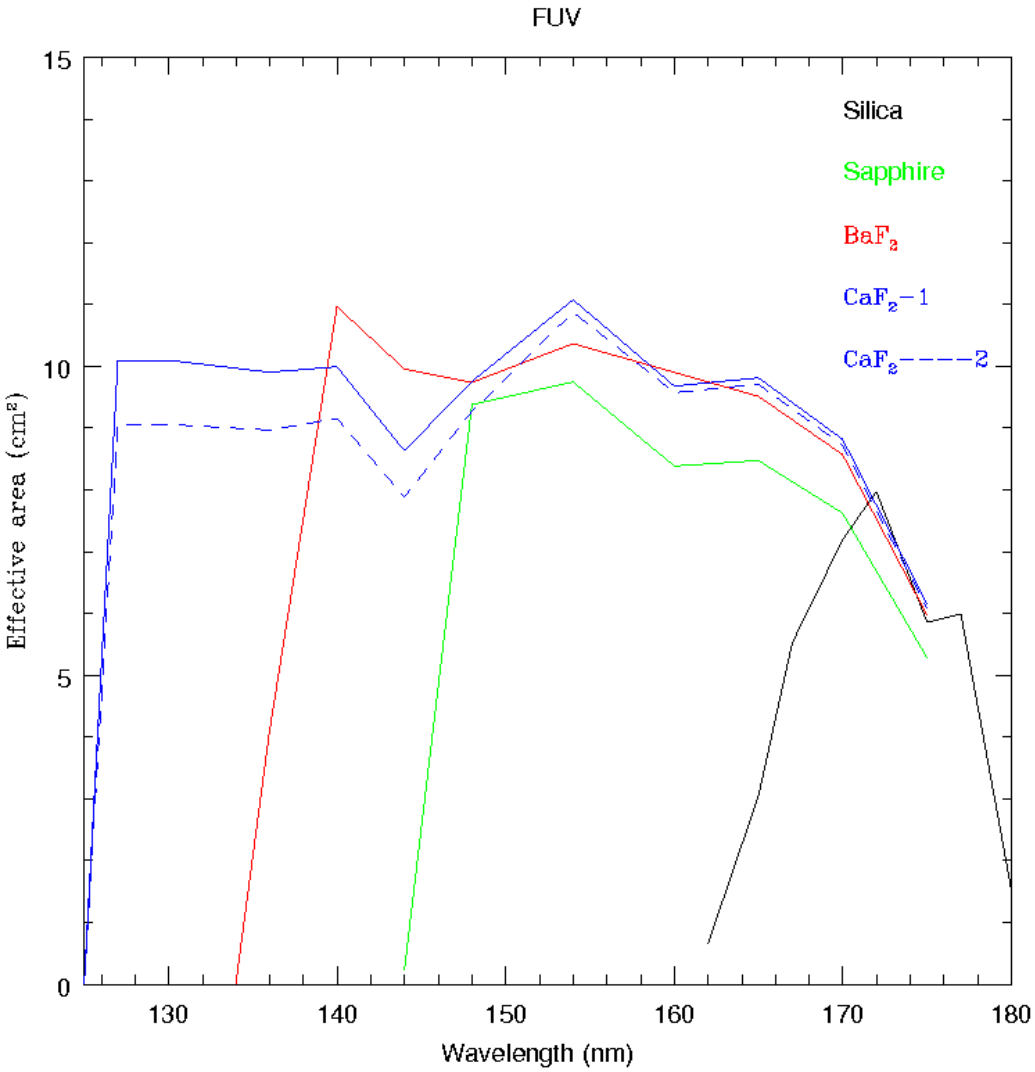


*Fig. 2.25: Estimates of the effective area are shown for the filters of FUV channel. The effective area at 200 nm (250 nm) is estimated as 1.85 (0.1) sq cm. "*

## Calibration details

The calibration of the UVIT instrument is achieved through ground-based as well as in-orbit tests. The individual components of the UVIT instrument are tested and calibrated in the ground. The performance of the integrated system is planned during the performance verification phase after the launch.

### Ground based tests:

**Detectors:**

The CMOS-intensified imagers used in the three UVIT channels are tested at the Canadian facility in the University of Calgary. The tests performed on the detector include tests for sensitivity, response as a function

of wavelength, spatial variation of sensitivity, tests to estimate the centroid of the photons detected, gain as a function of MCP voltage etc., and distortions. These tests were done on both the EM and the FM detectors. The estimated parameters will be integrated with the rest of the parameters

**Filters and gratings:**
The EM and the FM filters are tested and calibrated at MGKM Lab. (CREST, Hosakote facility of IIA).1The parameters estimated are: transmission of each filter as a function of wavelength, spatial variation of transmission, parallelism of the sides, shift in focus due to refraction. The gratings are tested for dispersion and spectral transmission in different orders

**Integration of parameters**
The parameters estimated above are integrated together with the transmission and sensitivity of the mirrors to estimate the overall throughput of the system. This is incorporated in the exposure time calculator developed by the Canadian team. The calculator estimates the expected counts/sec for any object, when one provides its magnitude and the spectral energy distribution (or equivalent). This will be used to estimate the exposure times by the users at the time of proposal submission. The deliverables from the calibration tests will be presented in the form of a tables or plots.

### In orbit calibrations:
This subsection describes the overall goals of the in-orbit calibration and outlines a set of calibration tasks. A calibration task is the configuration, observation and analysis required to calibrate a specific aspect of the instrument. The primary goal of this calibration is to ensure that the scientific quantities obtained from the UVIT instrument conform to the requirements set forth by the instrument document. This also needs to fulfill the requirements set forward by the science projects.

UVIT-in orbit calibration is designed to allow automated processing of UVIT data by the pipeline with the goal of producing a calibrated set of images and spectra which can be used for quantitative data analysis in order to achieve the scientific objectives. The activities listed in this document pertain to four types of calibrations. Photometric calibration will yield a conversion of a measured count rates into a broadband flux for any given filter-detector combination. The spectroscopic calibration consists of estimation of wavelength coverage, wavelength and flux calibrations. Astrometric calibration is the measurement of the relation between a point on the detector based on the image created by the telescopes and the absolute position in the sky. In addition, point sources are used to find PSF of the instrument for short exposures (which are not affected by drift of the S/C) and for long exposures (which are affected by drift of the S/C, and depend on how well the drift is corrected during the processing on ground).

The in-orbit tests are performed during the performance verification (PV) phase of ASTROSAT. The total exposure time required for these is approximately one month. The photometric calibration tasks along with the other calibration will be performed in this time. The in-orbit calibration tasks will be performed during the PV phase and repeated at regular intervals to monitor any drifts in the performance of the system as well as to improve the already estimated parameters. Hence, some of the calibration activities or tasks will be repeated at regular intervals. As per the recommendations of the monitoring team, certain calibration tasks may be included while planning the observing cycles also.

The following table summarises various calibration tasks planned to be taken up during the PV phase and later:

1. Photometric zero-point calibration (FUV, NUV, VISUAL)
2. Secondary photometric calibration (FUV, NUV, VIS)
3. Calibration of the gratings for dispersion and effective area
4. Astrometric positional calibrations
5. Astrometric angular separation estimations
6. Linearity of photometric response and bright star limits
7. PSF estimations
8. Timing calibrations
9. Estimation of background
10.

## Limits on Brightness for Observations with UVIT

1. **Introduction**

UVIT uses intensified imagers which can suffer permanent damage if exposed to excessive flux of photons. Therefore, it is required that observations are only allowed for those fields which have objects below defined levels of brightness in the field and its close neighbourhood. While a detected photon rate of 500/s can be considered as a safe upper-limit for any point source is the field of the detectors, there are two other considerations in defining a practical limit on the rate. Firstly, the hardware has a provision for safety which initiates "BOD-trigger" if an excessively bright object (defined by some parameters) is in the field; BOD-trigger initiates actions which bring all the detectors to OFF condition. Next, there are very few point sources which would give rate > 29/s in the FUV-CPU for the full field and the full band. The recommended limits on rate are based on all these three considerations.

2. **Recommended Limits on Count Rates**

2.1 The field and its neighbourhood

a) The field of view for UVIT is ~ 28' in diameter. However, the pointing error can be up to 3' and there could be some drift during the exposure. Therefore, for avoidance of bright sources we define the field as 40' diameter.
b) Scattered light from sources near edges of the field can reach the detector. For a source 30' away from the axis, ~ 0.5% of light can reach the detector- most of which would fall in one half of the detector. For sources at 60' from the axis, ~ 0.1% of light can reach the detector. *Direct tests with the telescopes show that < 0.5% of the light reaches the detector for sources at 30' and 60' from the centre, and that there are no ghost images in the field. We take the value of 0.5% for defining limits on the brightness.*

2.2 Count Rates in the Field

The following upper limits on count rates are recommended for any point source, or any 1600 sq arcsec part of an extended source, in a field of 40' diameter around the centre: a) for VIS-CPU: 3770/s (in integration mode with an intensification ~ 1/10 of that used for photon-counting), b) for NUV-CPU: 377, and c) for FUV-CPU: 29/s (in integration mode with an intensification ~ 1/10 of that used for photon-counting). (*We note that the intensification in the FUV-CPU is a factor ~ 1.5 lower as compared to the other two CPUs and it*

*requires a higher voltage for the intensifying multi-channel-plates. Given this comparision it is possible that this CPU has smaller life and we want to be more conservative in exposing it.).*

The above limits are to be followed for most of the observations, but in special cases it may be possible to allow exposures to brighter sources with a suitable protocol.

*2.3* Count rates in neighbourhood of the fields

A total rate of 10^5/s over the full face of the detector can be considered safe in photon-counting mode. Therefore, a source with count rate < 2 X 10^7/s can be allowed within 60' (but beyond 20') of the axis for observations with NUV and FUV CPUs. For the VIS-CPU, used in integration mode with a lower gain (by a factor ~10), a count rate of < 10 X (2 X 10^7)/s can be allowed.

Possibility of the ghosts at certain angles cannot be ruled out yet, and in the initial periods of the mission it would be best to keep the limit to a smaller number, e.g. 10^6/s, and look for possible ghosts.

**Sky Backgrounds Information (**these data are reproduced from Chapter 6 of STIS Instrument Handbook for Cycle 21)
>>>>>>>>>>>>>>>>>>>>>>>>>>>>>>>>>>>>>>>>>>>>

---

---

Geocoronal Emission lines (Taken from Table 6.5 of STIS Instrument Handbook for Cycle 21, Ch. 6 )

| | Low (Night?) | High (Day?) |
|---|---|---|
| 1216 | 2 kR | 20 kR |
| 1304 OI | 0.013 kR | 2 kR |
| 1356 OI | 0.001 kR | 0.2 kR |
| 2471 OII | <0.001 kR | < 0.2 kR |

Conversions from R (Rayleighs) to counts are: 4.3 X 15 (eff. Area in sq cm) ph./R/s for FUV detector of UVIT, and 4.3 X 40 (eff. area in sq cm) ph./s/R for NUV detector of UVIT.

---

---

**All the material below is reproduced from STIS Instrument Handbook for Cycle 21, Ch. 6**

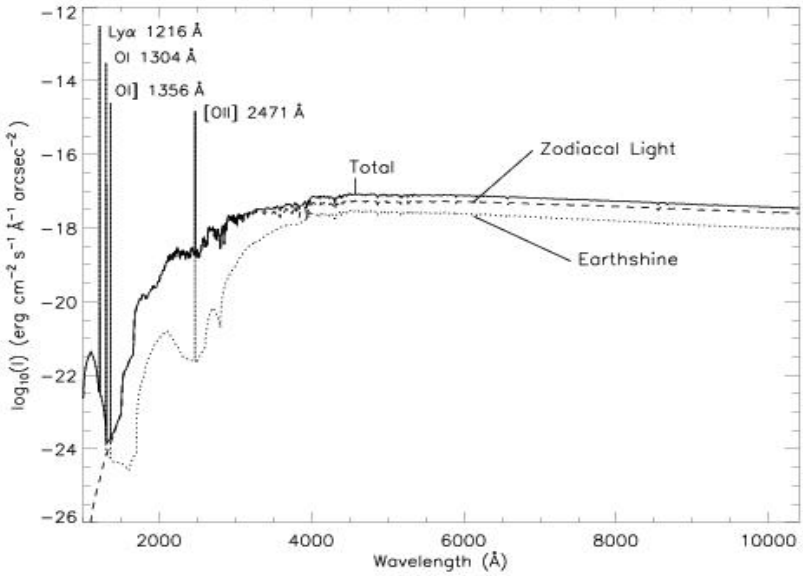


6.5 Detector and Sky Backgrounds



When calculating expected signal-to-noise ratios or exposure times, the background from the sky and the background from the detector must be taken into account.

6.5.1 Detector Backgrounds

Table 6.1 shows the read noise and dark current characteristics of the detectors, taken from Chapter 7.

Table 6.1: Detector Backgrounds

| Background | CCD | NUV-MAMA | FUV-MAMA |
|---|---|---|---|
| Read noise (electrons $pix^{-1}$) | 5.4 (for CCDGAIN=1)<br>7.7 (for CCDGAIN=4)[1] | 0 | 0 |
| Dark current (electrons $sec^{-1}$ $pix^{-1}$) | ~9.0 × 10–3 | ~1.3 × 10–3 | 0.07 - 3.0 × 10–4 |

[1] To convert to counts $sec^{-1}$ $pix^{-1}$ for CCDGAIN=4, divide by 4.039.

6.5.2 Sky Background

The sources of sky background which will affect STIS observations include:

- Earthshine (ES)
- Zodiacal light (ZL)
- Geocoronal emission (GC)

The continuum background in counts sec-1 pixel-1 for *spectroscopic observations* can be computed as:

$$B^{\lambda}_{sky} = \frac{I_{\lambda} \times S^{d}_{\lambda}}{G}$$

where:

- $I_\lambda$ is the surface brightness of the sky background, in erg $sec^{-1}$ $cm^{-2}$ $Å^{-1}$ $arcsec^{-2}$;
- $S_\lambda^d$ is the diffuse-source sensitivity for the grating mode

The background in counts $sec^{-1}$ $pixel^{-1}$ for *imaging observations* can be computed as:

$$B_{sky} = \frac{\int I_\lambda \times S_\lambda^d d\lambda}{G}$$

where:
$I_\lambda$ is the surface brightness of the sky background, in erg sec-1 cm-2 Å-1 arcsec-2;
$S_\lambda^d$ is the diffuse-source sensitivity for the imaging mode;
The integral is over the bandpass.

In Figure 6.1 we plot the "high" sky background intensity as a function of wavelength, identifying the separate components which contribute to the background. The information in this figure is presented in tabular form in Table 6.4. In the Exposure Time Calculators (ETCs) and in this Handbook, the choices for Earthshine of "shadow", "average", and "extremely high" correspond to 0, 50% of, and twice the "high" values in Table 6.4. For the zodiacal sky background, the values in Table 6.4 correspond to a high value of $m_V$ = 22.1 $arcsec^{-2}$ from Table 6.2, while the low and average zodiacal light are scaled to $m_V$ = 23.3 $arcsec^{-2}$ and 22.7 $arcsec^{-2}$, respectively. The strength of the geocoronal (airglow) line emissions are as shown in Table 6.5.

Figure 6.1: High Sky Background Intensity as a Function of Wavelength. .

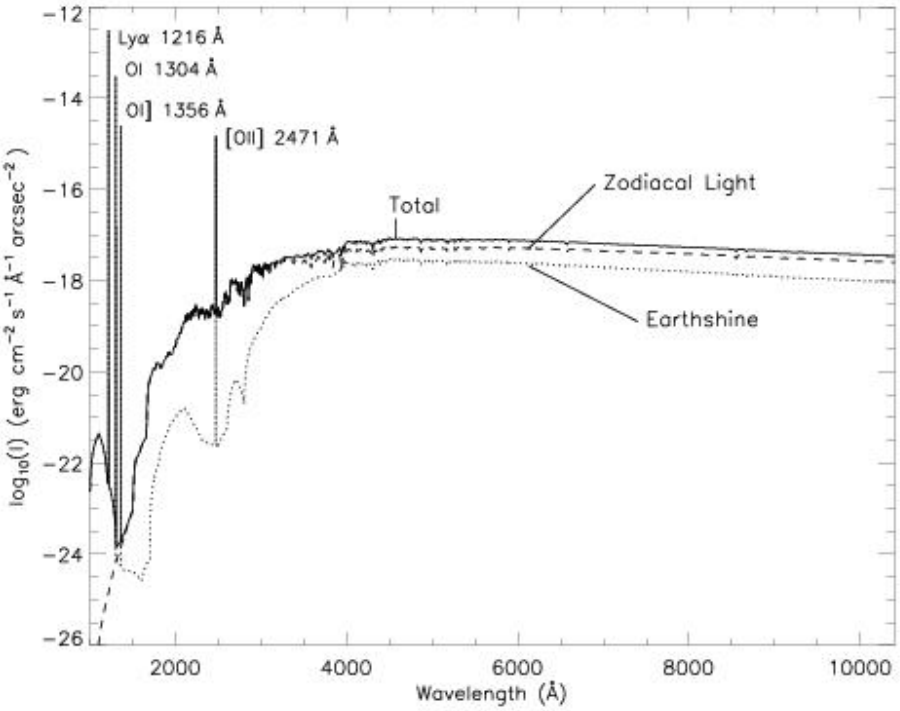


The zodiacal contribution corresponds to $m_v$ = 22.1 $arcsec^{-2}$. The Earthshine is for a target which is 38° from the limb of the sunlit Earth. The upper limit to the [OII] 2471 Å intensity is shown. Use Figure 6.2 to estimate background contributions at other angles. The geocoronal airglow line intensities are in erg $cm^{-2}$ $s^{-1}$ $arcsec^{-2}$.

Background Variations and LOW-SKY

In the ultraviolet, the background contains important contributions from airglow lines. These vary from day to night and as a function of HST orbital position. The airglow lines are an important consideration for imaging mode observations and can be for spectroscopic observations as well. Away from the airglow lines, at wavelengths shortward of ~3000 Å, the background is dominated by zodiacal light and is generally much lower than the intrinsic detector background. The contribution of zodiacal light does not vary dramatically with time and varies by only a factor of about three throughout most of the sky. Table 6.2 gives the variation of the zodiacal background as a function of helio ecliptic latitude and longitude. For a target near ecliptic coordinates of (50,0) or (-50,0), the zodiacal light is relatively bright at mv = 20.9 arcsec$^{-2}$, i.e. about 9 times the polar value of mv = 23.3 arcsec$^{-2}$.

Earthshine, on the other hand, varies strongly depending on the angle between the target and the bright Earth limb. The variation of the Earthshine as a function of limb angle from the sunlit Earth is shown in Figure 6.2. The figure also shows the contribution of the Moon which is typically much smaller, and the full range of the zodiacal contribution. For reference, the limb angle is approximately 24° when the HST is aligned toward its orbit pole (i.e., the center of the CVZ).

Figure 6.2: Background Contributions in V Magnitude arcsec$^{-2}$ from the Moon and the Sunlit Earth as a Function of Angle between the Target and the limb of the Earth or Moon.

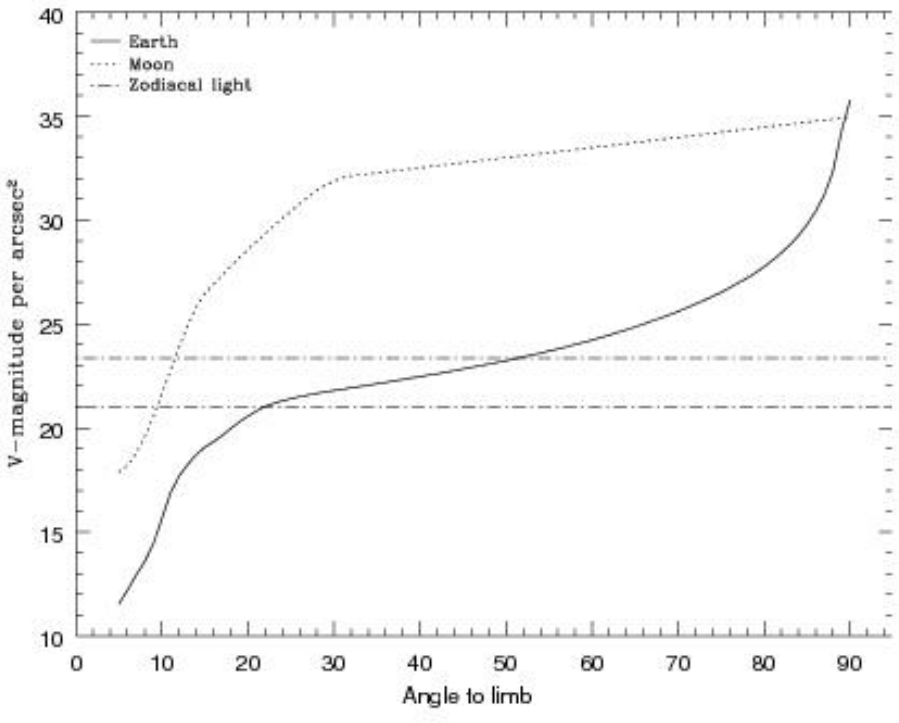


For observations longward of 3500 Å, the Earthshine always dominates the background at small (<22°) limb angles. In fact, the background increases exponentially for limb angles <22°. The background near the bright Earth limb can also vary by a factor of ~2 on time scales as short as two minutes, which suggests that the background from Earthshine also depends upon the reflectivity of the terrain over which HST passes during the course of an exposure. The total background at limb angles greater than the bright-Earth avoidance angle

of 20° appears to show no significant dependence on position within the small HST fields of view. Details of the sky background as it affects STIS are discussed by Shaw et al. (STIS ISR 1998-21) and Giavalisco et al. (WFC3 ISR 2002-12).

Table 6.2: Approximate Zodiacal Sky Background as a Function of Helio ecliptic Latitude and Helio ecliptic Longitude (in V magnitude arcsec-2).

| Helio ecliptic Longitude (deg) | Helio ecliptic Latitude (deg) | | | | | | |
|---|---|---|---|---|---|---|---|
| | 0° | 15° | 30° | 45° | 60° | 75° | 90° |
| 180° | 22.1 | 22.4 | 22.7 | 23.0 | 23.2 | 23.4 | 23.3 |
| 165° | 22.3 | 22.5 | 22.8 | 23.0 | 23.2 | 23.4 | 23.3 |
| 150° | 22.4 | 22.6 | 22.9 | 23.1 | 23.3 | 23.4 | 23.3 |
| 135° | 22.4 | 22.6 | 22.9 | 23.2 | 23.3 | 23.4 | 23.3 |
| 120° | 22.4 | 22.6 | 22.9 | 23.2 | 23.3 | 23.3 | 23.3 |
| 105° | 22.2 | 22.5 | 22.9 | 23.1 | 23.3 | 23.3 | 23.3 |
| 90° | 22.0 | 22.3 | 22.7 | 23.0 | 23.2 | 23.3 | 23.3 |
| 75° | 21.7 | 22.2 | 22.6 | 22.9 | 23.1 | 23.2 | 23.3 |
| 60° | 21.3 | 21.9 | 22.4 | 22.7 | 23.0 | 23.2 | 23.3 |
| 45° | SA | SA | 22.1 | 22.5 | 22.9 | 23.1 | 23.3 |
| 30° | SA | SA | SA | 22.3 | 22.7 | 23.1 | 23.3 |
| 15° | SA | SA | SA | SA | 22.6 | 23.0 | 23.3 |
| 0° | SA | SA | SA | SA | 22.6 | 23.0 | 23.3 |

Note: A value of “SA” denotes positions in the solar avoidance zone

Table 6.3 contains the expected count rates from different sky backgrounds in various STIS modes, which you can use to determine whether your observations would be background limited.

Observations of the faintest objects may need the special requirement LOW-SKY in the Phase II observing program. LOW-SKY observations are scheduled during the part of the year when the zodiacal background light is no more than 30% greater than the minimum possible zodiacal light for the given sky position. LOW-SKY in the Phase II scheduling also invokes the restriction that exposures will be taken only at angles greater than 40° from the bright Earth limb to minimize Earthshine and the UV airglow lines. The LOW-SKY special requirement limits the times at which targets within 60° of the ecliptic plane will schedule and limits visibility to about 48 minutes per orbit.

The ETC provides the user with the flexibility to separately adjust both the zodiacal (low, average, high) and Earthshine (shadow, average, high, extremely high) sky background components in order to determine if LOW-SKY is advisable for a given program. However, the absolute sky levels that can be specified in the ETC

may not be achievable for a given target; e.g., as shown in Table 6.2 the zodiacal background minimum for an ecliptic target is mv = 22.4, which is still brighter than both the low and average options with the ETC. By contrast, a target near the ecliptic pole would always have a zodiacal=low background in the ETC. The user is cautioned to carefully consider sky levels as the backgrounds obtained in HST observations can cover significant ranges.

Table 6.3: Count Rates by Sky Background and STIS Mode

| Mode | Count Rates (counts sec–1 pix–1) | | | | |
|---|---|---|---|---|---|
| | | Earthshine + Geocoronal Lines | | | |
| | Zodiacal[1] | Ex. High Earth[2] High Air Glow | High Earth[3] High Air Glow | Avg Earth[4] Avg Air Glow | Shadow Earth[5] Low Air Glow |
| CCD Clear | 1.1 × 10-1 | 9.6 × 10-2 | 4.8 × 10-2 | 2.4 × 10-2 | 0 |
| CCD Longpass | 6.5 × 10-2 | 5.5 × 10-2 | 2.7 × 10-2 | 1.4 × 10-2 | 0 |
| NUV-MAMA Clear | 6.4 × 10-5 | 2.4 × 10-3 | 2.3 × 10-3 | 1.2 × 10-3 | 2.0 × 10-4 |
| NUV-MAMA SrF2 | 5.8 × 10-5 | 3.7 × 10-4 | 3.6 × 10-4 | 1.8 × 10-4 | 1.6 × 10-5 |
| NUV-MAMA Qtz | 5.6 × 10-5 | 1.3 × 10-4 | 1.3 × 10-4 | 6.4 × 10-5 | 0 |
| FUV-MAMA Clear | 2.2 × 10-8 | 2.2 × 10-2 | 2.2 × 10-2 | 1.1 × 10-2 | 2.1 × 10-3 |
| FUV-MAMA SrF2 | 1.9 × 10-8 | 1.3× 10-3 | 1.3 × 10-3 | 6.5 × 10-4 | 8.0 × 10-5 |
| FUV-MAMA Qtz | 1.8 × 10-8 | 8.3 × 10-9 | 7.3 × 10-9 | 3.7 × 10-9 | 3.3 × 10-11 |
| FUV-MAMA Lyman-α | 1.4 × 10-11 | 1.6 × 10-3 | 1.6 × 10-3 | 8.1 × 10-4 | 1.6 × 10-4 |

[1] Zodiacal contribution is the same as in Figure 6.1 and Table 6.4 (mV=22.1 arcsec-2).
[2] Corresponds to HST pointing 24° from the limb of the sunlit Earth.
[3] Corresponds to HST pointing around 38° from the limb of the sunlit Earth, where the Earthshine is 50% of the “extremely high” value.
[4] Corresponds to HST pointing around 50° from the limb of the sunlit Earth, where the Earthshine is 25% of the “extremely high” value.
[5] Earthshine for shadow is 0 in the continuum, while the UV geocoronal emission lines are reduced from the high to the low values in Table 6.5.

*Geocoronal Emission and Shadow*

Background due to geocoronal emission originates mainly from hydrogen and oxygen atoms in the exosphere of the Earth. The emission is concentrated in a very few lines. The brightest line is Lyman-α at 1216 Å. The strength of the Lyman-α line varies between about 2 and 20 kilo-Rayleighs (i.e., between $6.1 \times 10^{-14}$ and $6.0 \times 10^{-13}$ erg $sec^{-1}$ $cm^{-2}$ $arcsec^{-2}$ where 1 Rayleigh = $10^6$ photons $sec^{-1}$ $cm^{-2}$ per 4π steradians) depending on the time of the observation and the position of the target relative to the Sun. The next strongest contribution is from the doublet [O I] 1302 + 1306 Å, which rarely exceeds 10% of Lyman-α. The typical strength of the [O I] 1302 + 1306 Å doublet is about 2 kilo-Rayleighs (which corresponds to about $5.7 \times 10^{-14}$ erg $sec^{-1}$ $cm^{-2}$ $sec^{-1}$ $arcsec^{-2}$) at the daylight side and about 150 times fainter on the night side of the HST orbit. O I] 1356 Å and [O II] 2471 Å lines may appear in observations on the daylight side of the orbit, but these lines are at least 10 times weaker than the [O I] 1302 + 1306 Å line. The widths of the lines also vary. The line widths given in Table 6.5 are representative values assuming a temperature of 2000 K.

The geocoronal emission lines are unresolved at the first-order resolutions of STIS but the emission fills the slit in the spatial dimension. A wider slit or slitless observing does not increase the background counts per pixel from geocoronal emission but does increase the area (range of wavelengths or pixels in the dispersion direction) over which that background is received. Observations with a slit which is *n* pixels wide in dispersion will be affected by geocoronal emission in a roughly *n* pixel region centered on the relevant geocoronal emission line wavelength. For slitless spectroscopy in the UV, the effects of geocoronal emission must be taken into account at all pixels, unless a long pass filter is employed to block off the short wavelength emission (see also Section 5.3.5 and Section 12.1).

It is possible to request that exposures be taken when HST is in the umbral shadow of the earth to minimize geocoronal emission (e.g., if you are observing weak lines at ~1216 or ~1304 Å) using the special requirement SHADOW. Exposures using this special requirement are limited to roughly 25 minutes per orbit, exclusive of the guide-star acquisition (or reacquisition) and can be scheduled only during a small percentage of the year. SHADOW reduces the contribution from the geocoronal emission lines by roughly a factor of ten, while the continuum Earthshine is set to 0. If you require SHADOW, you should request it in your Phase I proposal (see the Call for Proposals).

An alternate strategy for reducing the effects of geocoronal emissions is to use time resolved observations, so that any data badly affected by geocoronal emission can simply be excluded from the final coaddition. This can be done either by doing the observations in TIME-TAG mode or by just taking a series of short (~ 5 min.) ACCUM mode exposures over the course of each orbit.

Observers should also remember that geocoronal lines will also produce weak absorption features in the spectra of extended targets.

---

Chapter 3

# Soft X-ray Telescope

Soft X-ray imaging Telescope (SXT) onboard Astrosat will be sensitive to soft X-rays in the energy range of 0.3 – 8 keV. X-rays in this energy range are amenable to focusing and will lead to: a) nearly 1000 times better sensitivity over non-focusing instruments of similar areas making over 10,000 sources detectable; b) separation of confusing sources; c) arc min imaging; d) spatially resolved spectroscopy; and e) variability studies.

SXT will cover a very important energy range of the broadband spectrum observed with Astrosat, and will be able to investigate the following scientific problems.

1. Resolving the K line emission from Si, S, Ar, Ca and Fe in hot thermal coronal plasmas, as well as fluorescent line emission from these elements in the medium photo-ionized by strong X-ray continuum in accretion powered X-ray sources (neutron stars, stellar mass black-holes, supermassive black-holes etc.).
2. Carrying out spectroscopy of hot thin plasmas in galaxies, clusters of galaxies, nuclei of active galaxies, quasars, supernova remnants and stellar coronae.
3. Studying the physics of shocks and accretion disks, coronae, photo-ionized regions and their density, temperature, ionization degree, and elemental abundance.
4. Studying low energy absorption and the nature of absorbers, for example, whether these are cold (neutral) or warm (ionized).
5. Studying soft X-ray excesses due to a blackbody emission in AGNs, and in binary X-ray pulsars in conjunction with other higher energy X-ray instruments.
6. Carrying out Spatially resolved spectroscopy of Supernova Remnants and Clusters of galaxies.
7. Carrying out simultaneous wide-band spectral studies and time-resolved spectra of thermal as well as non-thermal plasmas in the universe using the unprecedented combination with sensitive hard X-ray detectors.

## Telescope

The telescope consists of a tubular structure housing the X-ray reflecting mirrors and other components. There is a “Charge Coupled Device” (CCD) camera at the focal plane of the mirrors in order to image the cosmic sources.

### Basic Components

The basic components of the telescope (apart from the mirror assembly) are given below (see Fig. 3.1).

a) A deployable cover/door at the top end of the telescope which covers the optical elements on the ground and protects them from contamination. It will be deployed in 4 to 6 weeks after launch. It can be closed only manually on ground. Once opened in space, it will be deployed at an angle of $270^{o}$.

b) A “Thermal Baffle” placed between the mirror assembly and the telescope door. All parts are made up of aluminum alloy 6061 T6. The function of thermal baffle is to protect the telescope from the Sun, and to provide a base for mounting the heaters to maintain the optics within a certain specified range of temperatures, and to block the unwanted area of the optics. The sun avoidance angle with the thermal baffle is ~45$^{o}$.

c) A “Forward tube” made up of Composite Fiber Reinforcement Plastic (CFRP). Forward tube extends from the bottom of the “Top Lid”. It covers the thermal baffle assembly.

d) Ring 2 as an interface ring between the forward tube and the middle flange of the optics. Ring 1 provides an interface between the Rear tube-2 and the middle flange of the optics.

e) Rear tube-1 made up of CFRP is a hollow cylinder of diameter 343 mm ID and 347.8 mm OD. Rear tube-1 extends from Ring-1 to “Deck Interface Ring” (DIR). It houses 3α Optics while forward tube is the house for 1-alpha assembly (see below).

f) “Deck Interface Ring” (DIR) is made up of Al alloy 6061 and is used to assemble rear tube-1 and rear tube-2 to the main deck of the satellite.

g) Rear tube-2 made up of CFRP is a hollow stepped cylinder with a top portion thicker than the bottom portion to provide stiffness. Rear tube-2 extends from the DIR to the CCD interface ring.

h) CCD interface ring is provided to align the CCD Camera with the tubular structure to the desired accuracy. This is made up of aluminium alloy 6061.

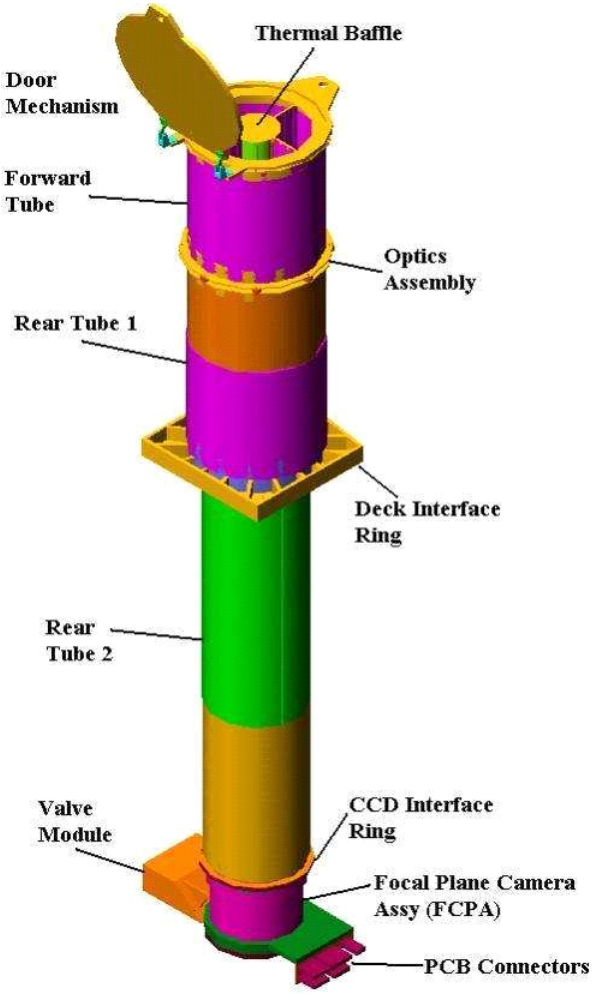


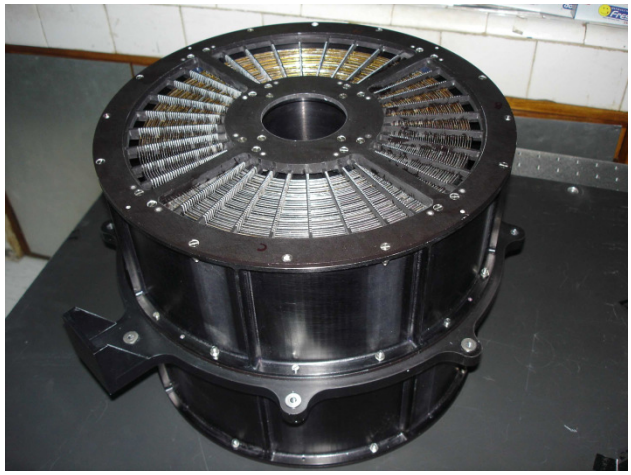

*Figure 3.1: Left: Structure and various components of the Soft X-ray Telescope from outside (simulated picture). Top: The optical modules with gold-coated mirrors (upper: 1-alpha; lower: 3-alpha; actual photo).*

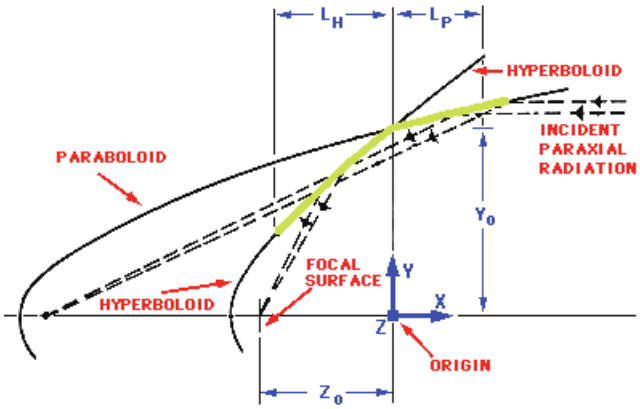


*Figure 3.2: The principle of the Wolter I optics using ray diagram. The green lines show the conical approximations of the paraboloidal and hyperboloidal mirrors.*

## Properties of the Mirror Assembly

The X-ray telescope in SXT consists of a set of coaxial and con-focal shells of conical mirrors approximating paraboloidal and hyperboloidal shapes and arranged behind each other. This geometrical arrangement is known as Wolter I optics (Fig. 3.2). X-rays are first reflected by an internally reflecting paraboloidal (1α) mirror and then reflected to the prime focus of the telescope by the internally reflecting hyperboloid (3α) mirror. At grazing incidence, the active region of the mirror is just a thin annulus giving a small collecting area even for a large diameter mirror. Thus nesting of Wolter I shells is incorporated to improve the filling factor of the circle defined by the outermost shell. Higher nesting is achieved by using shells made of very thin foils but figured in a conical approximation to Wolter I optics. SXT has 40 complete shells of mirrors assembled quadrants wise (total of 320 mirrors) for 1 and 3 mirrors (see Fig. 3.1). The focal length of the telescope is 2 meters, constrained by the available space in the launch vehicle flaring. Each mirror is made of aluminium (thickness ~0.2 mm) coated with gold on the reflecting side. The length of each mirror is 100 mm. The radius of the outermost shell is 130 mm, while that of the innermost shell is 65 mm. The on-axis half-power diameter of the point spread function (PSF) in the focal plane is expected to be about 2'. The on-axis effective area of the telescope, including CCD Quantum Efficiency (isolated and bi-pixel events 1-4) and the absorption by the optical blocking filter as measured, is expected to be ~128 $cm^2$ at 1.5 keV and ~22 $cm^2$ at 6 keV (see Fig. 3.3).

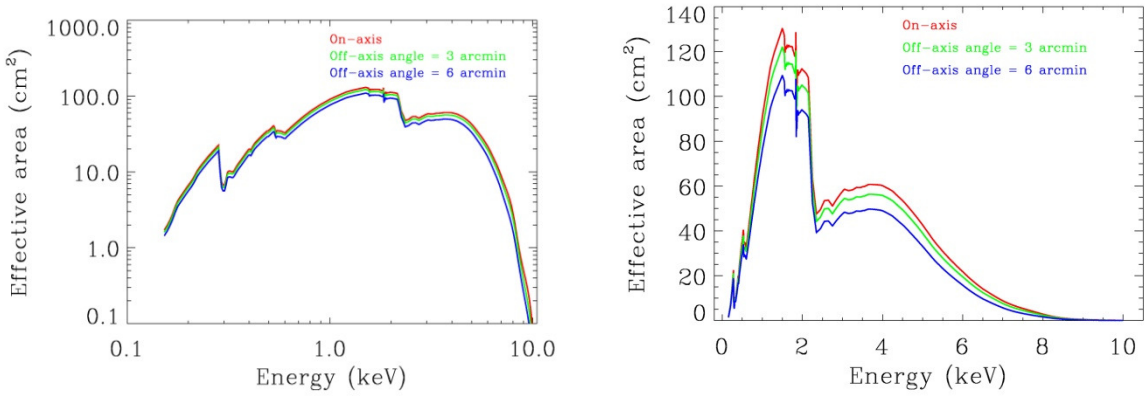


*Figure 3.3: Left: Telescope effective area (*including CCD Quantum Efficiency (isolated and bi-pixel events 1-4) and the absorption by the optical blocking filter as measured*) vs. energy for on-axis and two off-axis angles (simulation). Right: Same figure with linear scale in "effective area" axis.*

## Focal Plane Camera Assembly

The primary instrument of the Focal Plane Camera Assembly (FPCA; see Fig. 3.4) of the SXT is a CCD, which is the focal plane imager. The health and the operational condition of the CCD require vacuum, low temperature and protection from the optical light and energetic protons. Therefore, components such as thermo-electric cooler (TEC), optical blocking filter, proton shield, etc. have been included in FPCA. The operation of the CCD also requires the processing electronics, and the calibration of the CCD + processing electronics requires calibration sources (see Fig. 3.5).

### Focal Plane Camera Assembly Devices and Components

(i) Charge Coupled Device CCD-22 (a MOS device) built by E2V Technologies Inc., UK, specially for the European Photon Imaging Camera (EPIC) onboard the XMM-Newton observatory and supplied to the University of Leicester. For the characteristics of the CCD-22 see Fig. 3.6:

(a) A three-phase frame transfer device.
(b) Open electrode structure for useful band pass of 0.2 to 10 keV.
(c) Operating area of 610 × 602 array of 40 micron by 40 micron pixels.
(d) The storage region is a 600 × 602 array of 39 x 12 micron pitch.

(ii) Optical Blocking Filter:
A filter is installed in the front of the CCD to block optical light. The filter consists of a single fixed polyimide film 1840 A° thick coated with a coating of 488 Angstroms of Aluminum on one side. The typical optical transmission of the filter is less than $5 \times 10^{-3}$ (similar to the XMM-Newton thin filter). The filter design provides ~ 7 magnitude of optical extinction over the optical band. For the SWIFT SXT with a PSF of ~15" a 6th magnitude star gives an optical loading of ~ few $e^-$ per pixel, at which point the quality of the X-ray data begins to be affected. For the SXT with a ~7-8 times larger PSF and a 2 times larger (angular) pixel the safe optical limit should be closer to a ~4 magnitude star. This limit can be set more accurately in orbit using a bright non-X-ray emitting star. The X-ray transmission of the filter is shown in Fig. 3.7.

(iii) Operating Temperature of the CCD:
The X-ray CCD detector is cooled to 193$^{o}$ K by a thermo-electric cooler (TEC) and a radiator assembly during its operation for low dark current and to reduce sensitivity to radiation damage. The TEC is coupled to a cold finger connected to a “Heat Pipe” unit which is connected to a radiator plate designed by ISRO for effective heat dissipation and which provides a maximum temperature of −40° C at the junction between the heat pipe and the camera cryostat.

(iv) Proton Shield:
The camera is provided with a proton shield to minimize any damage of the device due to energetic protons. The degradation of energy resolution should be constrained during 5 years lifetime of the ASTROSAT mission. Due to the orbit of ASTROSAT being more benign than the orbit of SWIFT, the mass and size of the proton shield was significantly reduced from the original SWIFT design.

(v) Calibration sources:
Four individual $^{55}$Fe radio-active calibration sources are provided in the camera for in-flight calibration at energies of ~6.9 keV (Mn). These illuminate the corners of the CCD outside the Field Of View (FOV).

(vi) Readout Nodes:
Provision has been made for readout from either left node or the right node using node with two individual pre-amplifiers.

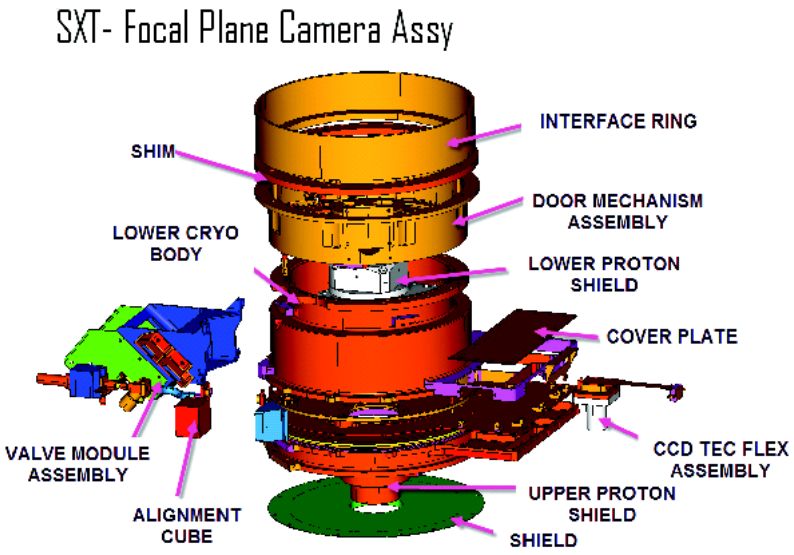


*Figure 3.4: Focal Plane Camera Assembly (FPCA) and its components.*

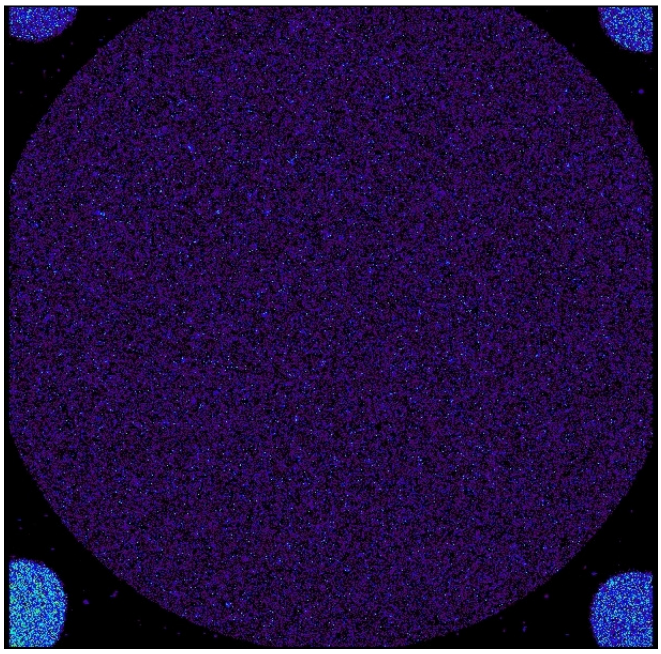

*Figure 3.5:* The CCD illuminated by 5 internal calibration sources.

### CCD Quantum Efficiency Curves

The flight device has been calibrated across the energy range giving the measured QE values for iso events, for events up to 4 pixels in size, and for "all" events, i.e. including those with 5 or more active pixels. The results of these calibration tests are shown in Fig. 3.8.

### The Energy Resolution

The energy resolutions estimated from the calibration data are given below.

| Line ID and Energy E (eV) | Resolution (ΔE) (FWHM in eV) | Resolution (%ge) |
|---|---|---|
| Al –Fl : 1487 | 90 ± 8 | 6.0 ± 0.54 |
| Si –K : 1740 | 92 ± 6 | 5.3 ± 0.34 |
| Cl –F : 2621 | 104 ± 5 | 4.0 ± 0.19 |
| Mn-Ka esc : 4155 | 120 ± 5 | 2.9 ± 0.12 |
| Ti –F : 4511 | 126 ± 6 | 2.8 ± 0.13 |
| Mn-Kb esc : 4750 | 128 ± 7 | 2.7 ± 0.15 |
| Mn-Ka : 5895 | 145 ± 9 | 2.5 ± 0.15 |
| Mn- Kb : 6490 | 150 ± 10 | 2.3 ± 0.15 |

### Charge Transfer Inefficiency (CTI) and Pile-up effects

The Charge Transfer Inefficiency (CTI) has been measured along both the serial and parallel readouts using the four corner sources. The serial and parallel CTIs thus measured are shown as a function of energy in Fig. 3.9.

The CCD camera door is always open and remains open during the data readout. Therefore, if the source is too strong or the PSF is too sharp then multiple photons can fall on the same pixel during the 2.4 s that it takes to readout the CCD, leading to a pile-up. The amount of pile-up will depend on the post-launch PSF of the telescope and will need to be corrected for when the source count rate at the maximum of the PSF becomes ~0.5 cts/pixel/frame. The ground measurements of the PSF suggest that it will not become an issue in the PC mode for sources fainter than 50-100 mCrab. For Chandra, XMM-Newton and Swift in imaging modes pile-up occurs at levels of ~0.1, 1 and 5 mCrab respectively. *The pile-up effect due to the sharpness of the PSF and the intensity of the source would be measured during the PV phase.*

### Observational Characteristics

| | |
|---|---|
| Detector: | E2V CCD-22. |
| Pixel Size: | 40μm × 40μm. |
| Pixel Scale: | 4.12" per pixel. |
| Useful Image Area: | 600 pixel × 600 pixel. |
| Field of View: | ~40'. |
| PSF: | 2.0' HPD |
| Position accuracy: | 0.5' |
| Energy Range: | 0.3-10 keV. |
| Energy Resolution: | 90 (tentative) eV at 1.5 keV (at launch);<br>145 (tentative) eV at 5.9 keV (at launch). |
| Effective Area (Telescope x CCD efficiency): | 128 $cm^2$ at 1.5 keV;<br>22 $cm^2$ at 6.0 keV. |
| Sensitivity (obs. time): | ~15 microCrab (5 σ) (10000 s) |

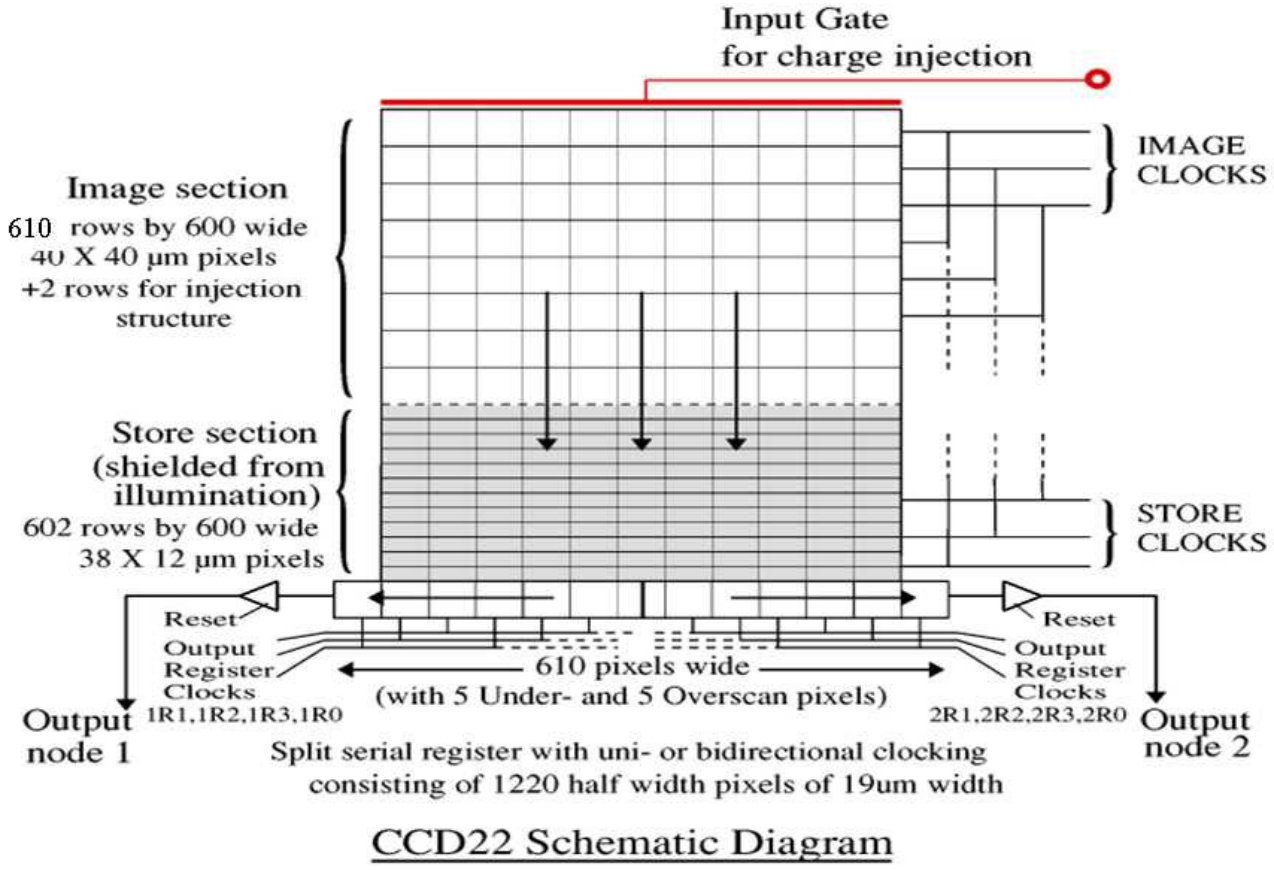


*Figure 3.6: Schematic Diagram of the CCD22.*

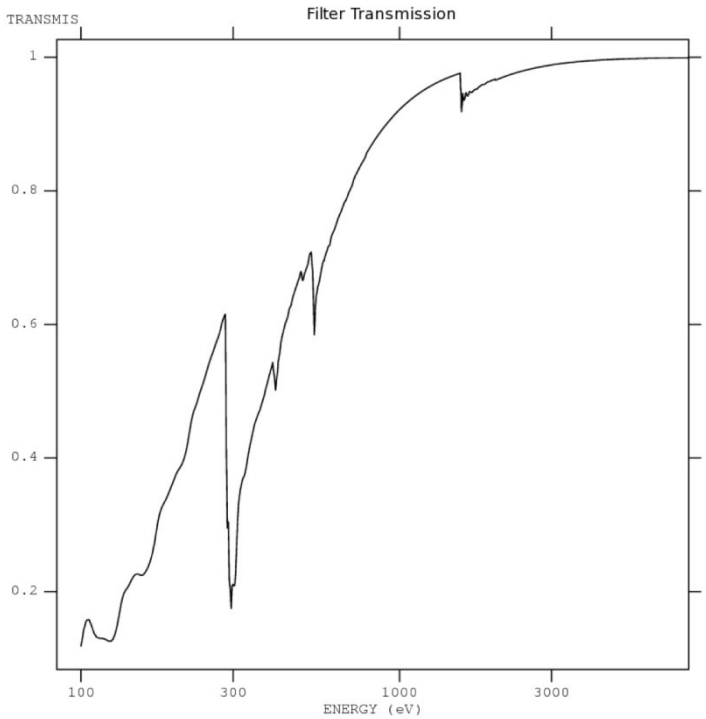


*Figure 3.7:* The transmission of X-rays through the optical blocking filter.

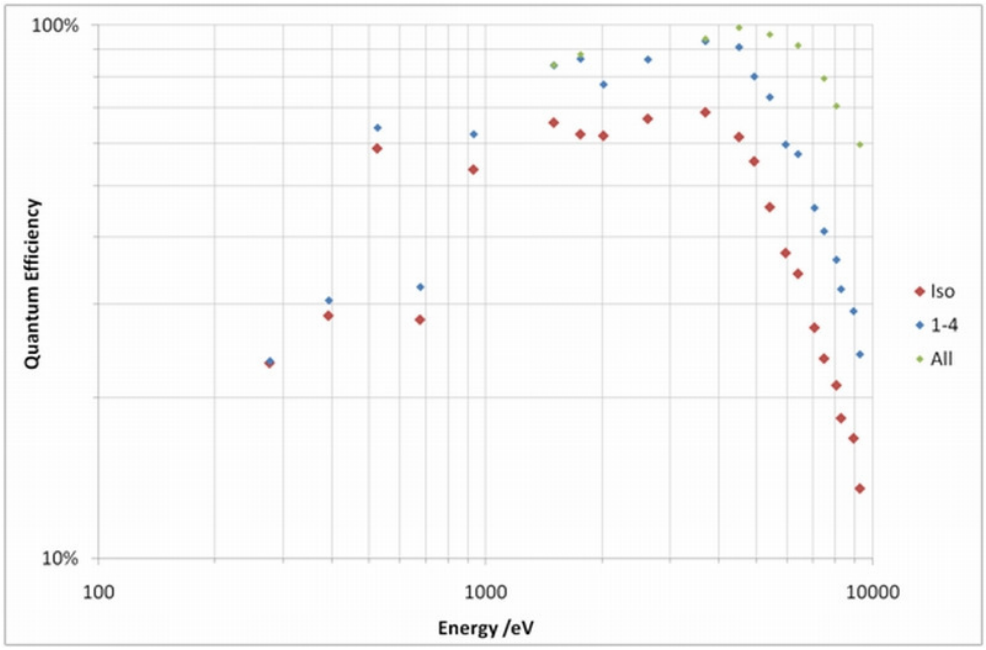


*Figure 3.8: CCD Quantum Efficiency points (refer to the subsection "CCD Quantum Efficiency Curves").*

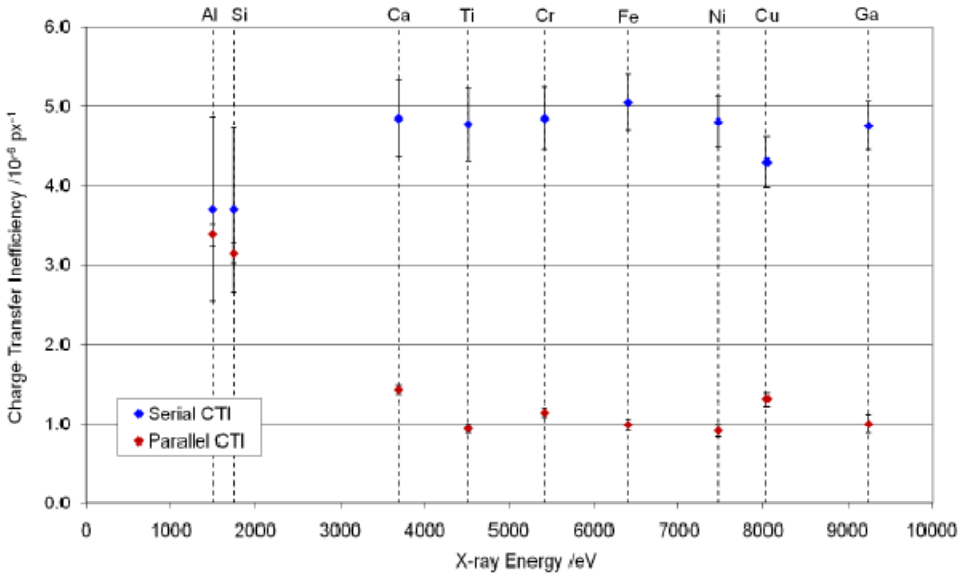


Figure 7. Serial and parallel charge transfer inefficiencies as a function of x-ray energy.

Figure 3.9: The serial and parallel CTI as functions of energy.

## Data Modes and Telemetry

Data from the SXT CCD will be stored on-board, and then will be sent to the ground station once in each orbit around the Earth. The SXT on-board memory quota is 280 Megabytes per orbit (~ 90 minutes). This puts serious constraints on the data modes and how the data are packaged. There will be six data modes. In each mode, data will be packed in 2 Kbyte (2K) segments. So the SXT memory per orbit will be filled with approximately 143360 2K blocks.

The six data modes will be "Photon Counting" (PC) mode, "Photon Counting Window" (PCW) mode, "Fast Windowed Photon Counting" (FW) mode, "Bias Map" (BM) mode, "Calibration" (Cal) mode and "House Keeping" (HK) mode. In the PC mode, data from the entire CCD (i.e., 600 X 600 pixels) will be collected. Data above a specified threshold energy (provided by tele-command; default value between 100 - 200 eV) only will be transmitted. Moreover, data from a maximum of 36000 pixels will be transmitted in this mode. The read-out time of this mode will be approximately 2.4 s. The PCW mode is similar to the PC mode, but the data are collected from a smaller rectangular or square window. The location and size of this window on the CCD is set by a tele-command. In the FW mode, a 150 X 150 pixel window will be used in the centre of the CCD. The read-out time of this mode will be approximately 278 ms. The data of the FW mode will be thresholded as in the PC mode. The Cal mode will be used to check the calibration of SXT. The read-out time of this mode will be approximately 2.4 s. Four X-ray radioactive iron sources of very low strength will be used in CM mode. They are mounted near four corners of the CCD, and for them four corners of the CCD will be used. BM mode is a separate mode in which the entire CCD frame will be sent with zero threshold. Incremental addressed 60 rows per CCD frame along with their co-ordinates are sent in this mode. On the ground, these rows of each incremental addressed CCD frame are mapped to generate individual CCD frame. It takes 24 seconds of data to generate one complete mapped CCD frame on the ground. The HK mode will be operated only when there is a failure of both LBT telemetry channels (main and redundant). When HK mode data command is uploaded, LBT data information in the form of HK data are sent in 2k data package. Hence only one frame will be generated and pushed in currently operating mode data package.

As mentioned earlier, data of each mode will be packaged in 2K blocks. However, the content of a 2K

block will not be same for all modes. For PC, PCW and FW modes (i.e., the science data), only a channel number above the pre-selected threshold will be stored in the 2K block along with the pixel coordinate and the CCD frame identification. These will be stored in the 15th to 2042nd bytes of the total 2048 bytes of a 2K block. Three bytes will be required to store each of (a) CCD frame identification, (b) CCD row number of the pixel, and (c) CCD column number of the pixel and the channel number. The bytes 1-14 (header) and 2043-2048 (footer) will store the 2K block number, mode information, on-board time, window location and numbers to check the validity of the 2K block.

### Operation Procedure

Normal operations will begin after the SXT door is opened and the CCD reaches its operational temperature. If all the observational constraints are met, the FPCA will normally operate under the PC mode with full CCD readout unless specified otherwise. The calibration data from the four corner point sources will be part of the observations. In case a window is specified to read only a part of the CCD, then a separate calibration mode data will be required. Thus normal data will have full energy resolution and time resolution of 2.4 sec.

## On-board Electronics

The SXT electronics box consists of ten cards of circuits (EL-01, ..., EL08, EL-3A, Motherboard), including three Field Programmable Gate Array (FPGA). The science data and the bias map data from the CCD will be passed on to the EL-03, where the analog to digital conversion will happen. The science data will then be stored in a memory (M1) in EL-05 via the 1st FPGA (EL-04). This memory has two portions: upper and lower. When the the 1st FPGA will store the data in the upper memory, the 2nd FPGA (EL-06) will take the previous set of data from the lower portion of memory M1. Next time, when the 1st FPGA will store in the lower portion of memory M1, the 2nd FPGA will take from the upper portion of memory M1. This way data will be continuously passed on from the 1st FPGA to the 2nd FPGA. The bias map data will be stored in the memory M2 of EL-05, after being passed through the 1st FPGA. Whenever the bias map data will be required during the PC mode, the flow of the science data will stop for a few seconds, and the bias map data will be passed on from M2 to the 2nd FPGA via the 1$^{st}$ FPGA. In the 2nd FPGA, the data will be packaged in 2 Kbyte blocks (as mentioned in the previous section), and will be passed on to the 3rd FPGA (EL-07). Here the data will be sent to the satellite memory (allocated for SXT) via high bit rate telemetry (HBT; rate is 4 MHz). The Housekeeping (HK) data from the FPCA will be passed on to the 3rd FPGA via EL-3A. These data will eventually be sent to the satellite memory via low bit rate telemetry (LBT; rate is 40 kHz). The power from the satellite interface will be supplied to various cards via the relay card (EL-02) and the DCDC tray (EL-01). The input of the DCDC tray will be between 18 V and 42 V, and its output to each card will be a regulated voltage. The tele-commands from the satellite interface will be passed on to the various cards, and eventually to the FPCA via EL-3A and EL-02.

## Observational Constraints

There will be several pointing constraints on the SXT observations, primarily to protect the CCD, the optical blocking filter above the CCD, and the mirror coating. The most important one will be the Sun avoidance angle (> 45 degree). The others are the Moon avoidance angle, the Earth limb avoidance angle and the ram direction avoidance angle. For faint or diffuse objects, these values are > 30 degree, 30 degree and > 12 degree respectively. For brighter point sources (> 30 mCrab), the lower limits of these three angles may be 5-10 degrees, depending on the observations done during the PV phase.

## In-flight Performance

Once the satellite is launched, a description of the in-flight information about each relevant component and operation will be available here. Examples of these are quantum efficiency behavior, energy and location dependent area and PSF, filter properties, response matrix, pileup, suitable threshold, spectral resolution, aim points, hot pixel information, background, suitable grades, telemetry limit, etc.

## Data Analysis Tools

SXT data will have various levels: 0, 1, 2 and 3. The users will be provided with the levels: 1, 2 and 3 data. Ideally, a user will start from the calibrated level 2 data, which he/she will screen in various ways according to his/her scientific requirements. It will be necessary to start from the level 1 data when there will be a significant change in calibration. Level 3 data consisting of automatically created high level products will be for a quick reference, and not for scientific publications.

Several tools will be used to process the data. The tool “Sxthkproc” will process the SXT house keeping header packets file, and “Sxtfilter” will run in sequence ‘prefilter’ and ‘makefilter’ to create a filter file from housekeeping data. The level 1 uncalibrated FITS file data will be processed with a series of tools. Here are some examples. The “Coordinator” tool will transform coordinates from raw data to detector and sky coordinate. The “Sxtpcbias” tool will adjust the bias subtraction. “Sxtflagpix” will flag events for bad pixels and calibration source location. “Sxtpcgrade” will calculate the PHA values and will assign event grades. The “Sxthotpix” tool will search for hot pixels and flickering pixels, and the “Sxtpccorr” tool will correct on ground bias subtraction for the photon counting mode. “Sxtcalcpi” will update the PI column in the SXT event files. Finally the “Sxtscreen” will generate GTI and use them together with other criteria to screen the data. The level 2 data will be somewhat screened, but the user will perform further screening (e.g., on pixels, channels, time) according to the scientific necessity. The user will then produce the higher level products, such as light curves, PHA files and response matrices. These higher level products will be compatible to the standard X-ray data analysis tools, such as XSPEC, FTOOLs, etc. The “Sxtpipeline” tool, which will employ many tasks, including those mentioned above, in series, will also create high level data product files by running the “Sxtproducts” tool for a quick reference.

## Writing an SXT Proposal

Once the satellite is launched, a description of the SXT-specific required information, for example, expected maximum and minimum count rates from the target source and from the field, viewing, simulations, etc., will appear here.

Chapter 4

# Large Area X-ray Proportional Counter

The Large Area X-ray Propositional Counter (LAXPC) is one of the major payloads on Astrosat, which covers energy range of 3 – 80 keV and with its large area of collection, about 8000 $cm^2$, it is well suited for timing and spectral measurements. The large detection volume (15 cm depth) of LAXPCs and being filled with xenon gas at 2 atmospheres pressure, results in detection efficiency greater than 50%, in 30-80 keV band. These three LAXPC units on Astrosat will thus have the largest effective area and sensitivity among all the satellite missions flown so far for X-ray astronomy studies above 20 keV.

The principal scientific objectives of LAXPC are as follows:

- Search for black hole sources will be conducted by repeated surveys in the limited regions of the galactic plane with the LAXPC. Detection and detailed studies of stellar-mass black holes with masses ~ 3-10 $M_\Theta$ in our Galaxy and the neighbouring galaxies and massive black holes (~$10^6$ to $10^9$ $M_\Theta$) in AGNs will be realized with the LAXPC instrument. This will be achieved by measuring variations in the luminosity of sources and the time scales of variations.
- Studies of periodic (pulsations, binary light curves, QPOs etc.) and aperiodic (flaring activity, bursts, flickering and other chaotic variations) variability in X-ray pulsars and other X-ray binaries, coronal X-ray sources, Cataclysmic Variables (CVs), Active Galactic Nuclei (AGNs) and other galaxies etc. by high time resolution (~10μsec) photometry over a wide spectral band covering 3-80 keV with a single instrument. Rapid variability studies e.g. sub-second variations, high and low frequency QPOs and kHz QPOs in soft and hard x-ray bands, probe astrophysical processes closest to the central source.
- Low to moderate spectral resolution studies of continuum X-ray emission over a broad band of 3-80 keV for X-ray binaries, Supernova remnants (SNRs), CVs, Stellar Coronae, AGNs etc. This will be done using large area and low to moderate energy resolution ( Δ E / E ~ 10 to 12%) of LAXPCs.
- Correlated time variations of intensity in 3-80 keV band with those in the visible, UV and soft X-ray (0.3-8 keV) bands to investigate the origin and mechanism of emission of radiation in different wave bands.
- Discovery of non-thermal components in the X-ray spectra of SNRs and Clusters of Galaxies by accurate spectral measurements in 3-80 keV band combined with simultaneous measurements from SXT in 0.3-8 keV region to estimate their magnetic field strength as well as understand the acceleration processes and origin of cosmic rays in the case of SNRs.
- Measuring magnetic fields of neutron stars by detection and studies of cyclotron lines, most of which lie in 15-60 keV regions in the X-ray spectra of x-ray pulsars.

## Payload configuration

The LAXPC instrument sensitive in 3-80 keV band, consists of 3 identical units, each with its own independent front-end electronics, HV supply, and signal processing electronics to facilitate easy replacement of the entire LAXPC unit in case any problem is encountered before the launch. The Time mark generating electronic unit is common for all the 3 LAXPCs. The data from all the 3 LAXPCs are independently acquired preserving the identity of each unit. These data are merged in a single telemetry data stream from which data for each LAXPC is recovered.

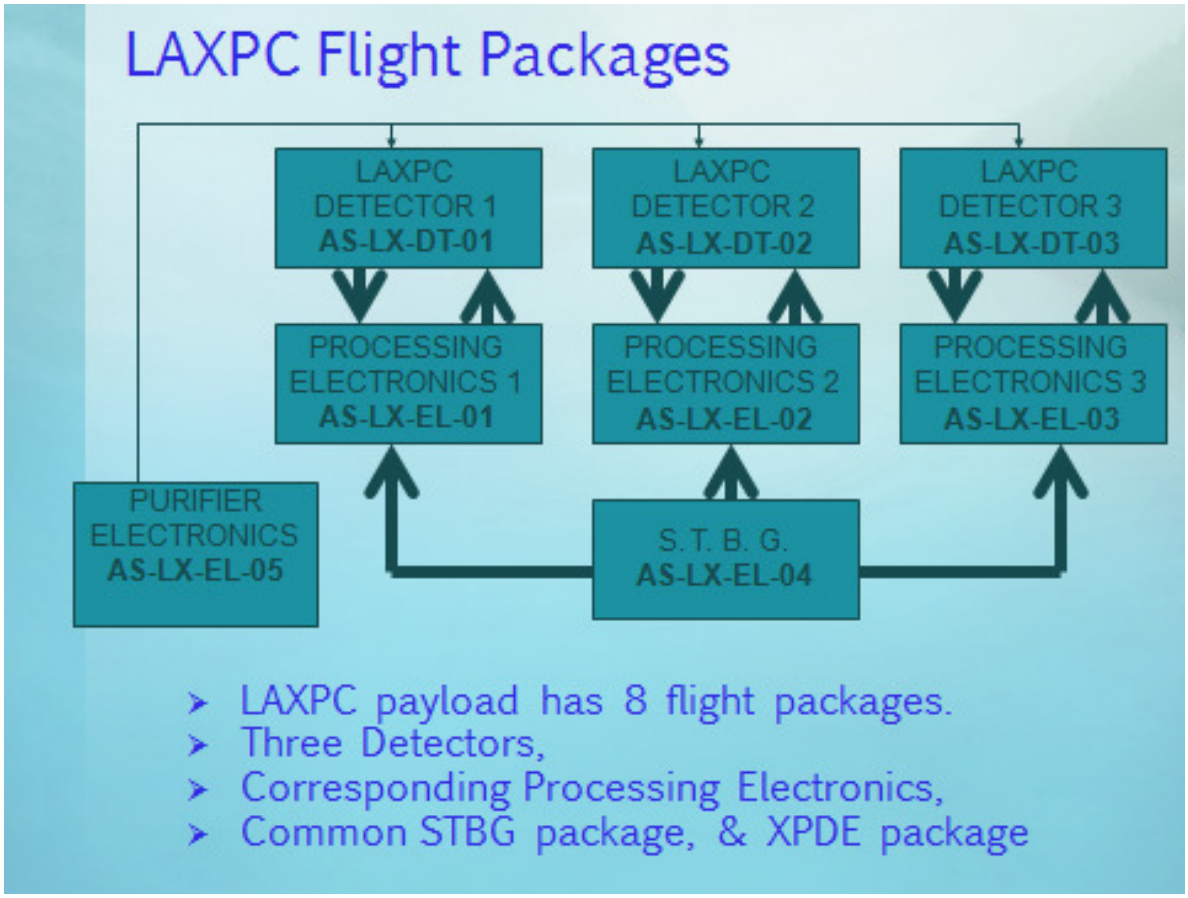


## Instrument Specification

| | |
|---|---|
| No. of LAXPC Detectors | Three (3) Identical units |
| Detector size | 120 cm x 50 cm x 70 cm |
| X-ray detection volume | 100 cm x 36 cm x 15 cm |
| No. of anode layers | 5 anode layers : each has 12 anode cells surrounded on 3 sides with Veto cells |
| Veto layers | 46 anode cells each with cross-section of 1.5 cm x 1.5 cm arranged on three sides of X-ray detection cells |
| Collimator field of view | $1^{o}$ X $1^{o}$ for all the LAXPCs |

| | |
|---|---|
| Collimator Height | 45 cm for WSC+FOV collimator |
| Counting Gas | Xenon + Methane |
| Gas Pressure | Two atmosphere (1520 torr) |
| Energy range | 3-80 keV |
| Total Effective Area of 3 LAXPC Detectors | About 8000 $cm^2$ in 5-20 keV |
| Total Weight of LAXPC | 414 Kg (Detector + Electronics) |

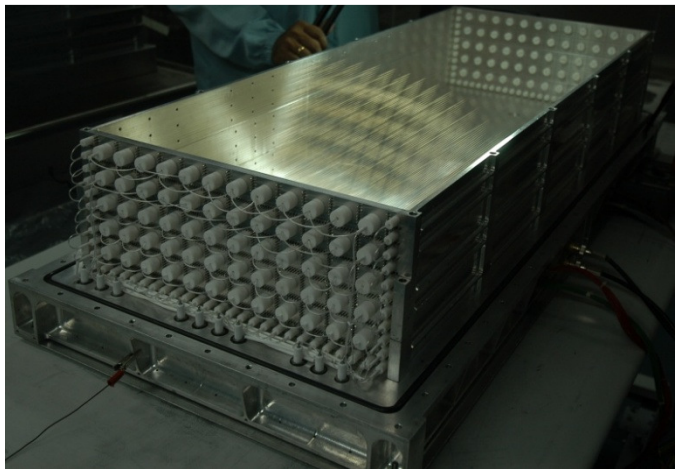

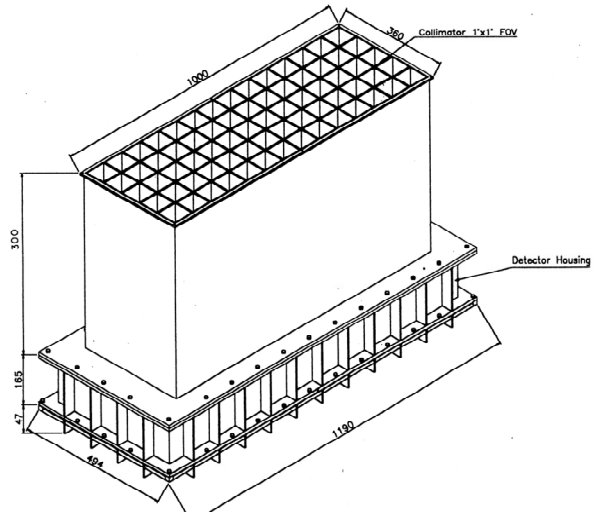


**Details of detector system:**

Each LAXPC detector consists of 60 anode cells of 3 cm x 3 cm cross-section and length of 100 cm, arranged in 5 layers providing a 15 cm deep X-ray detection volume. Each Anode Layer thus has 12 anodes with a total width of 36 cm. A Veto Layer made up of 46 anode cells each with cross-section of 1.5 cm X 1.5 cm surrounds the main X-ray detection volume on 3 sides to reject events due to charged particles and interaction of high energy photons in the detector. The alternate anode cells of Layer 1 and 2 are linked together and thus 4 outputs are obtained from Layer 1 and Layer 2. The anode cells in each of the Layer 3, 4 and 5 are linked together to provide one output from each layer. Thus there are 7 anode outputs that are operated in mutual anticoincidence to reduce the non-cosmic X-ray background The Veto layer is divided in 3 parts providing 3 Veto Layer outputs. The left side and right side veto anodes are linked together to provide one output from each one and the third veto output is from the bottom layer veto anodes linked together. The configuration of anodes is shown in the figure.

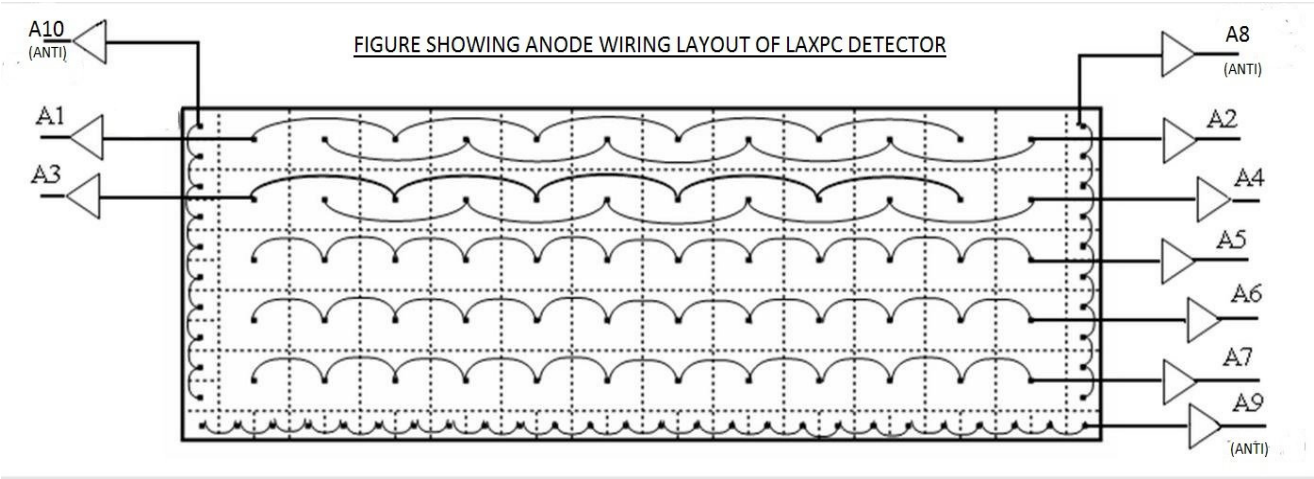


To suppress background from charged particles all events which register in multiple anodes or those which trigger the veto anodes are rejected, except for the situation where one of the energies is in the K X-rays for Xenon. For X-rays with energy above the K-edge of Xe, a K-electron may be ejected and the ion can radiate a K X-ray photon in energy range 29.4 - 34.4 keV. These X-ray may escape from the detector or be absorbed in a different anode. In order to include such events the anti-coincidence logic is modified to detect this energy range. If two main anodes register an event and at least, one of them is in the energy range of 25-35 keV, then the energy of the two anodes are added and the event is accepted. The lower threshold for this (KLLD) and the upper threshold (KULD) can be set through tele-command.

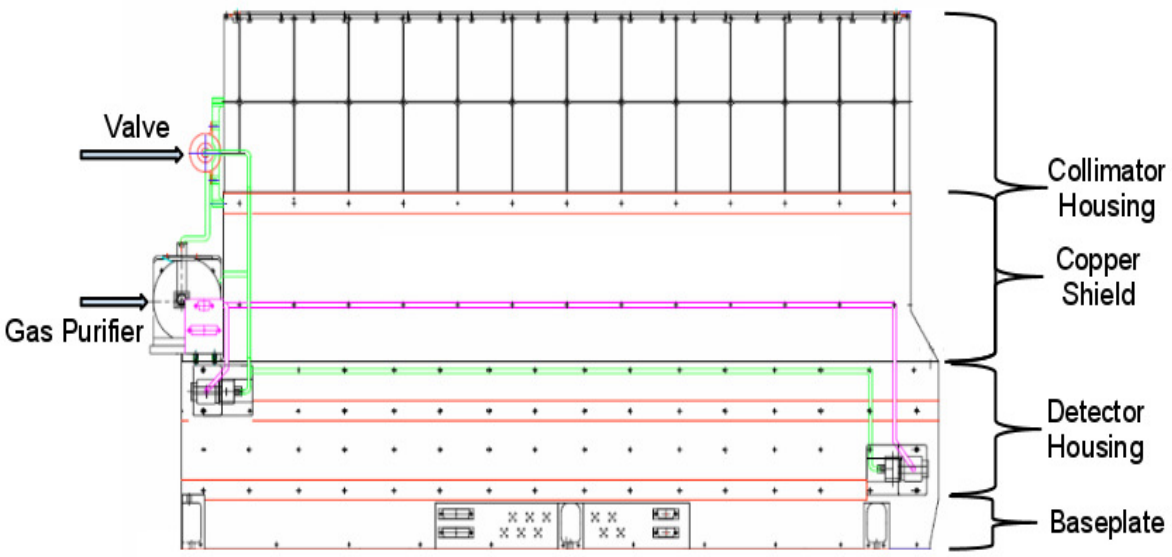


A 50 micron thick aluminized mylar film serves as the gas barrier as well as the X-ray entrance window for the detector. The detector is filled with a mixture of 90 % Xenon + 10 % Methane at a pressure of 1520 torr. The mylar window is supported against the gas pressure by a honey comb shaped collimator made of square geometry aluminium cells termed as Window Support Collimator (WSC). The Field Of View Collimator (FOVC) is placed above the WSC and is aligned with the openings in the WSC. The FOVC is made of sheets of tin, copper and aluminium and is placed in a collimator housing. The total height of the collimators is about 45 cm giving a Field of View (FOV) of

about 1 degree X 1 degree. A one mm thick tin sheet coated with copper serves as the shield for X-rays entering the detector from the side walls.

## Processing electronics and Timing capability:

There are 7 anode outputs from the X-ray detecting cells and 3 veto outputs from each detector that are fed to 10 charge sensitive preamplifiers (CSPAs). High voltage to the anodes is supplied from a command controlled HV unit whose HV output can be varied by command. The 7 X-ray anode and 3 Veto layer outputs from the CSPAs are sent to the peak detectors and events satisfying the selection logic as true X-ray events are further processed by signal processing electronics for

(a) Broad Band (BB) counting

(b) for time tagging of every event with its energy to an accuracy of 10 micro-sec.

For the purpose of BB counting the Bin time can be selected in multiple of 2 from 16 msec to 2048 msec, 128 msec. being the default value. The Bin times for the BB counting is selectable by command.

For BB counting output of all the 12 anode cells of Layer 1 and Layer 2 are combined and fed to the counters. Outputs of the Layers 3, 4 and 5 are also combined and given to a single counter for each energy band. All the events in each LAXPC above a lower energy threshold of 3 keV (LLD), upper energy threshold of 80 keV (ULD), all the three Veto layer counts termed as Anti counts and several other count rates detailed below, are also recorded in separate counters.

**Details of Broad Band Counting:**

**Counters Pulses for LAXPC counters from Event Processing Logic**

There are 7 Main Anodes and 3 Anti Anodes structured as follow:

Layer-1: Anode-1 & Ande-2. (Frame-1)
Layer-2: Anode-3 & anode-4. (Frame-2)
Layer-3: Anode-5 (Frame-3) & Anode-6 (Frame-4) & Anode-7 (Frame-5).
ANTI-1: Right-side Anti-Anode.
ANTI-2: Left-side Anti-Anode.
ANTI-3: End (Bottom) Anti-Anode.

| Sr.No. | COUNTER | WIDTH | REMARK |
|---|---|---|---|
| 1 | LLD | 13 (12+1) | Events crossing 3keV in any of 7 Main Anodes (A1 to A7) |
| 2 | ULD | 12(11+1) | Events crossing 80keV in any of 7 Main Anodes (A1 to A7) |
| 3 | ANTI | 13 (12+1) | Event in any of 3 Anti Anodes (A8 to A10). |
| 4 | MTO | 12 (11+1) | More than One Simultaneous Events (within 4uS) in any of 10 Anodes (A1 to A10). |
| 5 | MTT | 12 (11+1) | More than Two Simultaneous Events (within 4uS) in any of 10 Anodes (A1 to A10). |
| 6 | ANTI-1 | 12 (11+1) | Events crossing 3keV in Right ANTI Anodes (A8). |
| 7 | ANTI-2 | 12 (11+1) | Events crossing 3keV in Left ANTI Anodes (A9). |
| 8 | ANTI-3 | 12 (11+1) | Events crossing 3keV in Bottom ANTI Anodes (A10). |
| 9 | JE | 13 (12+1) | Genuine Events which has satisfied the criterion (may not be Digitized, depending of Mode of Operation) |
| 10 | NK | 12 (11+1) | MTO Events, None of the events is in K-band. |
| 11 | DEK | 9 (8+1) | MTO Events, One in K-band and another in Non-K-band for Particular Layer / Anode. |
| 12 | DK | 9 (8+1) | MTO Events, both events are in K-band. |

| | Colour Counts | L1 | L2 | L3 | |
|---|---|---|---|---|---|
| 13 - 15 | 3-80K | 12 (11+1) | 12 (11+1) | 12 (11+1) | Non-MTO Events between 2-80keV in Particular Layer / Anode. |
| 13 - 18 | 3-6K | 12 (11+1) | 9 (8+1) | 9 (8+1) | Non-MTO Events between 2-6keV in Particular Layer / Anode. |
| 19 - 21 | 6-18K | 12 (11+1) | 9 (8+1)) | 9 (8+1) | Non-MTO Events between 6-18keV in Particular Layer / Anode. |
| 22 - 24 | K (25-35K) | 9 (8+1) | 9 (8+1) | 9 (8+1) | Non-MTO Events in K-Band (i.e. between 25-35keV) in Particular Layer / Anode. |
| 25 - 27 | 18-40K | 9 (8+1) | 9 (8+1) | 9 (8+1) | Non-MTO Events between 18-40keV in Particular Layer / Anode. |
| 28 - 30 | 40-80K | 9 (8+1) | 9 (8+1) | 9 (8+1) | Non-MTO Events between 40-80keV in Particular Layer / Anode. |

**Note:**

**All Colour counts are counted for Single events only,**

**Total = 30 counters =>3x12 ibt, 12 x 11 bit & 15 x 8 bit counters. Each counters has an Over flow flag**

## Modes of operation of LAXPC:

The LAXPC payload consists of three independent LAXPC units with identical operational modes. There are three different modes of operation and each instrument can be operated simultaneously in more than one mode.

The LAXPC data carries information about cosmic X-rays detected with the instruments and it has three dimensions:

(a) time of detection

(b) energy (spectral channel) of the X-ray photons and

(c) identity of the detecting element (detector/anode-layer) including double-identity in some cases.

The signals generated by the instrument after detection of X-rays are processed and stored in any of the following modes.

- **Normal (or Default) Modes of Operation :**
  In Normal operation there are two modes running simultaneously and data are acquired from each LAXPC.

  (a) Broad Band Counting Data: Records the rate of occurrence of events in various energy bands with selectable time Bin (16 msec to 2048 msec). Default value is 128 msec. Details of the count rate capabilities of the various counters are given in the table. There are 15 counters for the broad band counting of the valid X-ray events in different energy bands covering 3-80 keV from 3 layers as discussed earlier.

  (b) Event Mode Data: In this mode arrival time of each event is time tagged to an accuracy of 10 microseconds. Simultaneously the energy and identity of each event is also recorded. This mode generates 5 bytes data for each accepted and analyzed event. In this mode the dead time of the detector is around 54 microseconds.

- **Fast Counter Mode:**
  In this mode the event rate is measured only from the top layer of each LAXPC detector in 4 energy channels covering 3-20 keV band with a fixed time bin of 160 microsecond. In this mode dead time is about 10 microsecond. Each of 4 counters are 8 bit deep and cover 3-6, 6-8 , 8-12 and 12-20 keV energy bands. This mode is to be used for studying rapid variability during the short duration flares or outbursts of sources.

Data from different modes of observation will be treated separately. The extraction criteria will be user defined and will require input from the housekeeping parameters. The auxiliary data will have to be processed separately. Certain housekeeping information will be derived independently from detector raw data.

## Detection Efficiency and Effective Area

Detection efficiency is determined by the thickness of entrance window at the low energy end and by the probability of photoelectric interaction in the detector gas volume at the higher energy end. GEANT4 simulations of detector have been used to estimate the effective area and field of view. The simulations were validated by comparing the simulations with observations using radioactive sources. The field of view (FWHM) is found to be 43' at 15 keV, 47' at 50 keV and 52' at 80 keV. The increase in field of view with energy is due to some part of the collimator becoming nearly transparent to high energy X-rays. The effective area calculated through simulations is reduced by 7% to account for imperfections in collimator as estimated by calibration using radioactive sources. A plot of effective area of the detector as a function of energy of X-rays is shown in figure which also shows the same for RXTE.

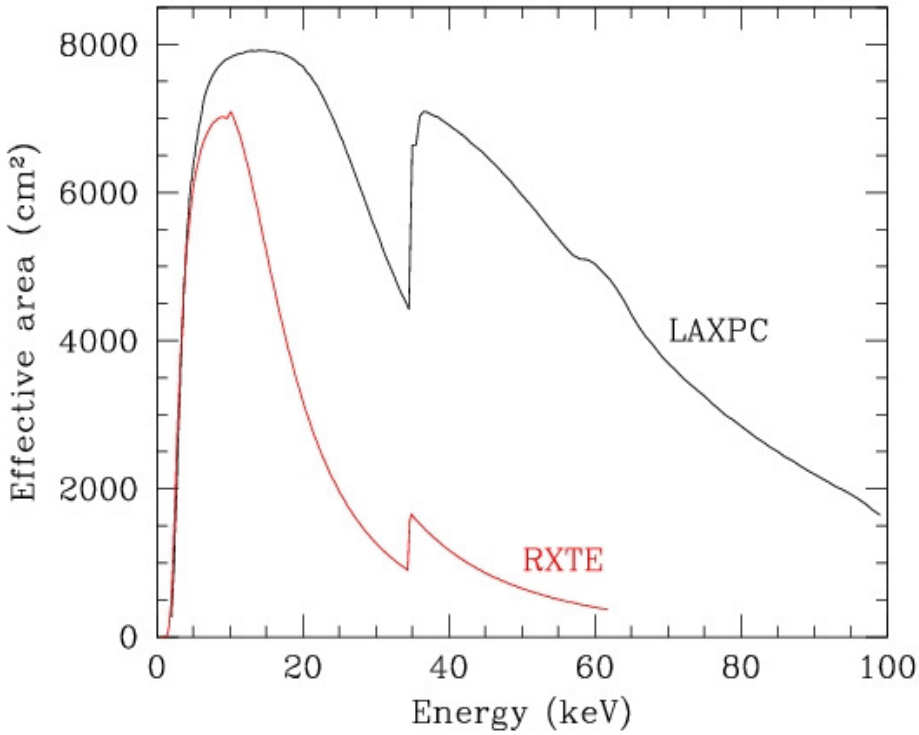


## Dead Time Measurement of LAXPC Detector

The test has been carried out using commercial mini X-ray gun (MINI X) mounted on specially designed X-Y source motion jig. The jig allows movement of the X-ray gun in controlled speed along both X and Y axis over the complete area of LAXPC detector. To avoid overexposure at one spot on detector, the X-ray gun is kept moving at slow speed along the length of cell. A commercial MCA is used to record the spectrum and counts for deferent event rates. The MCA provides dead time corrected incident event rate. The same setting of X-ray gun and jig is then used and event data are acquired with LAXPC PE and STBG unit. The counts as measured by MCA, is used as actual input counts and using the measured counts, the dead time is calculated as shown in figure. This measurement confirms with the number arrived at from analysis of processing time in electronics and the timing diagrams for the same.

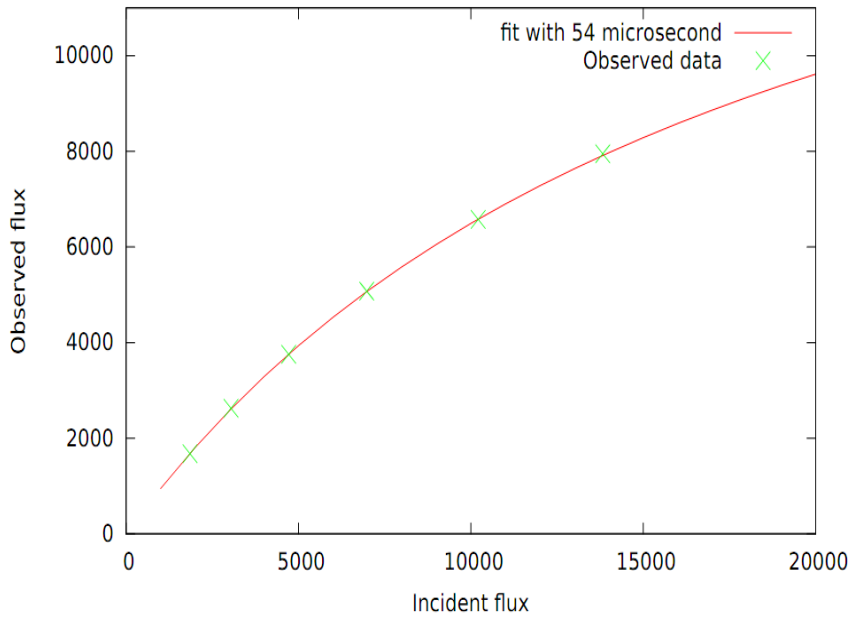


## Instrument Calibration

### Ground calibration

To obtain the energy response of detectors, 3 radioactive sources at different energies in the range of LAXPC detector were used. The calibration was repeated at 3 temperatures of 10°C, 20°C and 30°C to study the temperature dependence of detector response. The following 3 sources were used:

1. **$Fe^{55}$ with energy 5.9 keV**. These X-rays are absorbed in the top layer and hence only the two top anodes A1, A2 register these events.

2. **$Cd^{109}$ with energies, 22.1 keV (54.5%), 21.9 keV (28.8%), 24.9 keV (13.7%), 88.0 keV (3.0%).** The first two peaks cannot be resolved by the detector, while the third one gives a small feature at the high end of the main peak, which can be fitted with some effort. The last peak is beyond the range of the detector, but it can give a small contribution when the Xe-K X-ray escapes the detector. However, the resulting peak is too weak to be detected.

3. **$Am^{241}$ with energy 59.6 keV**. This sources also gives additional peaks because of loss of energy due to Xe-K X-rays escaping the detector. The detector logic is built to add contributions in 2 channels if one of them is in the range of Xe-K (25 –35 keV). Hence, the 59.6 keV peak consists of 2 parts, one where the entire energy is absorbed in the same anode and second where the Xe-K X-ray is absorbed in a different anode and the two contributions are added to one of the anode. If only one anode is in the Xe-K range the energy deposited in that anode is added to the other anode where remaining energy is deposited. If the energy deposited in both anodes is in the Xe-K range then the lower of the two energies is added to the anode which has higher energy. The Xe Kα X-rays have energies of 29.8 keV and 29.5 keV which account for about 81% of Xe-K X-rays, while the remaining fraction comes as Xe K-beta with energies 33.6–34.4 keV. Thus in addition to the 59.6 keV peak we also get two peaks when Xe-K X-rays escape from the detector giving the energies of about 30 keV and 26 keV. Because of limited resolution of the detector, the last two peaks are not well separated.

In order to estimate detector background, the counts are recorded without any source, before and after the source measurements are done. The background counts over a time interval equal to that for source are then subtracted from counts with source to get the net contribution from the source. All these measurements were done inside the thermovac.

In order to perform the calibration inside the thermovac chamber, an x–y motion platform for movement of radioactive sources above the Field of View (FOV) Collimator was designed. This can hold all three sources and expose one or more of them at a time. The x–y motion platform can function in vacuum and its movements and source on/off status can be controlled remotely. The movement of sources is controlled by a program to move the source at predetermined rates in x or y direction. To cover the entire area of the detector the source was moved along the y direction which moves it across the 12 cells followed by a movement along x axis. The sequence is repeated until the entire range is covered. Figure below shows the route traced by the source. To determine the characteristics of individual cells some scans were also done along each of the 12 cells, where the movement was restricted to x direction only along the wire.

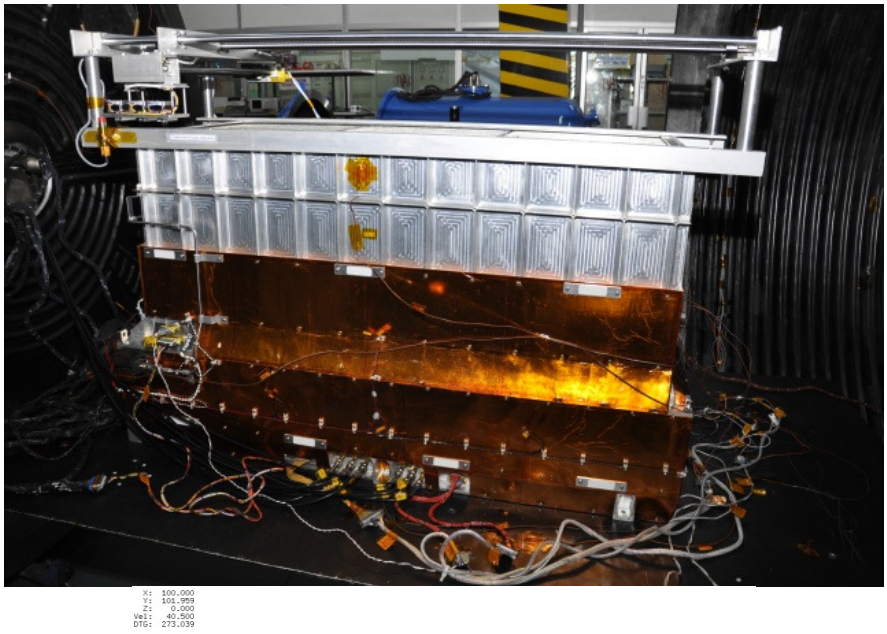


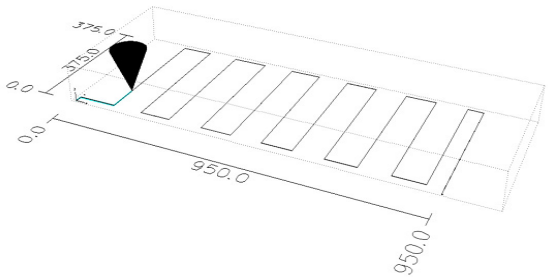

**Energy Resolution as a function of energy**

The energy resolution and channel to energy mapping were calibrated using three radioactive sources, $Fe^{55}$ (5.9 keV), $Cd^{109}$ (22 keV/ 24.9 keV) and $Am^{241}$ (59.6 keV). In order to perform the calibration inside a thermovac chamber, an x-y motion platform for movement of radioactive sources above the FOVC was designed. This can hold all these sources and expose one or more of them at a time. The movement is controlled remotely and can be programmed. The movement of source across the detector also allows us to estimate the transmission efficiency of collimator due to possible imperfections in the collimator fabrication. The calibration was repeated at temperatures of 10 C, 20 C and 30 C to study the temperature dependence of energy resolution and peak position.

The spectra of the three sources and background obtained from observations at 10 C and the energy resolution and the peak channel for the 4 main peaks in the spectra are shown in the following figure.

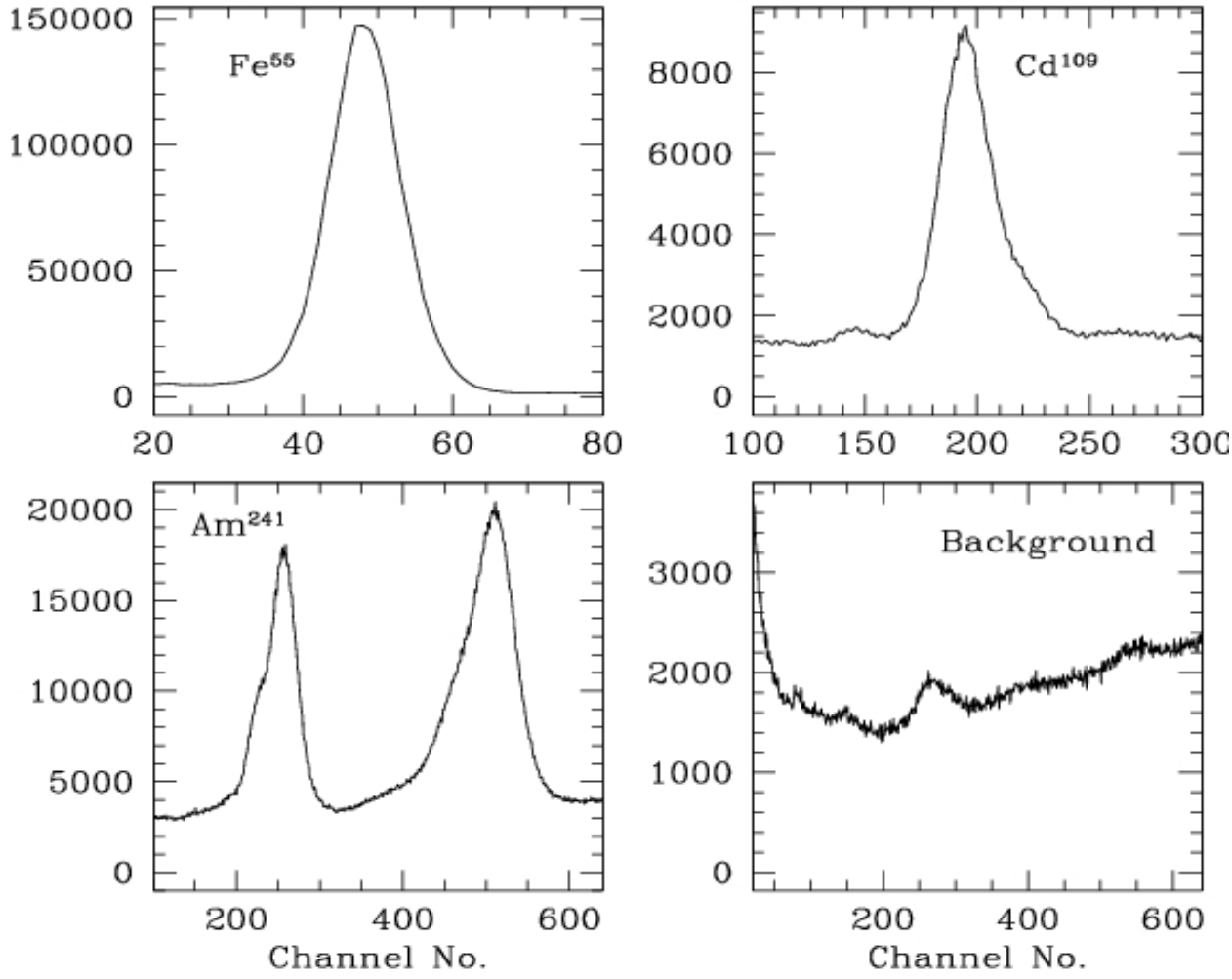

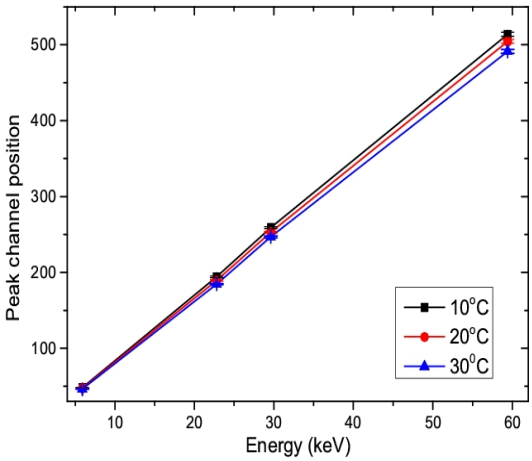


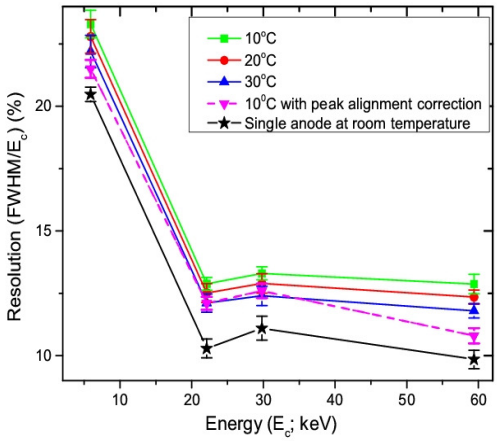


| Energy(keV) | Energy Resolution (%) | | | Peak Channel | | |
|---|---|---|---|---|---|---|
| | 10° C | 20° C | 30° C | 10° C | 20° C | 30° C |
| 5.9 | 23.4±0.6 | 22.9±0.7 | 22.2±0.7 | 48.2±0.6 | 47.4±0.6 | 46.3±0.6 |
| 22.1 | 12.9±0.3 | 12.5±0.4 | 12.1±0.6 | 194.2±2.5 | 189.5±2.3 | 184.6±2.4 |
| 29.8 | 13.3±0.3 | 12.9±0.4 | 12.5±0.4 | 259.0±3.4 | 253.0±3.0 | 247.0±3.2 |
| 59.6 | 12.9±0.4 | 12.4±0.3 | 11.8±0.3 | 513.9±6.7 | 504.5±6.1 | 491.2±6.4 |

To validate the GEANT4 simulation the events for each radioactive source were simulated. The total energy deposited in each anode was calculated for each event. In order to simulate the effect of finite energy resolution a random number with normal distribution is added to the energy in each cell. The random number is selected to have a zero mean and a standard deviation of σ. Here the relative standard deviation σ are treated as free parameters, which are chosen to get the best fit to observed spectra. For each peak in the spectrum we use a different σ. This gives 4 parameters, one each for $Fe^{55}$ and $Cd^{109}$ peaks and two for $Am^{241}$ spectrum. Although, some of these peaks have multiple energies which are not resolved, we use the same σ for the entire peak. The total energy, E, in each anode is translated to channel number, $n_c$, using

$$n_c = e_0 + e_1E(1+e_2E)$$

Here $e_2$ gives a small nonlinear contribution which is required to fit all spectra. Because of this nonlinearity the peak in $Am^{241}$ spectrum around 60 keV is split into two parts, one due to events where entire energy is deposited in one anode, and second where the energy is split between two anodes and is then added as one of the energy is the Xe K rays range. This gives rise to an asymmetry in this peak. The energy resolution of the two peaks is also different. The effective resolution of this peak quoted in the table above is in between that for the two peaks. The fitted resolutions for the four peaks are shown in figure, which also gives a linear spline interpolation for σ^2.

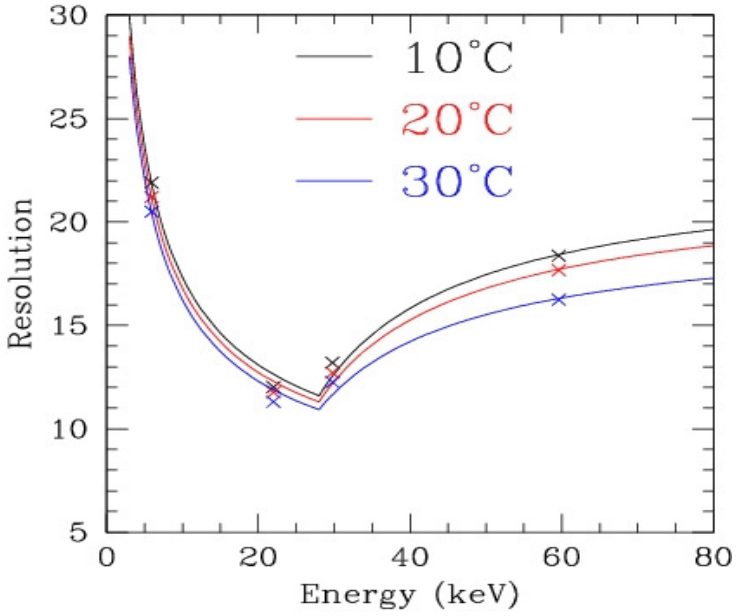


At 20 C, the channel number is given by $e_0$=-3.3 keV, $e_1$=9.16 $keV^{-1}$, $e_2$=0.0018 $keV^{-1}$. These fitted parameters are used to generate the response matrix for the detector.

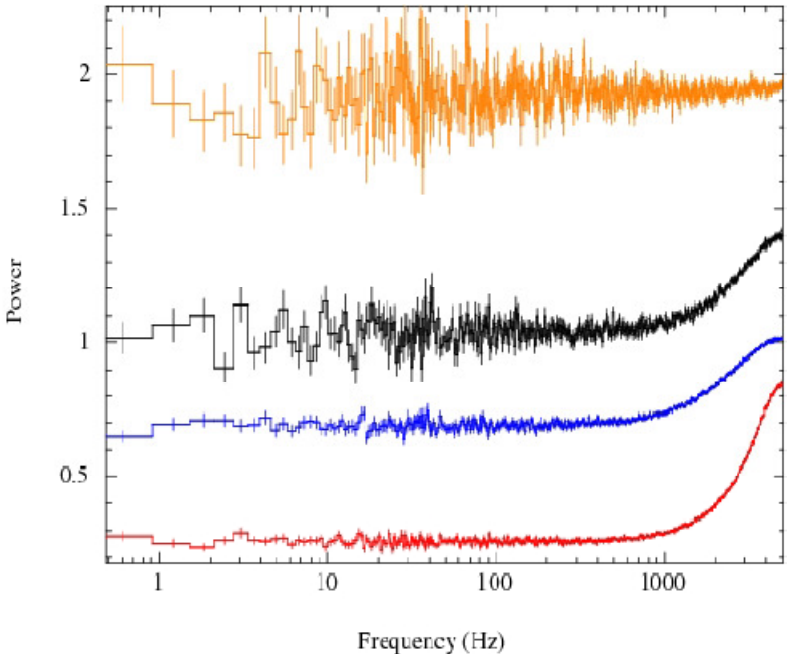


*Power spectra obtained from event mode data at different count rates.*

The timing characteristics of LAXPC event mode data is as expected (featureless) at frequencies below 390 Hz corresponding to bin size of 2.56 ms. The power density spectra obtained from light curves at different rates up to 12500 c/s are shown in above figure. At higher count rate, the spectra shows lesser power which is expected due to the dead time of the LAXPC processing electronics.

### Expected background in different energy bands

Background spectra in the laboratory is shown in figure below. To estimate the background in orbit we did GEANT4 simulations for photons and charge particles with various energies. These simulations included the collimator as well as shield surrounding the detector. It appears that major contribution may be due to diffuse X-ray background. For this purpose we assumed a background flux of 87.4 $E^{-2.3}$ $cm^{-2}$ $s^{-1}$ $keV^{-1}$ $steradian^{-1}$. The estimated background combining all 3 LAXPC detectors is shown in the figure. The actual background in orbit can only be measured after launch of Astrosat.

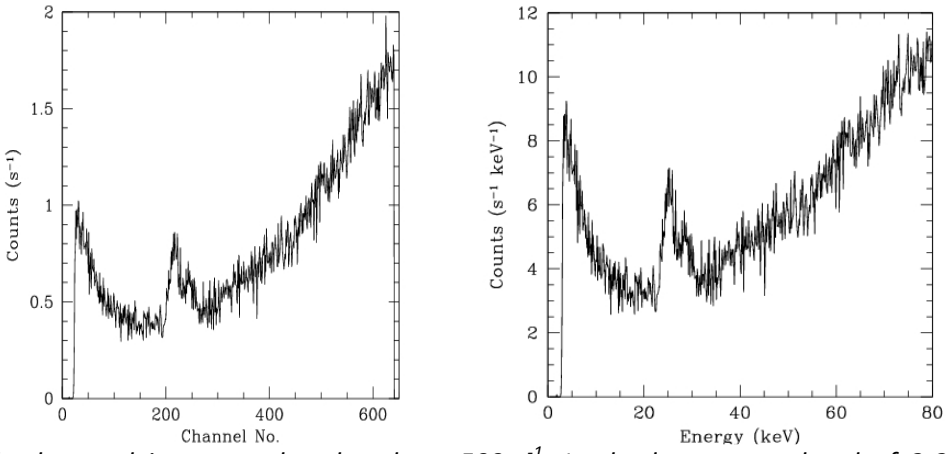


*The total background is expected to be about 500 $s^{-1}$. In the low energy band of 3-20 keV the background is about 80 $s^{-1}$.*

### Time exposure for sources of different intensity

Using the response matrix generated it is possible to simulate the response of detector at different energy spectra. The figure shows the response for different monoenergetic sources.

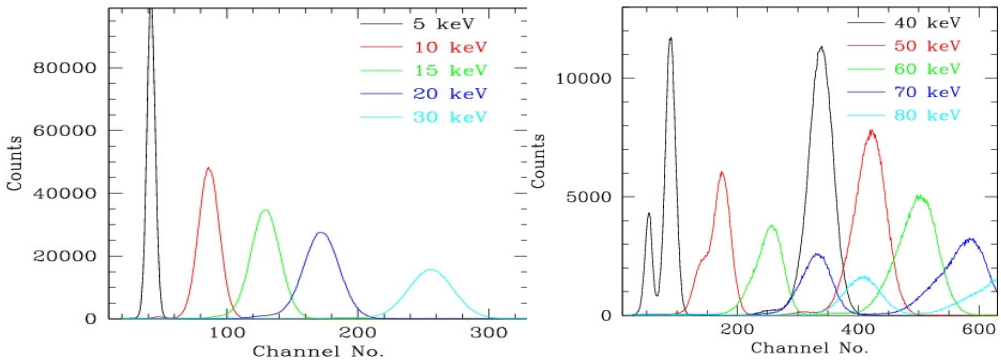


*The simulated spectra for the Crab source with 100 s observation is shown in the figure. This gives a count rate of about 6000 $s^{-1}$.*

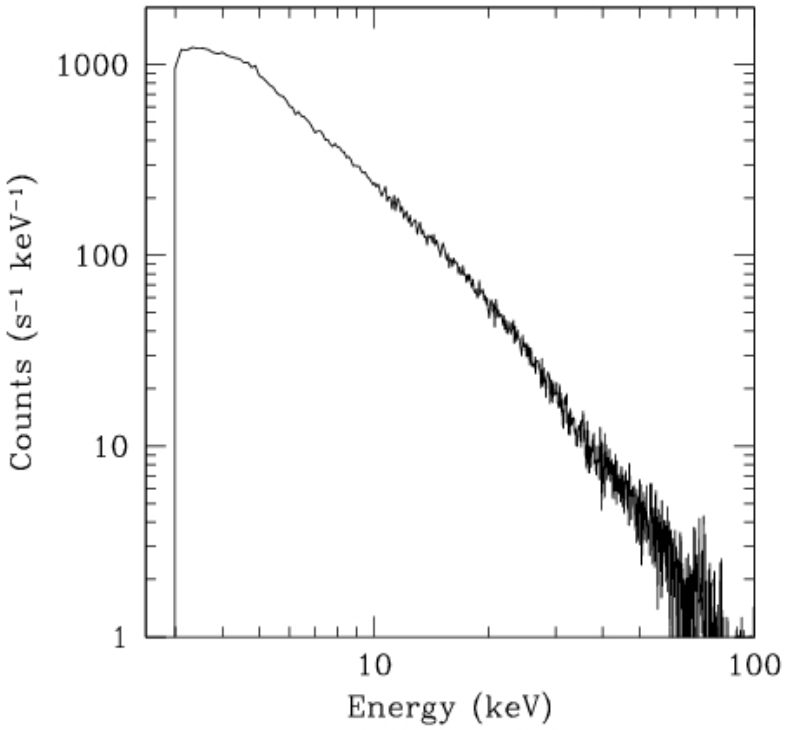


For a 1 mCrab source observation over 100 s can detect it at 3σ level in 3-80 keV. If the energy range is restricted to 3-10 keV, the detection improves to 6σ level.

## Observation Strategies for LAXPC

- Time tagged photons for periodic and fast time variability studies
- Spectral features using individual photon energy measurement data
- Fast timing mode data for bright and bursting sources
- Broad Band Counting (BBC) for quick study of time variability

Integration time for the BBC will depend on the source intensity and time scale of variability.

- For studying variability over time scale << 1 sec, use BBC integration time of 8 / 16 msec, for a few sec variability use 64 / 128 msec and for still slower variations use 1.024 sec BBC BIN time.
- For study of fast pulsars (e.g. 33 msec pulsar in Crab Nebula) or millisecond accreting pulsars or rotation powered pulsars of << 1 sec period use time tagged photon data**.**
- For very bright sources like Sco X-1, Cyg X-1, Crab Nebula, Bright Transients etc that may give a count rate of about 10 k per sec or more, use time tagged photon data for variability and spectral studies.

## On-board Purification

Each of the LAXPC detectors will have an onboard gas purification system. This system will be operated as and when required to purify the gas filled in the detector by command. Since operating power required for purification system is large, all the three LAXPC detectors as well as their associated processing electronics will be powered down before gas purification system is powered up.

Chapter 5

# Cadmium Zinc Telluride Imager

The Cadmium Zinc Telluride Imager (CZTI) is one among the four X-ray instruments on ASTROSAT. It is a hard X-ray imaging instrument covering the energy band from 10 to 100 keV, has a detector area of 976 $cm^2$ constructed using CZT modules and uses a Coded Aperture Mask (CAM) for imaging.

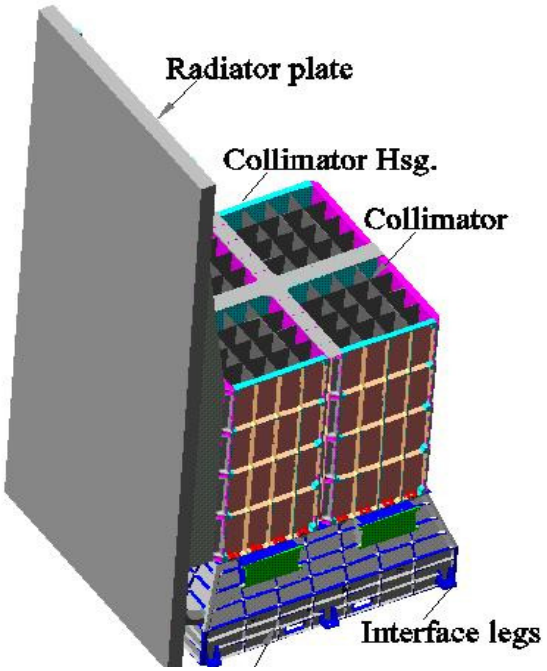


*Figure 5.1: The Cadmium Zinc Telluride Imager (CZTI)*

The characteristics of the CZT-Imager are given in Table 5.1 (Figure 5.1). The total detection area of 976 $cm^2$ is achieved by the use of 64 CZT modules of area 15.25 $cm^2$ each. These 64 modules are arranged in four identical and independent quadrants. The overall dimensions of the CZTI are shown in Figure 5.2 and the orientation reference is shown in Figure 5.3. The CZT detector is interfaced to a radiator plate which maintains an operating temperature of 0 to 15 deg Celsius by passive cooling. The instrument is mounted on the satellite deck with the radiator plate looking in the direction of the satellite +Yaw axis. Collimators above each detector module restrict the Field of View to 4.6deg x 4.6deg (Full Width at Half Maximum) at photon energies below 100 keV. At energies above that the collimator slats and the coded mask become progressively transparent. For Gamma Ray Bursts, the instrument behaves like an all-sky open detector.

The CZTI carries a Cesium Iodide (Tl) based scintillator detector for Veto measurements. This is located just under the CZT detector modules. Further, there is a gap of about 8 cm between the base of the collimator slats and the detector plane, in order to accommodate a radioactive calibration source module in each quadrant. This source shines alpha-tagged 60 keV photons on the CZT detector in order to help calibrate the energy response.

The science objectives of the CZTI include the measurement of curvature and reflection components in the spectra of Active Galactic Nuclei and X-ray binary systems, the study of Quasi-Periodic Oscillations at hard X-ray bands in accreting neutron star and black hole systems, cyclotron line spectroscopy of high mass X-ray binaries, the characterization of hard X-ray spectra of magnetars as well as the detection of gamma ray bursts and the study of their early light curves.

**Table 5.1: Characteristics of the CZT-Imager**

| | |
|---|---|
| Area | 976 $cm^2$ |
| Pixels | 16384 (64 modules of 256 pixels each) |
| Pixel size | 2.46 mm X 2.46 mm (5 mm thick);<br>edge row pixels are 2.31 mm wide instead of 2.46 mm |
| Read-out | ASIC based (2 ASICs per module) |
| Imaging method | Coded Aperture Mask (CAM) |
| Field of View<br>(10-100 keV) | $4.6^o$ X $4.6^o$ FWHM (primary FOV)<br>$11.8^o$ X $11.8^o$ FWZM (incl. illumination leakage) |
| Angular resolution | ~ 8arcmin (18 arcmin geometric) |
| Energy resolution | ~ 8% @ 100 keV |
| Energy range | 10 – 100 keV<br>Up to 1 MeV (Photometric); no imaging above 100 keV |
| Sensitivity | 0.5 mCrab (5 sigma; $10^4$ s) |
| Memory | 50 Mbytes per orbit |

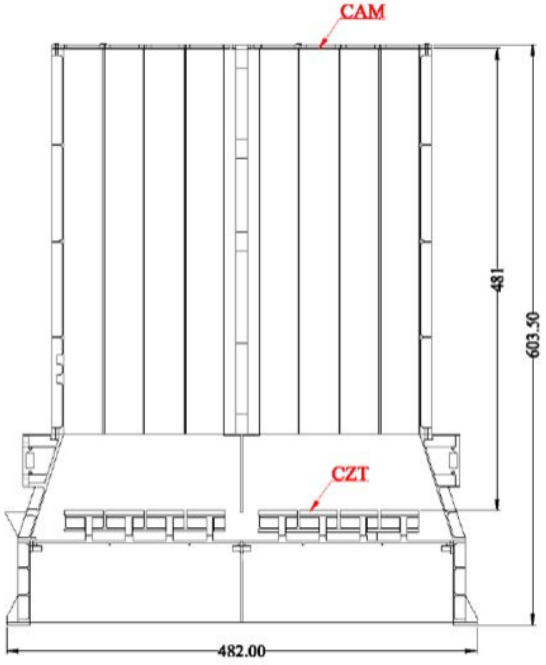


***Fig 5.2: Overall Dimensions of the CZT-Imager***

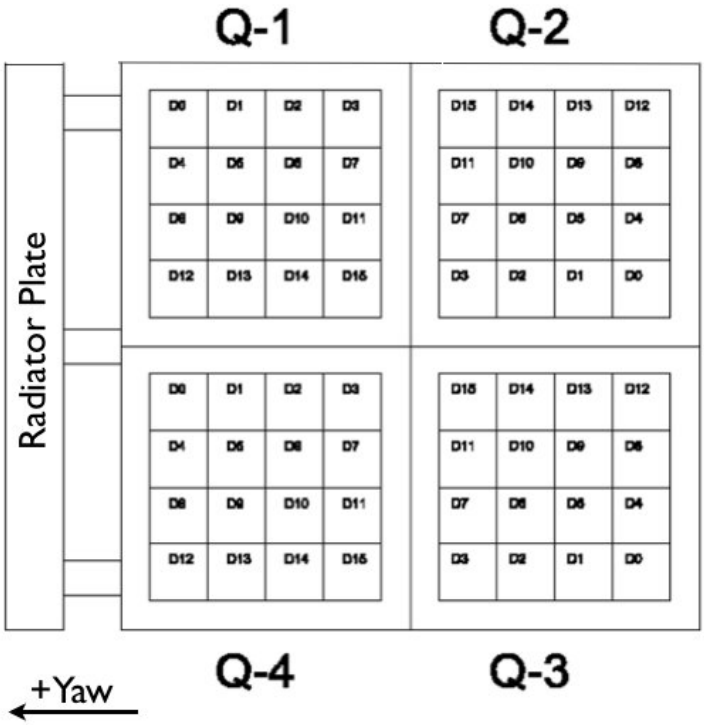


***Fig 5.3: Orientation of the CZT-Imager and the reference nomenclature of the four quadrants. The x-axis of the detector plane is identified with the negative Yaw axis of the satellite.***

## Detector Module Details

The CZT-Imager detector box contains Cadmium Zinc Telluride as the main X-ray detector and a CsI (Tl) crystal is used as a veto detector for background reduction. The Front-end electronics in the detector box handles the outputs from both the detectors for further analysis while low voltage and high voltage supplies provide the necessary power and biasing voltages to the detectors. In addition to these two detectors an alpha-tagged X-ray source is also used for calibration purposes (Rao et al. 2010, NIMA, 616, 55) .

a. The basic detector module is a CZT crystal of size 39.06 mm X 39.06 mm and 5 mm thick. It is pixelated by contact points on one side with a pixel size of 2.46 mm X 2.46 mm, except for edge rows which are 2.31 mm wide. The edge pixels are thus 2.31mm x 2.46 mm in size, and the corner pixels are of size 2.31 mm X 2.31 mm. One detector module thus becomes an array of 16 X 16 pixels of CZT. The overall geometric area (976 $cm^2$) of the instrument is achieved by using 64 detector modules divided into four quadrants, eachquadrant containing a 4 x 4 matrix of detector modules mounted on a special thermal conductive board called as the Detector board.

   A passive collimator (FOV of 4.6 deg X 4.6 deg FWHM) helps in allowing nearly parallel X-rays to enter the detector. A Coded Aperture Mask (CAM) made of tantalum is positioned above the collimator.Each individual pixel is connected to a pre-amplifier, which is embedded in an Application Specific Integrated Circuit (ASIC) containing 128 channels. Two ASICs are situated just behind the

detector wafer. The X-ray detector has a detection efficiency of 95% within 10 - 120keV and good energy resolution (~ 8 % at 100 keV).

The ASIC is a fully data-driven charge signal acquisition chip. It provides digital output corresponding to the detected X-ray energy and digital address of the incidental pixel.

b. The veto detector is a CsI (Tl) scintillator of size 167 mm X 167 mm and 20 mm thickness viewed by two one inch Photo-multiplier tubes (PMT) positioned on two sides of the crystal. Minimum detection sensitivity is 50 keV for incident photons. The CsI detector requires High Voltage (HV) of the order of 800 V, which is generated by the electronic circuits in the Crystal Holder.

c. Another CsI (Tl) 10 mm cube crystal viewed by a photodiode of 10 mm square area and embedded with a radioactive source $Am^{241}$ is placed on top of the CZT detector. At every disintegration of an $Am^{241}$ nucleus, a 60 keV photon is generated, accompanied by an alpha particle of energy of about 5 MeV. The alpha particle is absorbed in the small CsI (Tl) detector whereas the 60keV X-rays escape from this detector and in a very substantial number of cases interact in the CZT detector. The alpha particle gives a light pulse in the CsI (Tl) crystal which in turn is converted into an electrical pulse at the output of the photo-diode. Any output in the CZT detector coincident with the pulse output from the CsI (Tl) detector is deemed to be originating from a 60 keV photon. This method is used to calibrate the CZT detector for its energy response.

## Mechanical and Thermal Design

The mechanical parts of the CZTI consist of the following:

### CZTImager Housing

The housing is made out of blocksofAluminum alloy to increase the integrity of the payload. It has an overall dimension of 482 mm x 482 mm x 195 mm height. All peripheral walls (vertical & slant) of the housing are configured with suitable ribs and minimum wall thickness. The top half of the housing has circumferential as well as central flanges which are suitably stiffened by providing gussets and stiffeners to withstand load coming from collimator housing which will be integrated on this.

### Crystal Holder

CsI crystal holder is a sub-assembly interfaced with the Detector housing and it accommodates (1) the CsI crystal (2)a Power Card with HV DC-DC, pre-amplifier and power electronics**.** The CsI crystal is mounted on top of the housing and is held by a clamp specially designed for it. The Power card is assembled on the rear side of crystal housing.

### Detector Board Assembly

The Detector Board consists of a PCB to mount the 16 detector modules, Front-end Electronics Board (FEB), and a specially designed Internal Radiator Plate which acts as an interface between the detector modules and the heat pipes so that uniform temperature is maintained across all detector modules.

**Functions of detector board assembly:**

- Holding the CZT detector modules in a specified format.
- Providing interface to the Detector housing.
- Providing interface to the Calibration housing.
- Providing interface to the heat pipes.

### Radiator Assembly

The CZT modules perform best in a temperature range of 0° C to 15° C. To achieve this temperature, the heat produced by CZT module (300 mW/module) is drained continuously by the radiator assembly, which consists of (i) Heat pipes (3 nos.) (ii) Radiator plate and (iii) Spacers & clamps. The radiator plate area required to radiate the total power of 50 W is about 7000 $cm^2$.

### Collimator

The Collimator plates are made of 0.07 mm thick Tantalum sheet sandwiched between 0.2 mm thick precisely machined Aluminium alloy plates, providing a collimation of 4.6 (deg) X 4.6 (deg) FWHM directly under the collimator. However since a gap of 100 mm is left between the bottom of the collimator and the detector plane to accommodate the calibration housing, a certain amount of illumination leakage occurs from one collimated module to its adjacent neighbours. When this illumination overlap is taken into account, the net field of view works out to be 11.8 (deg) x 11.8 (deg) FWZM.

### Collimator housing

The Collimator housing is a hollow structure, configured quadrant wise, with a single quadrant 167.5 mm x 167.5 mm x 400 mm, made up of four aluminum alloy side plates, which are integrated side-by-side using M4 fasteners.

## The Coded Aperture Mask

The design of the CAM for the CZTI is such that the size of the mask plate is the same as that of the detector itself. The mask is made of a 0.5 mm thick Tantalum plate in which a pre-determined pattern of holes is cut to allow X-rays to pass through. The Coded Mask forms the topmost part of CZTI payload. It is coded by open and closed pattern of squares/rectangles matching the size of the detector pixels. Additional support bridges of thickness 0.2mm are introduced at a number of places within the pattern to improve its mechanical stability. In such a design (called a 'box-type' or 'simple' system) exposure to the full mask pattern is not possible anywhere except exactly at the middle of the coded field of view. At all other angles only a part of the shadow of the mask falls on the detector. The patterns are based on 255-element pseudo-noise Hadamard Set Uniformly Redundant Arrays. Of sixteen possible such patterns, seven were chosen on the basis of the mechanical support for individual pixels in the pattern. These seven patterns, with some repeats, were placed in the form of a 4 x 4 matrix to generate the CAM for one quadrant. This same pattern is placed on other quadrants, rotated by 90deg, 180 deg and 270deg respectively.

## CZTI Detector Electronics

The CZT detector box electronics consists of

1. The front end electronics for CZT module.
2. Pre and Post amplifiers for Veto detector Cesium Iodide {CsI (Na)}.
3. Pulse height (PH) analyzer for Veto.
4. Alpha source detector CsI (Na).
5. Logic circuits to handle the data.
6. The high voltage DC/DC converters.
7. Interface circuitry for communication with CZTI Processing Electronics.

The CZT-Imager detector box contains Cadmium Zinc Telluride as the main X-ray detector and a CsI (Tl) crystal is used as a veto detector for background reduction. The Front-end electronics in the detector box amplifies pulses from both the detectors for further analysis while low voltage and high voltage supplies provide the necessary power and biasing voltages to the detectors. In addition to these two detectors an alpha-tagged X-ray source is also used for calibration purposes.

The front-end electronics is made into four identical quadrants. All analog electronics is housed in the detector box itself and it contains ASIC control, amplifiers etc. Apart from Detector Board, Alpha card and the Power Card, there will be one electronics card per quadrant called the FEB which includes ADCs, digital control and FPGA. The Processing Electronics (PE) is housed separately and it contains an FPGA with an embedded processor. The PE controls all satellite interfaces, detector interfaces and it handles onboard memory and data management.

### Basic Design

One CZT module contains 2 ASICs and hence one quadrant will have 32 ASICs daisy chained to each other. A veto-detector of CsI (Tl) crystal is kept below the main CZT detector. An alpha-tagged radio-active source is used for onboard calibration. The CZT Detector houses four identical quadrants.

**List of Major Components of CZT-Imager Quadrant**

| **Name** | | **Components** | **Mechanical Location** |
|---|---|---|---|
| CZT Detector Assembly | | Detector Modules | Detector Board Assembly |
| | Detector Board | | |
| | Internal Radiator | | |
| | FEB | | |
| HV-CZT | | Pico DC/DC | Detector Board Assembly |
| Veto Detector | | CsI(Tl) + 2 PMTs | CsI Assembly |
| HV-Veto | | HV DC/DC (800V) | CsI Assembly |
| Alpha Tag | Am (241) | Alpha-Box | |
| FPGA Card | | FPGA, processor, | Processing Electronics Box |
| | interfaces | | |

The detector assembly consists of an array of Detector Modules which is an integrated unit of CZT detector and ASICs, procured from Orbotech Medical Solutions, Israel. The detector assembly contains a Detector Board with 16 CZT Modules with 32 ASICs daisy chained. An aluminized Mylar sheet of 50 micron thickness is kept on top of the detectors to provide thermal isolation.

### Veto Detector

A detector (CsI) covers the large area of 256 $cm^2$and the light collection is done using two photomultipliers (PMT), viewed from sides. On registering an event, a signal from the detector is sent to a pre-amplifier. This signal is processed and sent to the FEB for further analysis. After amplification of the signal from pre-amplifier, the signal is sent to a comparator via stretcher along with LLD level signal. If LLD is triggered the pulse is digitized to an 8-bit output by ADC through control circuit. This output is used to differentiate Compton scattered events and hence the background in main detector can bereduced.

### Power Card

The Power card, positioned in the Crystal Holder, has a Pico high voltage generator for biasing the veto detector. A positive high voltage around 800 V is used to bias the Photomultiplier tubes attached to Veto detector. Similarly another negative high voltage, from another Pico DC/DC converter, is used to bias the CZT detector. The Power Card also generates appropriate regulated low voltages for the CZT modules and it alos houses the amplifiers for the CsI detector.

### Alpha - Tag

A calibration source of Am (241), is kept to shine over the detector. A energy of 60 keV is released from the source along with an alpha particle simultaneously. This alpha particle gets detected in the CsI (Tl) detector volume which generates the signal. The photodiode which is coupled to this CsI (Tl) detector generates an electrical pulse, which is amplified in pre-amplifier and post-amplifiers. Postamplifier signal is fed to an analog comparator along with lower-level discriminator level. A relevant digitized signal generated with help of Monoshot is passed on to FPGA as an alphatag event.

### Front-end Electronics Board (FEB)

The FEB contains interface circuits required for the CZT modules as well as the Processing Electronics. A FPGA is used to handle the signals from the three different detectors (CZT, Alpha and CsI Veto) and data is stored in a memory to be transmitted to PE, every second. The coincidence among different detectors are done digitally by ground data processing.

## Processing electronics

The functions of the processing electronics includes reading, analyzing, storing and/or transferring detector data to satellite via data formatter. Also it controls the FPGA in the FEB using 16-bit serial commands.

There are two types of memories, namely

a. RAM: This holds all types of data like detector data and commands, telecommands and telemetry data.
c. EEPROM: This holds the basic software and the default parameters. Initially all parameters arecopied from EEPROM and then any changes sent bytelecommands are stored only in the RAM.

**About FPGA:** this is mainly a hardware compressor, in that it compresses the overall hardware into one single chip. This handles the following functions:

a. Timer.
b. Detector communications.
c. Telecommands.

During an event in the detector package, the same is analyzed and stored in one of its ping-pong memory, by its FPGA. The CPU interrogates the detector FPGA every 1 second. Upon receiving this signal the FPGA stops storage in the first of its ping-pong memory, resumes storage of data in the second memory and, upon command from the CPU, transfers data from the first memory to processing electronics. This FPGA based data are stored directly into a pre-determined space in the CPU memory. Data from all the 4 quadrants are read simultaneously (the entire data transfer at 500 kHz takes about 131 ms). The CPU then starts analyzing the stored data according to its operating mode.

**Data Organization in Detector Package**

The detector package contains a FPGA to analyze data from ASICs, store it in its RAM andsend it to the electronics package. All the ASICs are daisy chained hence the inputs and outputs of all 32 ASICs in a quadrant are controlled by a single FEB.

## Modes of Operation

The CZTI can operate in 16 possible modes. Fifteen of these are primary modes, and there is one Secondary Spectral Mode which runs in parallel with other primary modes. The description of these modes are as follows:

**Normal Mode:**
This mode transmits complete raw data received from the detector box. This takes up 144 Mbytes per 100-minute orbit. This is the default mode of operation of the CZTI.

**SAA Mode:**
When the detector is in the South Atlantic Anomaly (SAA), or if both the CZT and the Veto High Voltage supplies have been turned off by ground command, only header data is transmitted directly from the event frame. The header data of each second is extracted and compiled into one quadrant header packet every 100 seconds.

**Shadow Mode:**
The Shadow Mode is selected if the Earth Shadow Entry command is sent from ground. In this mode the header data of a 100-s window is sent at the 100-s boundary. The Frame/packet format is similar to the SAA mode. Each frame contains only one packet.

**Secondary Spectral Mode:**
This mode runs in parallel with any other selected mode. The on-board software prepares the spectral data of each quadrant every second. The integrated spectra so prepared is packetized and sent to the Satellite Bus storage (Solid State Recorder) once every 100 seconds.

### Reduced Data Modes

Reduced Data Modes can be entered either by ground command or due to limited memory availability.
The following reduced modes of operation are available:

**Fixed No. of Packets (FP):**
The frame format here is similar to the normal mode but a fixed maximum number of packets are generated from each quadrant.

**Veto Spectrum Disabled (VSD):**
Packets are generated without the Veto Spectrum.

**Two word event report (2WE):**
The number of words representing each event is reduced from 3 (as in normal mode) to 2, by sacrificing some resolution in time and energy.

**Memory Management (MM):**
The behavior of Memory Managed modes depends on the level to which the payload memory is occupied due to the Satellite Bus storage allocated to the CZTI being full. At different levels, Full data, only Secondary Spectral Mode data and Header data or the Header data alone could be recorded. Beyond a certain level no data is recorded.

A number of combinations of the reduced modes are possible, e.g., SAA+Shadow, VSD+2WE, VSD+FP, FP+2WE, FP+2WE+VSD, MM+SAA, MM+Shadow and MM+Shadow+SAA.

## Data Interfaces

The two main interfaces are namely:
1) Detector Interface.
2) Satellite Interface.

### Detector Interfaces:

The unit's interface with the detector electronics unit involves the following:

**Event Interface:**
The FPGA of each quadrant reads data from the detectors, arranges it in the form of a 2 x 2 Kbytes frames This is read periodically by the processing electronics every 1 second. This data is then further analyzed and accumulated or transmitted to the satellite via data formatter.

**Command Interface:**
The Command interface with the detector unit is done serially with clock & data lines.

### Satellite Interfaces:

The unit's interface with the satellite involves the following:

**Power Interface:**

The raw power is routed through a relay, which is switched ON/OFF by command from ground followed by a series of transfers to the motherboard. There are two separate lines for main & redundant power.

**Command Interface:**

There are 13 Pulse commands & one 32-bit data command with the facility of sending data commands in a time-tagged mode.

**Telemetry Interface:**

This interface is to a Solid State Recorder (SSR) via a data formatter. Data is sent periodically, typically every 8 ms, to the formatter in the form of 2 Kbytes frame at 2MHz clock rate.

## Background Estimation

The sources of background in the CZT detector are primarily cosmic diffuse gamma rays and gamma-rays originating from the satellite structure (spallation background) due to the interaction of cosmic rays.

To distinguish these background counts from the real source counts a slab of CsI is placed under each block of CZT. The high energy photons which deposit energy in CsI as well as CZT are rejected by anti coincidence techniques and hence do not contribute to the background counts in CZT. Only the photons which deposit partial energy in CZT but do not interact in the CsI block generate background counts in the (10 - 100) keV region.

### Compton Induced Background

Assuming an outer space environment where the satellite is deployed, some of the background count estimates have been simulated and the values are described here. The total number of background counts in the CZT due to single Compton scattering are calculated by summing up all the contributions over the entire energy range of injected gamma rays and the typical counts are about 20 counts/sec for CsI thickness of 2 cm.

### Fluorescent K-alphaBackground

Cosmic diffuse gamma ray photons in the energy range (10 - 100) keV interacts with Tantalum by photo-electric effect and produce fluorescent Kα X-rays. The fluorescent X-ray contribution to background contributions can be divided in 3 parts:

**(a) Contribution from the top surface,**

This surface is made up of Tantalum of thickness 0.5 mm. The total area of a module is 15.25 $cm^2$ but the effective area is half that due to the random holes of the CAM. It is far from the detector and subtends a small solid angle at the detector plane. The total counts from this surface are about 0.0025 counts / sec.

**(b) Contribution from 4 cm x 36 cm upper side surfaces.**
This side is made of Tantalum sheet of area 4 cm x 36 cm and thickness 0.1 mm. Though this surface is large compared to the detector surface, it is perpendicular to detector plane and makes a small solid angle to the detector. The total count from this surface is about 0.41 counts / sec.

**(c) Contribution from 20 cm x 14 cm lower side surfaces.**
This is the lower portion of the side surface and as it is closer to the detector it contributes the maximum. The numbers of counts at the detector depends very much on the height of the side surface. The total counts from this surface are about 5 counts/sec.

## Data Analysis

### Image Reconstruction

The standard procedure adopted for image reconstruction will consist of first binning the data to produce a detector plane image (DPI), which is then cross correlated with the mask pattern. Significant peaks from this image are picked and a least square fit is then made of the DPI with theoretically computed shadow patterns for sources these locations. This allows accurate determination of the intensities of these sources, and also helps identify and eliminate spurious peaks that might have been picked from the cross-correlated image.

### Operation Sequence to generate the Data products

- Step 1: Download telemetry data for an observation period.
- Step 2: The good time interval file is generated using the house keeping information
- Step 3: Read the attitude information and generate average position of the satellite for the period of observation.
- Step 4: Extract the relevant data and generate the raw DPH or raw DPI.
- Step 5: The detector data (DPH) is processed to generate information about noisy and dead pixels for the time of observation.
- Step 6: Using information generated in steps 3 and 5, process the raw DPH/ DPI and clean them. Generate a detector mask file that records the pixels removed in the cleaning process.
- Step 7: Perform cross-correlation imaging and pick candidate sources from the image
- Step 8: Perform shadow fitting to estimate fluxes of candidate sources, reject insignificant candidates and iterate until all sources have fitted flux values above the detection threshold. (In generating shadow patterns for fitting the detector mask must be accounted for).

Chapter

6

# Scanning Sky Monitor

The science objective of SSM is to scan a large portion of the sky every few hours to detect and locate transient X-ray sources in the outburst phase, in the energy band of 2 to 10 keV. Therefore, it is required that SSM has a large field of view (FOV) with a good angular resolution so that once detected the position of the sources is known to a few arcmin resolution in sky co-ordinates. This is to enable other instruments on ASTROSAT and ground based observatories to conduct detailed observations of the source. In addition to this, SSM will observe known transient X-ray sources in it subsequent scans which will be used to generate long term light curves of these binary systems. This will help study of long term behavior of the observed transient systems.

## Instrument Description

SSM consists of three nearly identical one dimensional position sensitive gas-filled proportional counters with a coded-mask and associated electronics, each having a FOV of the order of ~$22^{o}$ × $100^{o}$. The assembly is mounted on a rotating platform to scan the sky. Figure below shows the picture of the three units of SSM mounted on a single platform. SSM is composed of three elements: the imaging element, the detector element and the associated electronics.

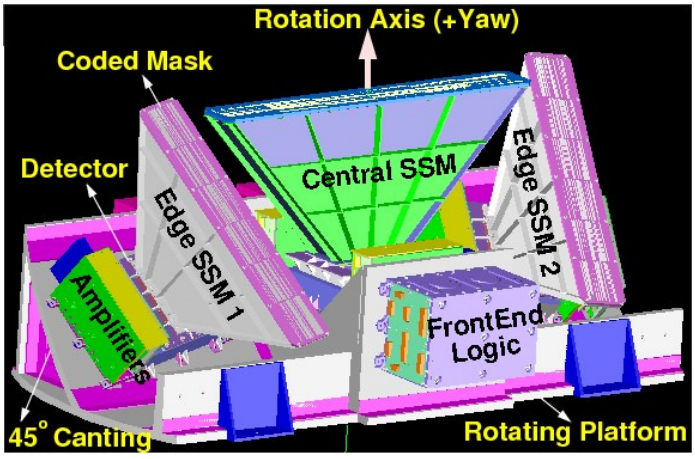


***Figure** 6.1 : Scanning Sky Monitor: Each of the three SSM cameras have their own electronics system (they are seen only for Edge SSM 1 in the figure and all others are obscured). The Central SSM will point towards the +Yaw axis, while the two Edge SSMs will be canted away by 45$^{o}$ from that axis. The entire assembly will rotate about the +Yaw axis.*

Effective area of SSM at 5 keV is 60 cm$^{2}$ and that at 2 keV is 12 cm$^{2}$. The window of SSM is aluminized Mylar of thickness 25 microns and this limits the detection efficiency at 2 keV. SSM detectors are position sensitive

detectors, position resolution of SSM at 6 keV is ~0.7 mm. Angular resolution of SSM is ~12 arcmin in the coding direction and that across is $2.5^0$. Energy resolution of SSM is 20% at 6 keV. Sensitivity of SSM is ~24 milliCrab for 10 minutes integration. Figure 1.1 shows the sensitivity curve for SSM.

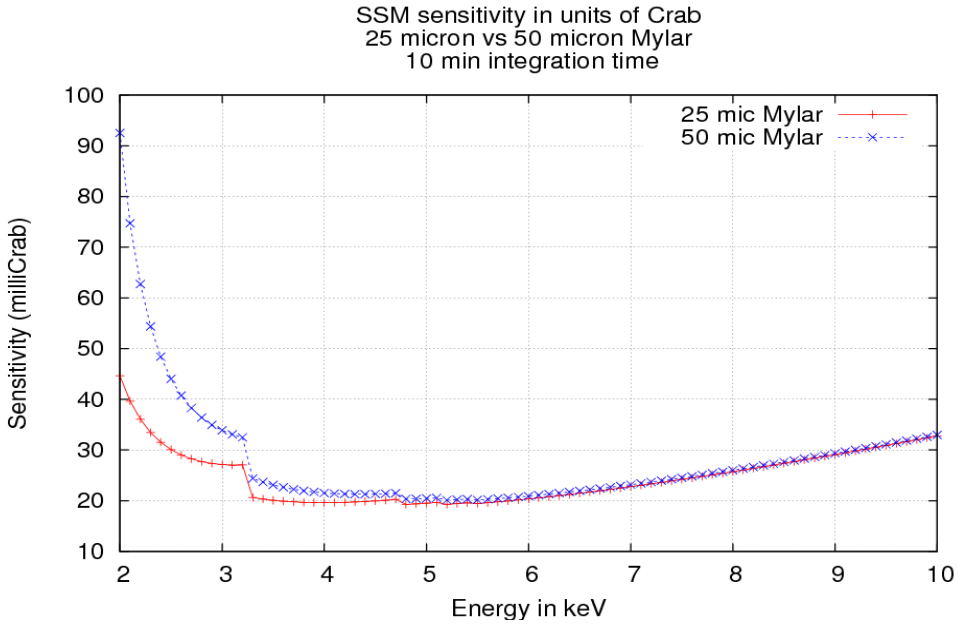


*Figure 6.2: Sensitivity of SSM with 25 micron Mylar window and 50 micron Mylar window*

## Detectors for SSM:

All three units for SSM have a position-sensitive proportional counter as the detector element. The detectors are multi-wire position sensitive proportional counters. There are eight anodes in each detector and the anodes are powered with a high voltage (HV) of the order of 1500 volts as compared to that of cathodes which are at zero potential. Many such cells (as shown in figure below) constitute the geometric area of a detector. These cells are enclosed in a gas-filled chamber having an entrance window thin enough to allow the incident X-ray photons into the counter. Figure 2 shows the schematic view of the cells inside

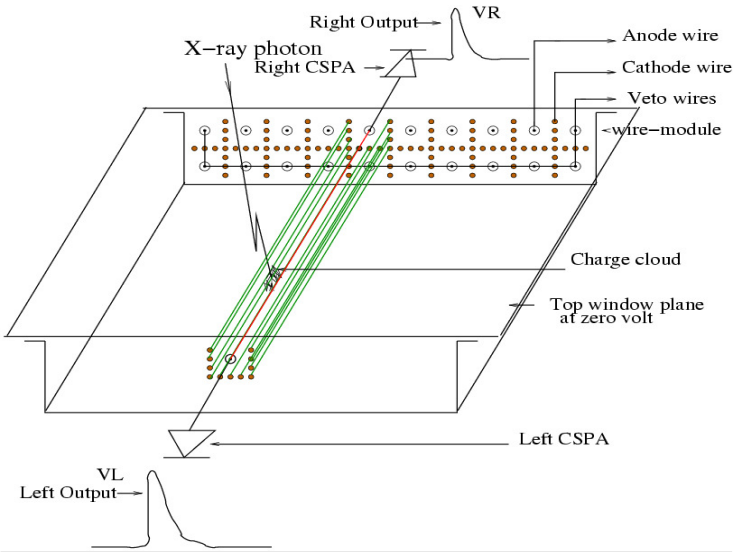


*Figure 6.3 : Schematic view of SSM cells. Only one of the cells is shown lengthwise, with a photon incident on the cell producing charge cloud at the anode.*

an SSM detector. The top layer consists of position-sensitive anode wires surrounded by wire-walled cathode forming individual cells. Figure 6.4 shows the photo of the wire module inside the detector.

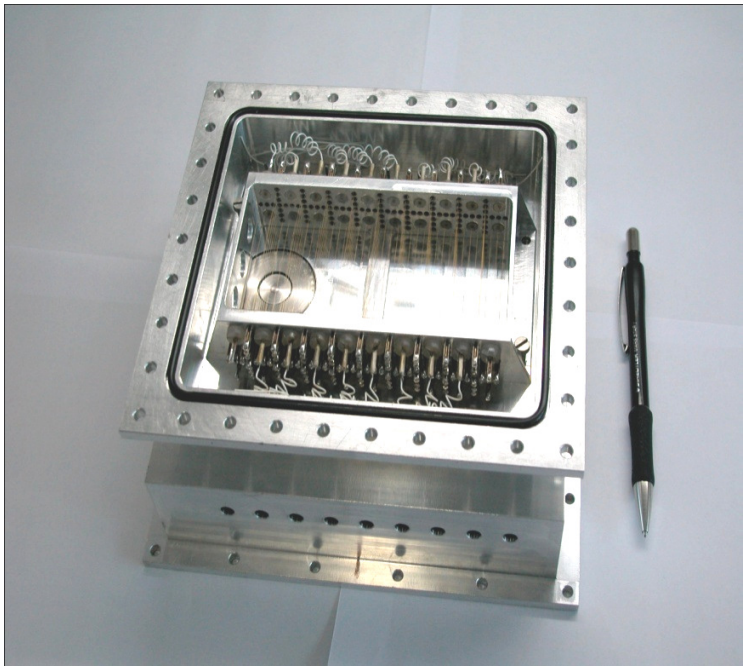

*Figure 6.4 : Wire module kept inside the detector*

**Principle of Operation:**

When an X-ray photon enters the gas chamber it ionizes the gas by photo-electric effect which leads to formation of several electron-ion pairs. The electrons are accelerated towards the anode resulting in further multiplication of the charge which is collected at the anode. In a position-sensitive detector the anode being resistive, the charge is proportionately divided to the two ends depending on the position where the charge cloud is collected along the anode wire. This charge is converted into voltage using a charge sensitive preamplifier (CSPA) at both the ends. The corresponding voltage pulses at either ends of the anode are referred to as left ($V_L$) and right ($V_R$) outputs of the anode. The total amplitude of both the outputs is proportional to the energy of the incident photon. The position (P) of the incident photon on the detector plane is given by $P=(V_L-V_R)/(V_L+V_R) *C_1+C_2$, where $V_L$ and $V_R$ are the amplitudes of the left and right output pulses and $C_1$ and $C_2$ are the calibration constants of that particular anode on which the photon is incident.

The SSM detector plane consists of two layers of wire-cells, central eight of the top layer being active anode cells. The two edge cells of the top layer and the ten cells in the bottom layer are all connected together to form the background or veto layer. The information that we get about every photon that is incident on the detector are 1. Time of arrival, 2. Energy and 3. Position of incidence. All the three parameters are measured using the electronics system of SSM.

## Design of Mask

Six different coded mask patterns could be generated for the constraints set in the specifications of SSM, with 50% transparency. They are joined sideways and the resulting complete mask plate is shown in figure 4. The design of the coded mask and the deconvolution software is developed in collaboration with Prof. D. Bhattacharya of IUCAA.

*Figure 6.5 : The coded mask plate with six different mask pattern used in each of the three SSM cameras.*

## Electronics for SSM

The Electronics system for SSM is composed of three units: (a) Charge Sensitive Pre-Amplifiers (CSPA) and post amplifiers (PA), (b) Front end electronics consisting of low voltage DC-DCs, HV programmer, logic unit for LLD/ULD/event-analysis, peak detectors, ADC, etc and (c) the Processing Electronics (PE) consisting of FPGA based system for event processing, buffer memory, telecommand and telemetry interfaces and the interface circuits for data transfer to Data Handling package. The detector is powered using High Voltage distribution unit mounted behind the detector. Figure 5 shows the block diagram of the detector with the electronics.

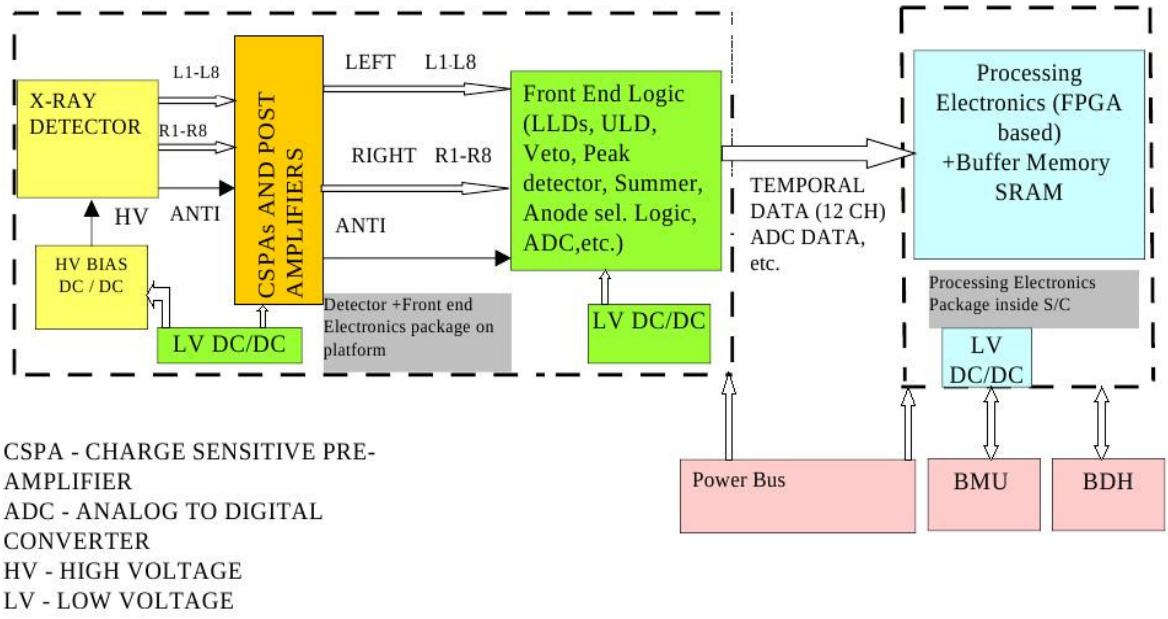


*Figure 6.6 : Block diagram of the Electronics System of SSM*

### Processing of an event

The charge collected at the anode for every photon incident is converted to a voltage pulse using a CSPA on either sides of the anode. The CSPA output is further shaped and amplified. There are seventeen such chains for each SSM detector unit, sixteen of them are connected to both ends of eight anodes and one of them is connected to the veto layer. The front end logic unit processes signals from each of these chains. Event outputs between Lower Level Discriminator (LLD) and Upper Level Discriminator (ULD) are accepted for processing. Charge particle rejection is done by the technique called anti-coincidence, where the event is rejected when (a) signals are present in both the top anode layer as well as the bottom veto layer simultaneously, or (b) more than one anode has an event simultaneously. The amplitude of every accepted event is measured and digitised and then the ADC output of each event, both left and right sides, are sent to the PE unit. In addition several channels regarding count rates of the anodes and veto, etc. are also sent to the PE. The PE which is a FPGA-based unit accepts these events, stores them in buffer memory and interfaces with the Data Handling system of the spacecraft. The PE also acts as both telecommand and telemetry interface for the complete SSM electronics system. The time of incidence of every photon is tagged with the event by the PE using an onboard SSM clock. This clock is periodically synchronised with the spacecraft BMU

clock. In addition, the electronics system also has circuitry for sensing and reducing High Voltage during high charge particle regions based on command-set thresholds and also corona sensing with auto-shutoff. Data from the PE is sent from the buffer memory through Data Handling and stored in the main spacecraft Solid State Recorder package for readout during visibilities. The detector and front end electronics packages are mounted on a rotating platform on the anti sun side of the spacecraft whereas the processing electronics is mounted inside the S/C. A flexible cable bunch is used between the packages.

**Table 6.1 : Technical details of SSM**

| | |
|---|---|
| **Detector** | One dimensional position sensitive gas-filled proportional counter |
| **Gas mixture** | 25% Xe + 75% P-10 (P-10 is 90% Argon + 10% Methane) |
| **Gas pressure:** | 800 torr |
| **Diameter of anode** | 25 micron |
| **Active length of anode** | 60 mm |
| **Type of anode wires** | Carbon-coated Quartz |
| **Diameter of cathode wires** | 75 microns |
| **Entrance Window** | 25 micron thick Aluminized Mylar |
| **Detector operating voltage** | ~1500 volts |
| **Unit Slit size of coded mask** | 0.95 mm |
| **Memory required** | 200Mbyte per orbit |
| **Payload weight & power** | ~45 kg; ~49 W |
| **Geometric area** | ~180 $cm^2$ |
| **Effective area** | 12 $cm^2$ @ 2keV ; 60 $cm^2$ @ 5 keV |
| **FOV** | Edge SSMs: $26.8^o \times 100^o$, Central SSM: $22.1^o \times 100^o$ |
| **Energy resolution** | 20% at 6 keV |
| **Angular resolution** | ~12 arcmin in the coding direction and ~$2.5^o$ across |
| **Time resolution** | 1 ms |
| **Sensitivity (Obs time)** | ~24millicrab (600s) (3 sigma, for one SSM) |

## Ground calibration

SSM ground calibration includes spectral and positional calibration. Spectral calibration is done to study and keep track of the gain of the detectors for SSM. Positional calibration of SSM detectors give the calibration constants to derive the position of every photon incident on the detector. This will be used to generate the image of the FOV of the sky observed by SSM.

### Spectral calibration

SSM detector is calibrated for spectral response at different energies in the range of interest. The energy range of interest for SSM is from 2 keV to 10 keV. The detector is calibrated at different energies to derive the Energy-vs-Channel relation, the Energy-vs-FWHM relation and the energy resolution at different energies. These relations are required to generate the response matrix of the detector. The position resolution at different energies is also estimated for SSM.

**Experimental tests at different energies**

Radioactive source Fe-55 gives X-rays of energy 5.9 keV (Mn $K_\alpha$ ) and 6.4 keV (Mn $K_\beta$ ). These energies are detected under a single Gaussian in gas proportional counters as the energy resolution is not good enough to resolve the two lines. Characteristic X-rays are used to calibrate the detector at different energies. The photon energies used to calibrate the detector are Ca $K_\alpha$ (3.69 keV), Ti $K_\alpha$ (4.51 keV), Mn $K_\alpha$ (5.89 keV, Fe-55 radioactive source) and Cu $K_\alpha$ (8.04 keV). The Ca $K_\alpha$ , Ti Kα and Cu $K_\alpha$ are produced by shining the continuum spectrum of an X-ray gun onto foils of respective materials to produce the characteristic X-rays. Thus, the detector is calibrated with four different X-ray sources within the energy range of interest.

The peak channels corresponding to different energies are estimated using a Gaussian fit to these different energy spectra. The energy resolution at different energies is also estimated from these fits. The relation between incident X-ray photon energy and peak channel is linear as shown in figure 7.5.1. The relation between energy resolution and energy of the incident photon is derived by fitting a function f(x)=a/Eb +c to the data. Using these inputs, response for SSM is derived. This will be used for on-board calibration using Crab observations.

The position resolution at different energies for SSM is also estimated. The position of every photon incident on one of the anodes is calculated with the respective anode-calibration constants and a position histogram is generated. The position spectra generated for various energies are fitted with Gaussian function. The FWHM of the fit results give the position resolution at different energies. Figure 7.5.2 shows the position resolution as a function of energy for one of the anodes in SSM.

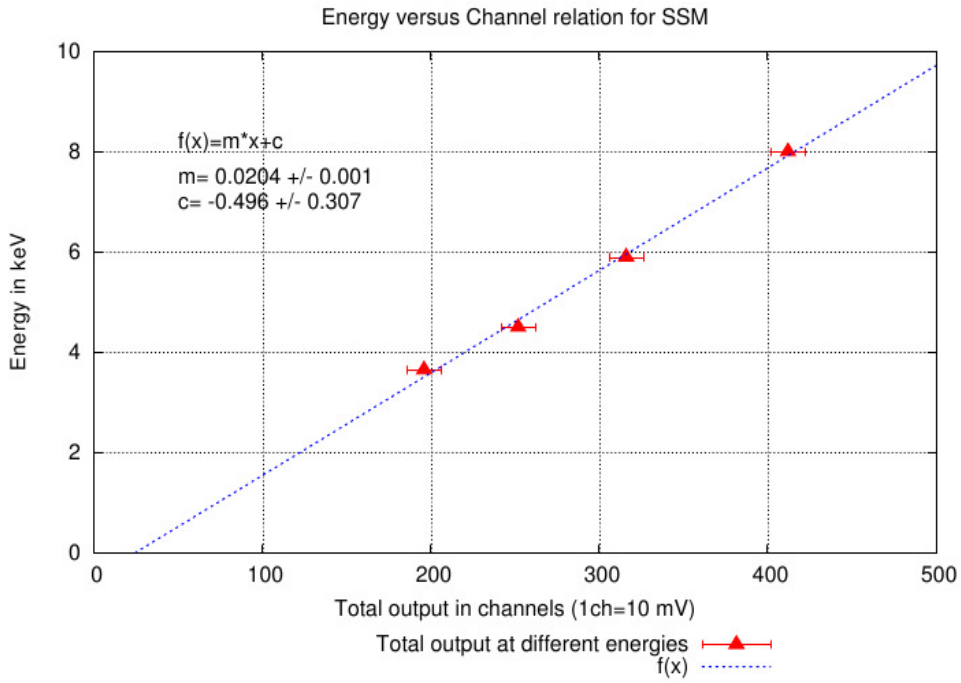


*Figure 6.7: Plot showing the energy-channel relation for SSM*

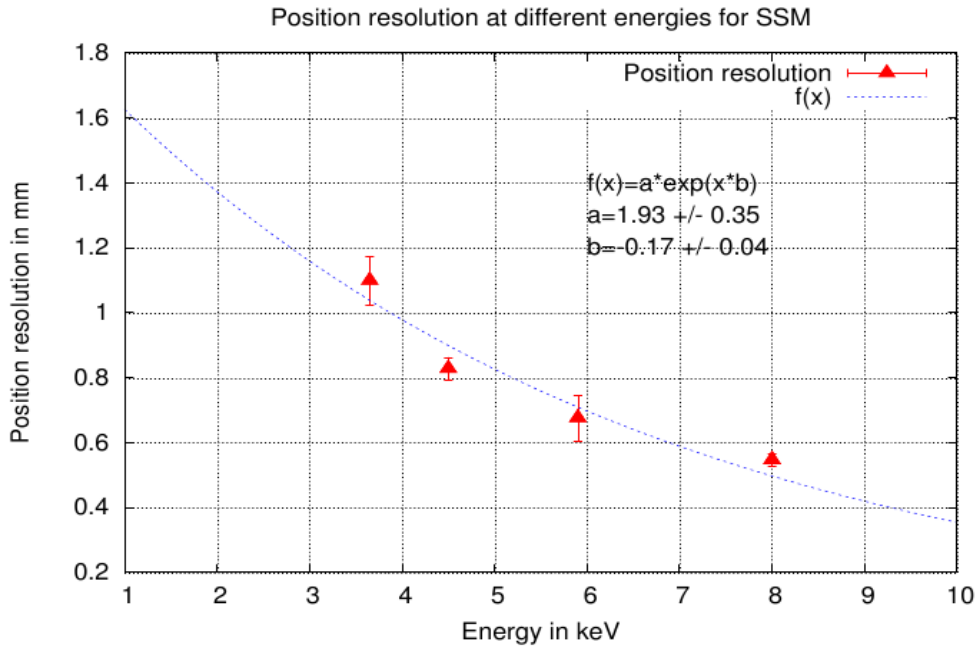


*Figure 6.8: Plot showing position resolution as a function of energy for SSM*

### Positional calibration

The position of a photon incident on the detector is determined from the ratio of the charge collected on either sides of the anode. It has been observed that for photons incident at the geometric centre of the anode, the left and the right output amplitudes are not the same and hence the calculated position using the charge ratio from the output pulses does not match with the geometric position. Therefore, it is required to calibrate the detector for its positional response and to get the correction factor, which are called the anode calibration constants, with respect to every anode in the detector. The anode wires are tested at every 1 mm along the length with collimated 55 Fe source and the non-uniformity is studied. In addition, the data from these tests are used to derive the anode calibration constants. Various experiments are carried out to verify the derived calibration constants. The details of the experiments and the results are discussed in SSM Test and Calibration document. The steps involved in positional calibration are discussed in the same.

## On-board Calibration

### Calibration with Crab nebula

The on-board gain calibration for SSM will be carried out using the Crab nebula. For any change in the gain, the energy-channel relation of the instrument changes. As the energy-channel relation changes, the spectral response also changes. Four different gains are considered here to study the variations in the observed spectrum of Crab. The gain factors which are the ratios of the nominal gain of SSM to the changed gain on-board (which could be due to contamination or leakage of gas) are taken as 0.5,1,1.5 and 2. These values indicate a variation of 50% decrease in the gain, the actual gain, 50% increase in the gain and 100% increase in the gain respectively. The spectral response for SSM is generated for these four different gains. Using these different responses, the pulse height spectrum of Crab is simulated. The pulse height spectrum shifts for

different gain factors. This indicates that the integrated counts in a defined range of channels is changing for different gain factors. Thus, from the observed Crab count at different epochs of the mission, the sensitivity of SSM can be calibrated.

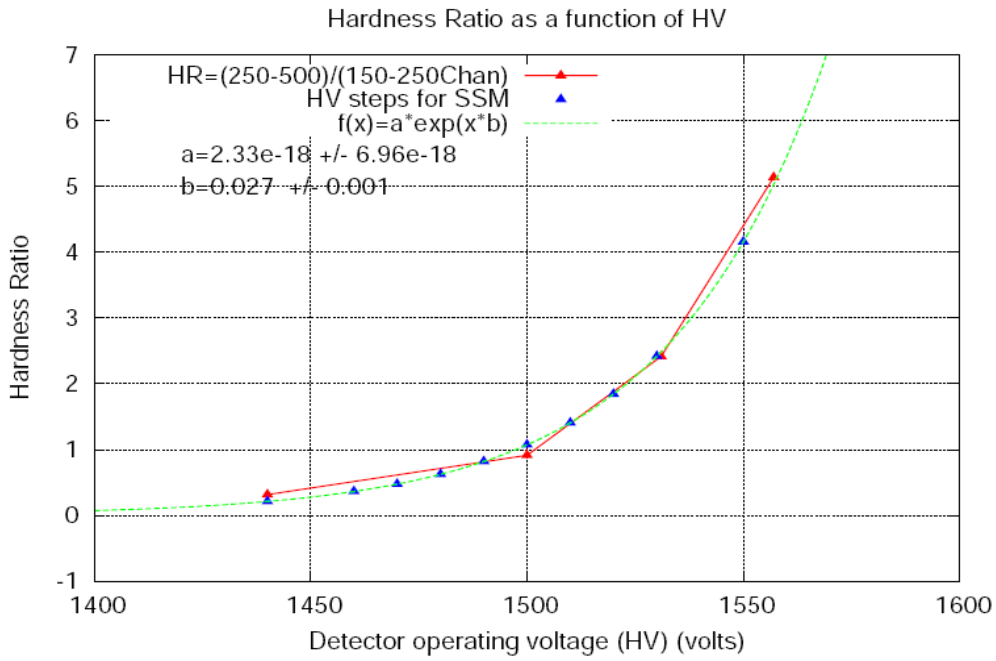


*Figure 6.9 : Hardness Ratio as a function of detector operating voltage*

The hardness ratio (HR2), which is the ratio of the counts in one band (250 to 500 channels) to the other band (150 to 250 channels) also changes. This hardness ratio is equivalent to the ratio of the flux in the energy bands 5 to 10 keV and 3 to 5 keV. Any 10% variation in the gas gain (ie. the gas factor is 1.1) can be detected from the variations in the hardness ratio calculated from observations of Crab nebula for an integration time of 10 minutes. Therefore, from the changes in the hardness ratio, the changes in the gain of the detector can be deduced.

Once the variation in the gain of the detector is estimated, the operating voltage of SSM can be tuned to bring it back to the nominally operating gain value. The HV for SSM are in steps of about 10 Volts around 1500 Volts, using which a 10% variation in the gain of the detector can be corrected. Figure 7.5.3 shows the variation in hardness ratio as a function of HV for SSM. The points in the plot shown in figure 7.5.3 give the steps available for tuning the operating voltage of SSM on-board. Thus, by observations of the Crab nebula, SSM can be calibrated on-board over a gain of ±50% about the nominal gain value, with the available small steps of HV, in the HV range 1440 to 1530 Volts.

Thus, the gain and sensitivity calibration of SSM can be done by observing the Crab nebula. Any variations in the gain, greater than 10% can be corrected by stepping the HV of SSM and for finer variations in the gas gain, correction factors can be applied to the data.

## Data Reduction and analysis methods

Data from SSM detectors are of two types, temporal and time-tagged. The temporal data gives the counts detected by the detector every 100 ms and the time-tagged data gives the information of every event detected in the detector. From the time-tagged data information like energy of the incident photon, position of incidence can be calculated. Using this data the shadow pattern cast by different sources in the FOV of SSM is derived, which is later used to derive the position of the sources in the FOV.

The Light curves of different sources in the FOV will be generated and will be made available to the public. The light curve in 4 different bands (2-10, 2-4, 4-6 and 6-10 keV) are expected to be made available in the SSM website.

(Reference for website and instructions will also come here)

Chapter 7

## Charged Particle Monitor

Satellites in the Low Earth Orbit (LEO) pass through the trapped radiation belts of the South Atlantic Anomaly (SAA), where the particle environment can change very drastically within a few tens of seconds. Due to high density of very high energetic particles (mostly protons), there are adverse scientific and technological effects like, glitches in the data, aging of the scientific instruments and even permanent damage to the detectors. Hence, this region should be monitored properly and all scientific instruments should be shut down/corrective action taken during the satellite's passage through the SAA region. The charge particle monitor (CPM) warns the satellite instruments about the approximate entry and exit points of this region and thus serves the purpose of a monitor.

The Charge Particle Monitor is an auxiliary payload on ASTROSAT. The main objective of CPM is particle count rate measurement above an energy threshold. The detector used for the Charge Particle Monitor is a CsI(Tl) scintillation detector. This has an entrance window of 0.12mm Teflon reflector along with 50 micron aluminized Mylar as the outermost layer. A thin copper box is put over the assembly as an IR protection. Specification of CsI(Tl) is mentioned in the table below. CsI(Tl) is preferred over more common NaI(Tl) which is hygroscopic in nature. A Si-Pin diode is placed on one surface of the scintillation crystal.

This crystal and photodiode assembly is much cost effective than semiconductor detectors, and lighter than scintillator photomultiplier assembly (as used in RXTE). Moreover, the photomultiplier needs high voltage biasing and the gain may vary with time. In such cases it is better to read out the detector output with a photodiode which can be rugged, compact and reliable.

| Scinti-llator | Type | Density | R.I. | Light output (% of an-thracene) | Decay con-stant (ns) | Wavele-ngth (nm) | Principal applica-tion |
|---|---|---|---|---|---|---|---|
| CsI(Tl) | Crystal | 4.31 | 1.788 | 95 | 1100 | 580 | Heavy Particle, $\gamma$ |

The detector light output peaks at 580 nm and the light intensity is proportional to the energy of the incident radiation. This light is proportionally converted to electrical signal by the photodiode. A charge sensitive preamplifier (CSPA) is used to amplify the photodiode output to milli volt range. CSPA is preferred over a voltage sensitive preamplifier as the output voltage of the CSPA does not depend on the intrinsic capacitance of the detector. Capacitance of the Si-Pin photodiode is likely to change with temperature. The detector, photodiode and CSPA are combined in a compact 1 $cm^3$ box made by SCIONIX, Holland to form the detector module.

We estimate that gamma-ray bursts and solar gamma-ray flares which give a measurable count (> 10 counts/s) above 0.5 MeV occur very rarely (a rate of less than once per year). The time-scale for detecting the entry and exit of SAA would be kept large enough to ignore even such rare events.

SAA occurs at an altitude of about 500 km spanning $-50^0$ to $0^0$ latitude and $-90^0$ to $+40^0$ longitude. This SAA region changes slowly over time dominant drift being westward of approximately 0.3 degrees/year (as reported in 1997) or somewhat greater. As a back up to CPM, it is envisaged that ASTROSAT will have time tagged commands to alert the entry/exit of SAA, based on a SAA model. The CPM will measure the intensity of energetic charge particle rates and help in refining this model.

## Instrument details

The Charge Particle Monitor (CPM) is a stacked assembly of 2 modules: CPM POWER MODULE at the bottom and CPM LOGIC PCB containing front end electronics, processing electronics and Detector mounted on it, at the top.

CPM Power Module (CPM PM) generates +5V, +12V, -12V voltages from Satellite Raw Bus of +42 Volts and consumes about 4W power. +5V supply is used to power the CPM logic circuits, +12V and –12V supply is used to power Detector and Amplifier circuits.

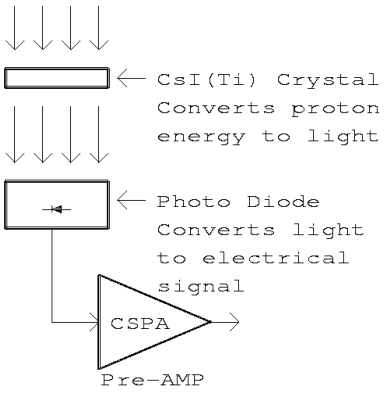


All electronics is mounted on this card along with detector module. The Detector module consists of Cesium Iodide Thallium activated [CSI (Tl)] crystal along with Si-Pin Photodiode and charge sensitive preamplifier (CSPA) eV product. All these are combined into small module of 1cc by SCIONIX, Holland. The energy of charge particle striking the crystal gets converted into photon (light energy). Photodiode converts this photon energy into electrical energy by generating electrons corresponding to energy of incident photons. CSPA amplifies this small electrical signal to a measurable milli-volt range.

The pulse corresponding to every energy particle from detector is passed through post amplification, where milli-volt signal is converted to volt level. The total gain of amplifier is kept around 500 with bandwidth such that it generates 0.5 microsecond rise time pulses.

These amplified pulses are passed through a Low Level Discriminator (LLD) circuit to cut-off noise level and select the Charge Particle signals above a defined value of 0.5 MeV or so. The LLD reference voltage value is programmable from ground station through telecommand. It is a 12 bit DAC and 4096 discrete values are possible.

The pulse signal from LLD circuit output is digitized and fed to a 14 bit counter. The 14 bit counter is a free running counter default gated every 5 sec and hence count rate profile will be every 5sec. Gate time is also programmable from ground through telecommand. All digital processing electronics is embedded in a FPGA. The telemetry and telecommand interface with the satellite bus is also embedded into FPGA. The general health of Instrument is monitored through the analog channels of satellite telemetry.

## CPM data / alert availability

The CPM count rate is transmitted through telemetry to ground station. Also it is available for onboard users in serial format as Data, Clock and a Latch. Maximum three users can be supported.

This count rate is compared with the preset value set from ground station through telecommand. Whenever count rate is greater than a preset value the output is activated. The output is de-activated whenever count rate is less than preset value. To avoid false triggering, output is activated/de-activated only after 3 successive confirmation of count rate (filtering). This SAA warning outputs are available for users. Maximum eight users can be supported.

All the digital processing electronics is embedded into FPGA. The telemetry and telecommand interface with the satellite bus is also embedded into FPGA. The general health of Instrument is monitored through the analog channels of satellite telemetry.

The energy threshold of CPM is nominally set at 500 keV and this can be changed upto 10 MeV with a few keV steps. The count threshold for the automatic onboard sensing of SAA can be set from 1 to 16384 counts with step of 1 count and the integration time can be set from 1 s to 32 s with a step of 1 s. Additionally, there is a command facility to automatically step up the energy threshold so that, at stable non-SAA regions, integral energy spectrum can be obtained.

Chapter 8

# Using ASTROSAT as a broad-band Observatory

So far we have discussed the details of individual payloads on ASTROSAT and its capabilities. However, since all these experiment are co-aligned (except SSM) and mostly operates in unison, ASTROSAT can effectively conduct broad-band multiwavelength observation from Optical to hard X-rays for select sources in the sky. Here we explore briefly the nature of such potential investigations.

For correlated variability in soft and hard X-rays use time tagged photons data from SXT and LAXPC.

- Correlated variability in X-ray and UV bands require time tagged data from X-ray instruments and fastest possible photometric data from UVIT.

- To study simultaneous broad-band X-ray spectrum from 0.3-100 keV, combine data from SXT, LAXPC and CZT and perform simultaneous spectral fits in XSPEC (X-ray analysis package).

- Search of Cyclotron absorption feature (usually in ~10 keV to 60 keV ) needs well calibrated spectral data with high statistics from LAXPC and CZT instruments.

- For constructing multi-frequency spectra (Spectral Energy Distribution) of AGNs, CVs, SNRs etc, simultaneous observations with all 4 instruments over a time scale less than the variability time of a source is needed.

Chapter

9

# Proposing to use ASTROSAT

## ASTROSAT time sharing plan

Allocation of observing time for the Performance Verification (PV) phase, Guaranteed Time (GT, next 6 months after the PV phase) and 3 years of regular observations is given in table below.

| *Instruments* | *PV Phase (6 months)*[3] | *Guaranteed Time (next 6 months)*[4] | *First Year Regular observations* | *Second year Regular observations* | *Third year Regular observations* |
|---|---|---|---|---|---|
| **X-ray Inst. Teams** | 67% | 4 months | 32.5% | 20% | - |
| **UVIT Teams** | 33% | 2 months | 17.5% | 10% | - |
| **Indian proposals** | - | - | 35% | 45% | 65% |
| **International proposals** | - | - | - | 10% | 20% |
| **CSA Team**[1] | - | - | 5% | 5% | 5% |
| **UoL Team**[2] | - | - | 3% | 3% | 3% |
| **TOO** | - | - | 5% | 5% | 5% |
| **Calibration time** | - | - | 2% | 2% | 2% |

- [1]Canadian Space Agency will get 5% of Guaranteed observing time from first year of regular observations for the entire life of the mission.
- [2]University of Leicester team will get 3% of the Guaranteed observing time from first year of regular observations for the entire life of the mission.
- In the PV phase the CSA and UoL teams will be part of the UVIT and SXT teams respectively in selecting appropriate targets for the calibration and performance verification of the instruments.
- During the Guaranteed Time (GT) phase (6 months time after PV phase) the CSA and UoL teams will be part of the UVIT and SXT teams respectively and the observing proposals and targets for the UVIT and SXT will be selected in close consultation with them.

**Distribution of observing time between 4 X-ray Instrument Teams**

The distribution of Guaranteed observing time amongst each x-ray P/L teams is given below.

| | *PV Phase (6 months)* | *Guaranteed Time (6 months)* | *First Year Regular Observations* | *Second Year Regular Observations* |
|---|---|---|---|---|
| Total % of time for X-ray instruments | 67% | 4 months (120 days) | 32.5% | 20% |
| LAXPC | 21% | 37 days | 10.5% | 7% |
| CZT | 9% | 16 days | 4% | 2.5% |
| SXT | 24% | 43 days | 11.5% | 7.0% |
| SSM | 13% | 24 days | 6.5% | 3.5% |

## Proposal Guidelines

### Submission guidelines

Proposers will submit completed proposals using the ASTROSAT Proposal Processing System (APPS) hosted at the ISSDC website. Detailed proposal guidelines are available at the APPS page.

### Observation policies

**Switch 'on' sequence of the Instruments**

| **Time** | **Instrument ON** |
|---|---|
| T0 | ASTROSAT in the orbit |
| T0 + 1 days | CPM switch ON |
| T0 + 7 days | SSM switch ON |
| T0 + 7 days | CZTI switch ON |
| T0 + 21 days | LAXPC switch ON |
| TO + 30 | SXT Door open |
| T0 + 45 | SXT switch ON |
| T0 + 42 | UVIT Door open, UVIT switch on |

PV phase will begin when the last ASTROSAT instrument is turned ON in orbit.

### Description of and Links to different tools

### Instrument specifications

UVIT
LAXPC
SXT
CZTI

SSM : SSM is not a proposal based instrument. Data will be made available on the web
CPM : CPM is not a proposal based instrument.

### Target of Opportunity Proposals

Targets of Opportunity (TOO) observations will mainly be aimed at new transient sources. It will include newly discovered GRBs, supernovae, novae or any other kind of new or known sources that might be undergoing outbursts of flaring that cannot be predicted in advance. Data from TOO source observations will be placed in public domain in ISSDC, as soon as they are processed and converted to useful format. Known sources that undergo regular or predictable outbursts, will not be considered under targets of opportunity. Such proposals will be processed for evaluation under normal observing time.

## Collaborators

The following institutes / centers have significantly contributed to the ASTROSAT payload development.

- Tata Institute of Fundamental Research (TIFR)
- Indian Institute of Astrophysics (IIA)
- ISRO Satellite Centre (ISAC)
- Laboratory for Electro-Optics (LEOS)
- Vikram Sarabhai Space Centre (VSSC)
- ISRO Inertial Systems Unit (IISU)
- University of Leicester (UoL)
- Canadian Space Agency (CSA)
- Inter University Centre for Astronomy & Astrophysics (IUCAA)
- Raman Research Institute (RRI)

Chapter

10

# Observing with ASTROSAT

**Introduction**
**ASTROSAT orbit**
**Observing Constraints**

- SAA
- Celestial constraints
- Sky Visibility
- Bright source avoidance
- Multiwavelength observations

**Field of View of Instruments**
**Instrument overheads**
**Observing Policies and Procedures**

- ASTROSAT Time sharating plan
- Observing Cycles
- Proposal Types
- ToO proposals
- Proposal review process and time allocation

Chapter

11

# Proposal Preparation & Submission

**About APPS**

**Planning an ASTROSAT proposal**

- General considerations
- Instrument Set up
- UVIT
    - Bright Point Source
    - Faint Point Source
    - Extended Source
    - Timing Observations
    - Grism Observations
- SXT
- LAXPC
- CZTI

**Proposal Preparation Tools**

**Preparing an ASTROSAT proposal**

**APPS Instructions**

**Acronyms**

**FAQs**

**Help desk information**

**References**